DOCTORAL THESIS
Doctoral Program in Engineering

Assisted-Control Strategies On Electric Vehicles In Order To Achieve Optimal Energy Efficiency

Author

Juan Diego Valladolid Quitoisaca

******

Supervisor:
Prof. Diego Alejandro Patiño, Ph.D

Doctoral Examination Committee:
Prof. Carlos Ocampo-Martinez, PhD, Universidad de Cataluña, España
Prof. Toufik AZIB, PhD, ESTACA'Lab, France
Prof. Rafael Diez, PhD, Pontificia Univerisidad Javeriana, Colombia

Pontificia Universidad Javeriana
2023

Acknowledgements

I would like to express my gratitude and special thanks to my advisor, Professor Diego Patiño, who assisted and guided me with patience and dedication during my doctoral study process and all my professors at Pontificia Universidad Javeriana.

I am grateful to Professor Giambattista Gruosso from Politecnico di Milano for supporting me during my international stay in Italy. Thanks to examiners Carlos Ocampo-Martinez, Toufik Azib, and Rafael Diez for their comments, feedback and contributions during my Ph.D. process. Also, I would like to thank Universidad Politecnica Salesiana for financial support throughout the doctoral program.

I would also like to thank my parents who have always been by my side, giving me encouragement in all the projects that I have undertaken. I have to really thank my wife, Soledad Carchi, for being my partner and for her unconditional support in every moment of my life.

This thesis is dedicated to my wife Soledad and my children Elias, Francisco, and Amelia; we did it !!!

Abstract

JUAN DIEGO VALLADOLID

Assisted-Control Strategies On Electric Vehicles In Order To Achieve Optimal Energy Efficiency

Electric vehicles (EVs) are capturing popularity, and the reasons behind this are many. The most outstanding is its contribution to the reduction of greenhouse gas emissions. Electric vehicles, with sufficient penetration in the transport sector, are expected to reduce those emission indicators.

The EVs are quiet, easy to operate, and the average cost : EV is 3 times cheaper than fuel internal combustion engine (ICE). As a mode of urban transport, it is beneficial. It uses no energy or emissions of harmful chemicals, gases and particle pollution while idling. EV is capable of frequent stop-and-go driving using minimal power and provides full torque right from the start and the instant torque makes it highly preferable for motorsports.

The next-generation power grid, called the "smart grid," is also being developed. Electric vehicles are seen as a significant contributor to this new energy system made up of renewable generation facilities and advanced grid systems. All this has led to a renewed interest and development in this mode of transport.

This doctoral thesis focuses on the proposal of strategies to improve the energy efficiency of electric vehicles through optimal assisted control. In order to generate a detailed description of the vehicle, experimental tests are accomplished on routes and in the laboratory, using a dynamometric bench and combining it with the mathematical model of the vehicle's dynamics.

The developed strategy shows that driving energy efficiency can increase between 2% and 3% depending on the driving style. On the other hand, for the regenerative braking system, an optimal assisted control strategy has been proposed based on achieving an improvement in energy recovery of up to 8%.

These results will allow the start of future work focusing on implementing assisted systems for current electric vehicles and proposals for energy optimization for autonomous vehicles.

Resumen

JUAN DIEGO VALLADOLID

Estrategias de Control Asistido en Vehículos Eléctricos para Alcanzar la Eficiencia Energética Óptima

Los vehículos eléctricos (*EVs*) están ganando popularidad, y las razones detrás de esto son muchas. La más destacada es su contribución a la reducción de las emisiones de gases de efecto invernadero. Se espera que los vehículos eléctricos, con suficiente penetración en el sector del transporte, reduzcan esos indicadores de emisiones.
Como vehículo, un *EV* es silencioso, fácil de operar y no tiene los costos de combustible asociados con los vehículos convencionales. Como modo de transporte urbano, es beneficioso. No utiliza energía ni emisiones mientras está en ralentí, es capaz de conducir con paradas y arranques frecuentes, proporciona par completo desde el principio. El par instantáneo lo hace muy preferible para los deportes de motor.
También se está desarrollando la red eléctrica de próxima generación, denominada "red inteligente". Los vehículos eléctricos son vistos como un contribuyente significativo a este nuevo sistema energético compuesto por instalaciones de generación renovable y sistemas de red avanzados. Todo esto ha llevado a un renovado interés y desarrollo en este modo de transporte.
Esta tesis doctoral se centra en la propuesta de estrategias para mejorar la eficiencia energética de los vehículos eléctricos mediante un control asistido óptimo. Para generar una descripción detallada del vehículo, se realizan ensayos experimentales en ruta y en laboratorio, utilizando un banco dinamométrico y combinándolo con el modelo matemático de la dinámica del vehículo.
La estrategia desarrollada muestra que la eficiencia energética en la conducción puede aumentar entre un 2% y un 3% en función del estilo de conducción. Por otro lado, para el sistema de frenado regenerativo se ha propuesto una estrategia óptima de control asistido basada en conseguir una mejora en la recuperación de energía de hasta un 8%.
Estos resultados permitirán el inicio de trabajos futuros centrados en la implementación de sistemas asistidos para vehículos eléctricos actuales y propuestas de optimización energética para vehículos autónomos.

Contents

List of Figures **vii**

List of Tables **x**

Nomenclature **xii**

1 Introduction **1**

1.1 Motivation and Research Problem 1

1.2 Objetives 3

1.2.1 General Objective 3

1.2.2 Specific Objectives 3

1.3 Contributions 4

1.4 Scientific Publications Resulting From This Document 5

1.5 Thesis Outline 6

2 Electric Vehicle System and Dynamic Modeling **9**

2.1 Dynamic Modeling 9

2.2 Battery Modelling 12

2.2.1 Deriving *SOC* model whit Temperature effects 14

2.2.2 Battery Model Proposed 18

2.2.3 Parameter Estimation 19

2.3 Inverter and Electric motor 23

3 A Virtual Sensor for Electric Vehicles' State of Charge Estimation **27**

3.1 Design of a virtual current sensor 28
3.2 Battery Model and SOC Estimation 35
3.3 Results and Discussion 38
3.4 Conclusions 40

4 Energy-Efficiency Optimization Approach Based on Experimental Tests 42
4.1 Energy Efficiency Optimizer 42
4.2 Results and Analysis 47
4.3 Conclusions 53

5 Assisted Regenerative Braking Control System 54
5.1 Model of Energy Recovery System 55
5.2 Proposal optimal torque control strategy of energy recovery system . . . 61
5.2.1 Formulation of assisted optimal control strategy 62
5.3 Simulation results and analysis 63
5.4 Conclusions of the chapter 66

6 Conclusions 69

References 71

Appendix A Dynamometric Bench MAHA 79

Appendix B Support Vector Regression 80

Appendix C Particle Swarm Optimization 82

List of Figures

1.1 Energy saved in the transportation sector in Ecuador [1] 2

1.2 Thesis organization 7

2.1 Architecture of the EV power train 10

2.2 Diagram of longitudinal forces acting on a vehicle. 12

2.3 Temperature influence during the discharge cycle of the batteries 15

2.4 Battery model using modified Thevenin circuit 15

2.5 Estimated and fitted V_{OC} vs. SOC 16

2.6 Evaluating *SOC* model of the battery *EV* for different routes. (a) Route 1, (b) Route 2, (c) Route 3 and (d) Route 4 18

2.7 Thevenin battery model (2RC model) 19

2.8 Measured and fitted V_{oc} vs. SOC 21

2.9 Modified Equivalent Circuit Model 22

2.10 Inverter and motor efficiency experiment setup on the dynamometer bank 24

2.11 Efficiency curves for inverter electrical device 24

2.12 Result of efficiency curves based on speed 25

3.1 General architecture for SOC estimation 29

3.2 Input variable vector representation in the principal components' space. 30

3.3 A sample of predicted current on the same route used for training—in this case Route 1. The PCA + PK6 model is not shown. 33

3.4 Normalized histogram of the DDR values for the four methods in the training stage. (a) PCA+GK-SVM, (b) PCA+PK-SVM, (c) GK-SVM and (d) PK-SVM 34

3.5 Current prediction: Training using a 15' sample of Route 1 and Testing on a small portion of Route 2. 34
3.6 Current prediction: Training using a 15' sample of Route 1 and Testing on a small portion of Route 3. 35
3.7 Current prediction: Training using a 15' sample of Route 1 and Testing on a small portion of Route 4. 35
3.8 Evaluating SOC model of the battery EV for Route 1 38
3.9 Evaluating SOC model of the battery EV for Route 2 39

4.1 Simulation schematic to optimization for drive cycles 43
4.2 Route 1: The route of the *EV* between two cities on the highway 44
4.3 Route 2: The route around local areas of the city, a short route around the city with medium-traffic roads 44
4.4 Route3: high energy consumption in mountainous roads 45
4.5 PSO Algorithm flowchart. 47
4.6 Particles convergence of PSO algorithm in different motor speed scenarios 48
4.7 Result of efficiency curves based on speed 50
4.8 Comparison of the original and optimal values for δ=5%: (a) Efficiency; (b) Speed 51
4.9 The computation time during optimizer execute 52

5.1 The general architecture 55
5.2 Pressure sensor placed at the end of the hydraulic brake line 56
5.3 Pressure sensor data 56
5.4 Braking mechanism 57
5.5 Torque calculation in braking mechanism. 58
5.6 Torque and recovered current of the RBS. 58
5.7 Numerical Subspace State Space System Identification (N4SID) performance. 60
5.8 General architecture of the control proposal. 62
5.9 Regenerative and friction braking torque generated by the MPC controller for test 2 64

5.10 Regenerative and friction braking torque generated by the MPC controller for test 2 65

5.11 Regenerative and friction braking torque generated by the *MPC* controller for test 3 66

5.12 Regenerative and friction braking torque generated by the MPC controller for test 1 67

5.13 Regenerative and friction braking torque generated by the MPC controller for test 2 67

5.14 Regenerative and friction braking torque generated by the MPC controller for test 3 68

5.15 Comparison of percent of recovery current according to α parameter . . 68

List of Tables

2.1 Parameters for the dynamic model on the EV 11

2.2 Relationship for the Charging State and Discharging State 16

2.3 Factor for the Number of Cycles 17

2.4 RMSE Test Result for Models Battery 22

3.1 Itineraries used for training and testing 28

3.2 RMSE (root mean square error) of SVR training for GK, PK2, PCA + GK, PCA + PK2 and PCA + PK6 models. 32

3.3 Mean absolute error (MAE) of SVR training for GK, PK2, PCA + GK, PCA + PK2 and PCA + PK6 models. 32

3.4 RMSEs of SVR PCA+GK, PCA+PK2 and PCA+PK6 models trained using four routes testedagainst the other routes. 36

3.5 MAEs of SVR PCA + GK, PCA + PK2 and PCA + PK6 models trained using four routes tested against the other routes. 36

3.6 Battery Parameters Estimation 37

3.7 SOC Estimation Results for Route 1 39

3.8 SOC Estimation Results for Route 2 40

4.1 Performance comparison of *GA*, *SA* and *PSO* algorithms 45

4.2 Results of energy efficiency in *EV* applying the driver cycle optimizer in 3 tests with different variations in the reference speed. 49

5.1 Parameters for Mechanical Friction Brake 57

5.2 Performance Experimentation test 59

5.3 Results of energy efficiency in EV applying the driver cycle optimizer in 3 tests with different variations in the reference speed. 63

A.1 Parameters for the dynamometric bench whit Roller Set R200/2 79

Nomenclature

Roman Symbols

f	complex function

Greek Symbols

β	The inclination angle of vehicle
η	Performance Between Charge and Discharge
η_{MI}	The efficiency factor of the PMSM
η_{Tr}	the efficiency factor of the transmission system
γ	a simply closed curve on a complex plane
$\imath$	unit imaginary number $\sqrt{-1}$
ω	The rotational speed of the PMSM
π	$\simeq 3.14\ldots$
ψ	Parameters Vector
ϖ	Internal Losses caused by Self-Discharge

Superscripts

j	superscript index

Acronyms / Abbreviations

AI	Artificial Intelligence
BMS	Battery Management System
C_d	Drag Coefficient

CAN Controller Area Network

ECU Electronic Control Unit

$EKFA$ Extended Kalman filter Adaptive

EMS Engine Management System

EV Electric Vehicle

$GK-SVR$ Gaussian Kernel Support Vector Regression

GNL General Nonlinear Model

HEV Hybrid Electric Vehicle

$iBAU$ Integrated Brake Actuation Unit

KF Kalman Filter

$LiCoO_2$ Lithium Cobalt Oxide

$LiFePO_4$ Lithium Iron Phosphate

$Lipo$ Lithium Polymer

$LOSPEE$ The Organic Law of Public Service for Electrical Energy

MAE Mean Absolute Error

$MEER$ Ministry of Electricity and Renewable Energy

ML Machine Learning

$N4SID$ Numerical Subspace State Space System Identification

OBD On Board Diagnostic

P_{elec} Electric Power

P_{mec} Mechanical Power

P_{tra} Power Output of the transmission

PCA Principal Component Analysis

$PHEV$ Plug-in hybrid vehicles

$PK-SVR$ Polinomial Kernel Support Vector Regression

$PLANEE$ National Plan of Energy Efficiency

$PMSM$ Permanent Magnet Synchronous Motor

$PNGV$ Partnership for a New Generation of Vehicles

PSO Particles Swarm Optimization

PSU Pressure Source Unit

R_{int} Internal-Resistor

RBS Regenerative Braking System

RC Resistor-Capacitor

$RMSE$ Root Mean Square Error

SOC State of Charge

SVR Support Vector Regression

T Temperature

T_e Torque Applied

T_{tra} Torque Output of the transmission

UN/ECE The Economic Commission for Europe of the United Nations

V_{batt} Battery Current

V_{batt} Battery Voltage

V_{oc} Open Circuit Voltage

Chapter 1

Introduction

In introducing this research study, this chapter shows an overview of the context in which it was conducted. Motivations, general and specific objectives are considered. Likewise, the contributions and limitations of this research are presented, as well as publications made during its development and the general structure of the chapters that make up the document.

1.1 Motivation and Research Problem

Society has been largely dependent on fossil fuels for energy, particularly for the transportation sector, which releases greenhouse gases that pollute the atmosphere, known as global climate change [1–3]. The electric energy generated by renewable sources contributes significantly to mitigate polluting gas emissions and the energy demand is expected to continuously increase in the coming years. Therefore, a significant reduction in the use of fossil fuels is the result of the substantial contributions of the electricity sector. Therefore, a substantial contribution of the electric sector gives as result a significant reduction of the use of fossil fuels.

During the last few decades, transport electrification technology has presented proposals around hybrid electric vehicles $(HEVs)$ and pure electric vehicles (EVs). These vehicles are the biggest bets of today's technology, especially the EVs with almost local zero emission, which is capable of reduce fossil fuels demand and environmental damage caused by the internal combustion engines used for transportation [3–6].

The automotive industry in Latin America is mainly occupied by vehicles that work with internal combustion engines. However, EVs sales have been increasing every year as a result of the acquisition cost reduction and the variation in oil prices worldwide. In

Latin America, an average increase in the range of 75% has been reported [7]. South American countries such as Colombia and Ecuador show an increase in sales during 2021 of 60% and 228% respectively in comparison to 2020 [7, 8].

In Ecuador, the Organic Law of Public Service for Electrical Energy (*LOSPEE*) determines that the Ministry of Electricity and Renewable Energy (*MEER*) establishes the creation of the National Plan of Energy Efficiency (*PLANEE*), which seeks to coordinate stakeholders, identifying and incorporating programs and projects that will be implemented nationwide to increase efficient energy use, during the 2016-2035 period, as shown in Figure 1.1.

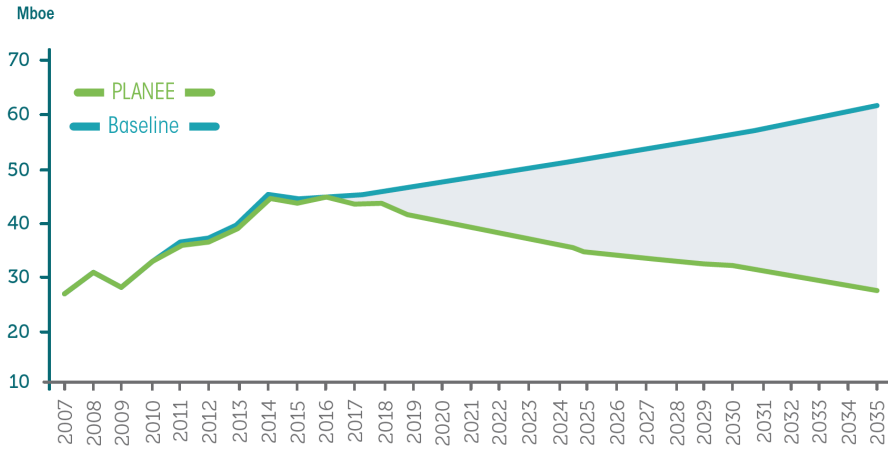

Fig. 1.1 Energy saved in the transportation sector in Ecuador [1]

The primary consumer sector identified is transportation, which corresponds to 42% of the total national energy consumption [1]. *PLANEE* aims to optimize energy consumption in freight and passenger transport compared with the industry baseline scenario by carrying out energy efficiency projects that generate benefits in the sector. This Project pursues to Incorporate *HEV*, *EV* and New Technology Vehicles to be commercially available in the future.

On the other hand, the increase of this technology in the automotive industry of Ecuador and Latin America sector suggests taking action on the limitations of the operation of these vehicles, such as the lack of charging points or charging stations, the repowering of the local electrical network and the insufficient autonomy. Studies have shown that electric motors are largely more efficient than internal combustion engines. However, the energy density of an electric vehicle (EV) battery pack falls short of that of fuel, and the constraints on recharging continue to be a vital factor to bear in mind when acquiring an EV.

This research focuses on improving energy efficiency in *comercialEVs*, where control and optimization strategies are proposed that can be executed while driving the vehicle. The initial step involves considering the study and modeling of vehicle subsystems using mathematical equations and lookup tables, accounting for the non-linearities inherent in the system dynamics. Then, test routes for the vehicle in order to determine its performance in each scenario are established. With this information, an optimizer is proposed to improve energy efficiency. Finally, proposals for optimal control are also presented in the vehicle's energy recovery system through the regenerative braking system (RBS). The optimization algorithms adequately consider the electrical and mechanical losses.

1.2 Objetives

The present study proposes to generate simulation tools and assisted control strategies that help improve *EVs*' efficiency, includiing : speed optimisation, driving cycle optimisation, motor efficiency optimisation. Based on this approach, the following general and specific objectives are established

1.2.1 General Objective

The main objective of this research is to develop assisted-control strategies for electric vehicles in order to achieve optimal energy efficiency, considering a dynamic model that includes losses and experimental data of the system.

It is essential to develop a model capable of representing the full dynamics of the EV, from the battery pack to the power in the vehicle wheel. Additionally, the vehicle experimentations must be considered in real conditions and in the laboratory, where there are controlled conditions.

1.2.2 Specific Objectives

In order to achieve the general objective, the following specific objectives are defined:

1. Determine an *EV* model that represents the interactions between electrical and mechanical components, as well as the losses of the system in each stage of operation.

2. Formulate a model for the problem of energy efficiency optimization to address the dynamics of the vehicle considering the effects of non-linearities and driving styles.

3. Propose a control scheme that includes formulating an optimization problem to increase energy efficiency in *EV* during the driving and regenerative braking action.

1.3 Contributions

The control strategies applied in EV are aimed to obtain an enhanced performance, taking into consideration the driver's driving profile or adapting to a defined speed trajectory, as discussed in detail in the following chapters. Nowadays, most EVs consist of driving modes, such as the NORMAL mode which offers regular daily performance, the ECO mode offers a setting to reduce energy consumption and the SPORT mode which adapts to a more aggressive driving mode ensuring maximum power. Unfortunately, most of the scientific researches and improvement strategies around EVs do not take into account the electrical and mechanical losses of all subsystems that guarantee the maximum energy efficiency point throughout the entire system during its operation.

This research aims to address the above challenges to present a formulation for an optimizer covering distinct scenarios of driving patterns for EVs; this proposal is developed with the mathematical model including a differential drive, lookup tables made from experimental data, and a solution of the objective function using a metaheuristic algorithm. The contributions of this thesis are the following:

1. We formulate a model for commercial EV that aims to include a realistic efficiency analysis for the whole system of the vehicle using a mathematical model, experimental tests in a dynamometer bench [9] and the On-Board Diagnostics (OBD), which provides access to the Electronic Control Unit (ECU) data allowing the inclusion of realistic nonlinear effects of EV in lookup tables.

2. A strategy is proposed to improve consumption and energy efficiency in an EV through an optimization algorithm that adapts to the user's driving pattern in real conditions, generating corrections in vehicle speed according to defined ranges. This formulation guarantees the improvement of EV's energy efficiency without the need to generate previous training for the identification or classification of driving styles.

3. We propose and evaluate an assisted control strategy to enhance the recovered current from the *RBS* during the braking process generating corrections in the torque target generated by the vehicle braking system. This formulation guarantees the improvement of the recovered current during the braking process without depriving the driver of the principal operation. By incorporating experimental tests, vehicle dynamics, and accessing data from the Electronic Control Unit (ECU) via the On-Board Diagnostics (OBD), we have developed a fourth-order multi-variable state space discrete-time linear model for the electric vehicle (EV) braking system. Furthermore, we have taken into account the guidelines outlined in regulation # 13 of the United Nations Economic Commission for Europe to establish the criteria for safe braking.

1.4 Scientific Publications Resulting From This Document

It is important to mention that this dissertation is based on several articles published in journals and conferences during this investigation. The publication topics during the development of this research are the following:

Accepted and published journal articles

- Valladolid, J.D., Patino, D., Gruosso, G., Correa-Flórez, C.A., Vuelvas, J., Espinoza, F. A Novel Energy-Efficiency Optimization Approach Based on Driving Patterns Styles and Experimental Tests for Electric Vehicles. Electronics 2021, 10, 1199. https://doi.org/10.3390/electronics10101199.
- Gruosso, G., Storti Gajani, G., Ruiz, F., Valladolid, J.D., Patino, D. A Virtual Sensor for Electric Vehicles' State of Charge Estimation. Electronics 2020, 9, 278. https://doi.org/10.3390/electronics9020278.

Accepted and published conference articles

- J. D. Valladolid, D. Patino, G. Gruosso and F. Espinoza, "Study on the Torque-Speed Allocation on PMSM to Improve Energy Efficiency in Electric Vehicles Using Metaheuristic Optimization," 2021 IEEE Vehicle Power and Propulsion Conference (VPPC), 2021, pp. 1-5, doi: 10.1109/VPPC53923.2021.9699274.

- J. D. Valladolid, R. Albarado, D. Mallahuari and D. Patiño, "Experimental Performance Evaluation of Electric Vehicles (EV) Based on Analysis of Power and Torque Losses," 2020 IEEE International Conference on Industrial Technology (ICIT), 2020, pp. 933-938, doi: 10.1109/ICIT45562.2020.9067241.
- J. D. Valladolid, D. Paladines, J. Vidal and D. Patiño, "Proposal of Fuzzy Controllers for Improve Features of Driven Style in Electric Vehicles Using Experimental Route Data," 2020 IEEE International Conference on Industrial Technology (ICIT), 2020, pp. 77-82, doi: 10.1109/ICIT45562.2020.9067208.
- G. Gruosso, G. S. Gajani, J. D. Valladolid, D. Patino and F. Ruiz, "State of Charge Estimation of LiFePO4 Battery Used in Electric Vehicles Using Support Vector Regression, PCA and DP Battery Model," 2019 IEEE Vehicle Power and Propulsion Conference (VPPC), 2019, pp. 1-5, doi: 10.1109/VPPC46532.2019.8952458.
- J. D. Valladolid, J. P. Ortiz, F. A. Berrezueta and G. P. Novillo, "Lithium-ion SOC Optimizer Consumption Using Accelerated Particle Swarm Optimization and Temperature Criterion," 2019 AEIT International Conference of Electrical and Electronic Technologies for Automotive (AEIT AUTOMOTIVE), 2019, pp. 1-6, doi: 10.23919/EETA.2019.8804490.
- J. D. Valladolid, D. Patiño, J. P. Ortiz, I. Minchala and G. Gruosso, "Proposal for Modeling Electric Vehicle Battery Using Experimental Data and Considering Temperature Effects," 2019 IEEE Milan PowerTech, 2019, pp. 1-6, doi: 10.1109/PTC.2019.8810611.

Summitted journal paper

- J. D. Valladolid, D. Patino, J. Vuelvas and P. Ortiz, "A novel proposal for assisted control to enhance the regenerative braking system performance in electric vehicles", Elsevier, Transportation Research.

1.5 Thesis Outline

The thesis document is organized in chapters and each one can be read independently. Fig. 1.2 shows the organization of the thesis, numbered by the respective chapter and their purpose in the assisted optimal control strategies for electric vehicles framework.

- **Chapter 1: Introduction**

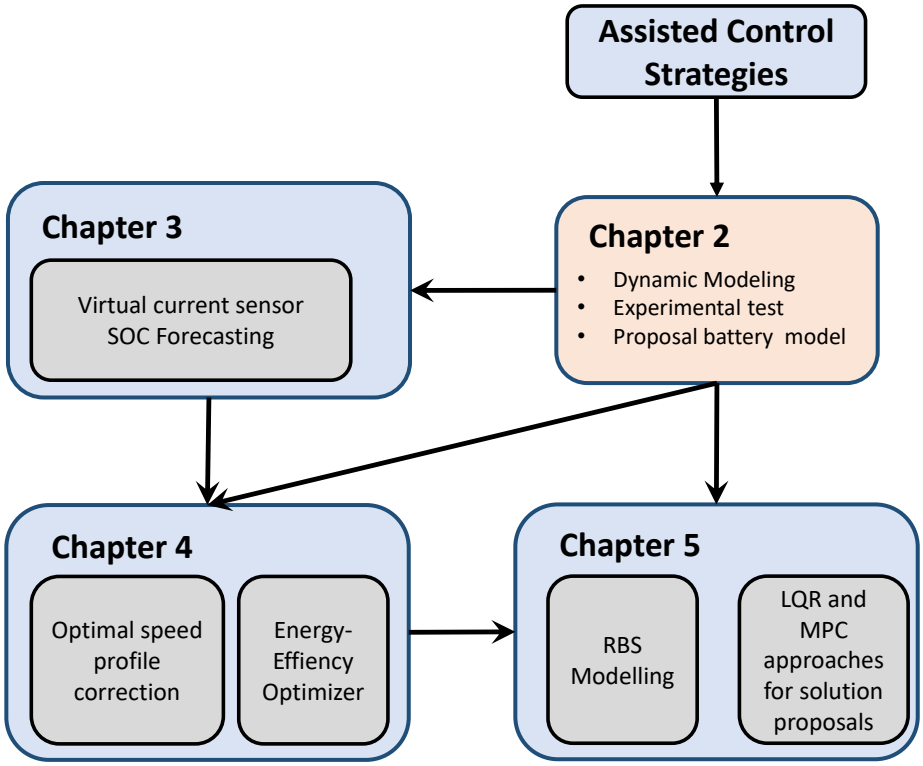

Fig. 1.2 Thesis organization

This chapter presents the initial information of this document and its general structure. The content refers to how the research problem is defined, its motivations, and the set of objectives considered . Additionally, the generated contributions are detailed and the scientific publications in congresses and journals are presented.

- **Chapter 2: Electric Vehicle System and Dynamic Modeling**

  The second Chapter considers that generating a model of *EVs* (Mechanical and electrical) is essential to provide accurate and useful representations of the knowledge needed to generate control and optimization proposals. The considered subsystems are battery pack, inverter, motor, representation of loss mechanical and electric inverter. Finally, the mathematical expressions and look-up tables necessary to establish a proposal for optimization strategies in the following chapters are exposed.

- **Chapter 3: A Virtual Sensor for Electric Vehicles' State of Charge Estimation**

  This chapter shows a new methodology for estimating the state of charge estimation in electric vehicles without the use of a conventional current sensor in the battery pack. It is important for the proposed optimization algorithms that the

battery current data are available directly or through a virtual current sensor. The virtual current sensor is based on the use of other available vehicle variables, such as speed, battery voltage and accelerator pedal position. The estimator was derived from experimental data, employing support vector regression, principal component analysis and a dual polarization battery model. It is shown that the obtained model is able to predict the state of charge of the battery in the case of a failure of the current sensor.

- **Chapter 4: Energy-Efficiency Optimization Approach Based on Experimental Tests**

  This chapter proposes a strategy to improve energy efficiency in EVs based on optimizing the speed profile during the electric vehicle's driving. The optimization problem is focused on maximizing energy efficiency between the wheel power and battery pack, while also improving the state of the battery. The solution to the optimization problem is found using a metaheuristic algorithm based on particle swarm optimization.

- **Chapter 5: Assisted Regenerative Braking Control System**

  The recovery of energy of EVs from the wheels to the battery pack through the braking process is analyzed in this chapter. A model of regenerative braking system is established, this one describes the system's dynamics and proposed assisted control strategies to improve its performance. The proposal is based on the modeling obtained through experimental data and optimal control strategies, such as model predictive control and finite horizon linear quadratic regulator.

- **Chapter 6: Conclusions**

  This section considers the obtained assumptions and results in Chapters 3, 4 and 5 and discusses all the most important conclusions of the investigation. Finally, this chapter presents the closure of all the research and a methodological proposal to implement the controllers in future studies.

Chapter 2

Electric Vehicle System and Dynamic Modeling

In recent years, vehicle electrification technology, including $HEVs$ and EVs, has gained popularity in public and private transportation systems [10, 3–6]. This chapter provides a detailed description of the state-of-art in the dynamic modeling of an electric vehicle.

Different studies of electric vehicles have been carried out around the world. Most of these studies focus on the battery and the losses that exist in its overall operation. For this reason, different authors are looking for a way to obtain greater battery autonomy and achieve a long-distance trip. To achieve it, different mathematical models help to understand EV behavior[6, 11–13].

The electric vehicle model gives primary importance to the electric propulsion system, which is comprised of an electric machine, power converters, and electronic controllers. This system is crucial to the functioning of the electric vehicle as it converts electrical energy into mechanical energy, propelling the vehicle forward.

2.1 Dynamic Modeling

In this section, first, the power-train modeling of the Battery EV (BEV) is detailed. Then, the longitudinal and lateral dynamic model is proposed. The architecture of the power train is shown in Fig. 2.1. The motor's command torque is dynamically coupled through simple gearbox and transmitted to front-wheels via a conventional differential drive.

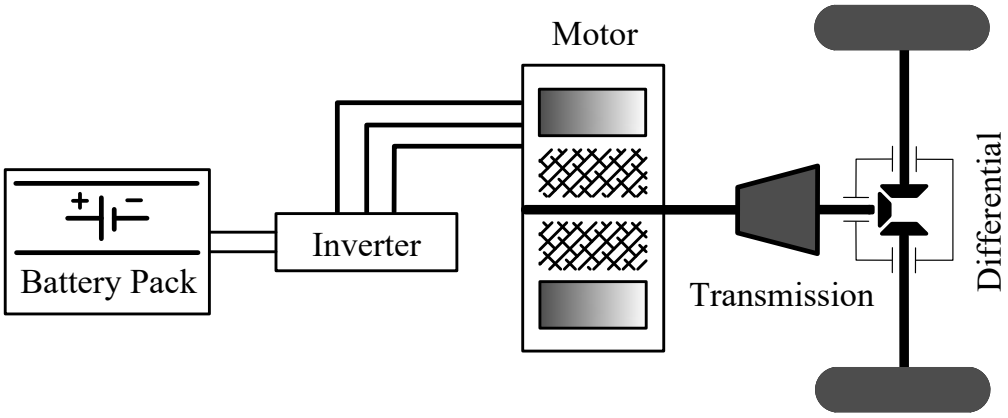

Fig. 2.1 Architecture of the EV power train

The power train modeling parameters and lookup tables were obtained through its technical specifications and laboratory experimentation in a commercial EV detailed in [12].

It is essential to mention that for *EV* modeling, the altitude of 2550 meters above sea level was considered. Experiments was performed in Cuenca-Ecuador. This information was factored into the calculation of the air density. Given that vehicle driving at higher altitudes, the air density would have lower values, and so the air resistance as well. According to [14], the air density of 0.96 $kg\ /m^3$ was considered.

On the other hand, the rolling resistance coefficient was calculated in relation to different types of roads and variable weather conditions. The value for this parameter is 0.017.

The Aerodynamic Drag Coefficient (C_d) is a rather complex parameter, and in practice, wind tunnels and coast down tests are often used to obtain it. For this document, the Kia Soul EV manufacturer provided the 0.35 value for C_d. Finally, the value of a vehicle's frontal area can be estimated as the multiplication of width and height. However, as the shape differs between model vehicles, this value is perhaps not applicable. Nevertheless, various estimations can be found in the literature [6] [15]. Based on the EV's model, the frontal area's estimate is found according to the weight and the C_d of the vehicle [15].

The parameters are shown in Table 2.1.

Table 2.1 Parameters for the dynamic model on the EV

Parameter	**Value**	**Unit**
Total mass of the vehicle	1670	kg
Aerodynamic Drag Coefficient	0.35	–
Frontal area vehicle	2.3	m^2
Air density	0.96	kg/m^3
Tire radius	0.325	m
Rolling resistance coefficient	0.017	–
Distance from gravity center to front axle	1.2	m
Distance from gravity center to rear axle	1.4	m
Track width	1.576	m
Max. torque of Electric Motor	285	Nm
Ratio in the transmission system	8.2	–

A system model is required for designing the vehicle motion control, with motor torque as input and *EV* speed as output. Tire forces influence the vehicle's longitudinal dynamics model, the aerodynamic drag force of the vehicle, rolling resistance forces, and the gravitational force related to the inclination of the vehicle as shown Fig. 2.2 [6, 16]. The external longitudinal forces acting on the vehicle are described in (2.1) as follows.

$$\dot{V}_x = \frac{T_e}{rm} - \frac{F_{aero}}{m} + g(-sin\beta - u_r cos\beta) \tag{2.1}$$

The torque T_e applied to the front wheels through the differential drive causes the vehicle to move. The aerodynamic drag force is defined as shown in Equation (2.2):

$$F_{aero} = \frac{1}{2}\rho C_d A (V_x)^2 \tag{2.2}$$

EV is driven by a transmission system between motor and wheel to improve vehicle performance. The primary function is to transfer power from the electric motor to the wheels, allowing the torque and motor speed to fulfill performance requirements [17]. The torque generated by the electric motor is distributed in the front wheels via differential bevel gear. Considering the effort to overcome these forces, the differential drive allows the drive wheels to turn at different speeds when turning a corner or

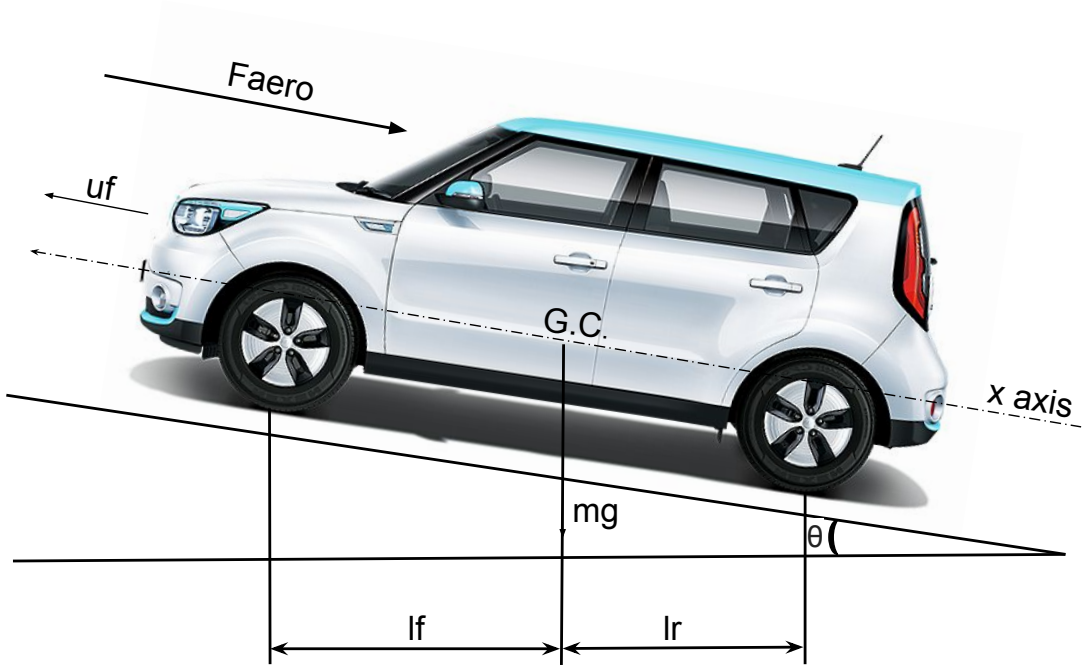

Fig. 2.2 Diagram of longitudinal forces acting on a vehicle.

maneuvers while driving the vehicle. Another essential feature is distributing equal torques on each of the wheels, even when rotating at different speeds.

2.2 Battery Modelling

The most valuable component involved in the operation of an *EV* corresponds to the battery storage system [18, 19, 11]. Manufacturers are highly devoted in the improvement of power and energy density of batteries, which makes necessary to establish reliable models to determine its performance and behavior during the charge and discharge processes. Batteries used in *EVs* have different characteristics depending on their chemistry composition. Lithium polymer batteries are more suitable for *EVs* due to the long life cycle, less self-discharge rate, high-energy density, high efficiency, low maintenance, and safe use [19].

The battery of *EV* consists of about 96 cells in the pack, which are monitored and controlled by a battery management system (BMS). The *BMS* need to be linked with all battery components, as well as with the vehicle's computer. The *BMS* will take several sensors readings A fundamental indicator used in *BMS*, is the battery state of charge (SOC). Numerously methods have been investigated in the literature for *SOC* modelling,

several strategies presented in [20–22] show a Coulomb counting methodology, where the Thevenin model is taken as a reference to represent the dynamics of a cell.

To establish the empirical model of the battery, we use some of the expressions described in [23–26], where the models used are: Unnewehr universal model, Shepherd model and Nernst model. Nernst model is considered due to its enhanced performance over other model structures. The expression for the battery model is expressed as:

$$\begin{aligned} V_k = V_o - \frac{k_1}{SOC_k} - k_2 SOC_k + k_3 ln(SOC(k)) \\ + k_4 ln(1 - SOC(k)) - R_{int} i(k) \end{aligned} \tag{2.3}$$

where, V_k is the output voltage of the battery, $k_1, \ldots, k_4$ are parameters of the model, R_{int} is the internal resistance of the battery and V_o is the initial voltage in the battery pack.

In addition, there are variations from this model to extended structures as the general nonlinear (GNL) and an improved model for a partnership for a new generation of vehicle $(PNGV)$, which includes a series capacitor to the open circuit voltage source (V_{OC}) [27–30].

However, these methods have the disadvantage of error propagation according to the study shown in [31].

The non-linear behavior of the *SOC* has also generated proposals based on Machine Learning (ML) and Artificial Intelligence (AI) [32–35] successfully combining recurrent neural networks and sliding mode observers to estimate the SOC and voltage of batteries. On the other hand, in [36] is shown the use of the Kalman filter (KF) for estimate synaptic weights of a dynamic neural network. The concept of adaptive extended Kalman filter $(EKFA)$ is used in [37] as well as the Thevenin model in order to establish the parameters of the equivalent circuit. These methods present a great performance in their estimation, however; its complex structure hinders its implementation.

There are models for battery packs in a series-parallel combination of cells; some strategies are shown in [38, 39], where Thevenin models are established as a reference for each element, increasing its complexity to a model of 96 combined series circuits. Therefore, the model will require a high computational cost.

For the development of this research, a package of Lithium polymer battery of a commercial *EV* is used, composed of 96 cells of $3.7V$ placed in series, with a load capacity of 80Ah and as an internal characteristic of self-discharge of less than 5% in the period of one month. The experiments described in [40] show that the self-discharge for

this type of battery is less than 3% per month. The expression of the SOC described in [41] is used for the models generation, the same as it governs a function of: the current, the temperature, the number of cycles and self-discharge.

2.2.1 Deriving *SOC* model whit Temperature effects

This model describes the battery state of charge (SOC) and the batteries' output voltage using experimental data gathered during the driving of the EV on pre-established routes. In addition, the temperature effect was considered [42]. The state of charge is formulated as

$$SOC(t) = SOC(t_0) - \frac{\beta}{Q}\int_{t_0}^{t} i(\tau)\cdot d\tau + \varpi \tag{2.4}$$

where $i(t)$ is the instantaneous current of the battery, considered as positive for discharge and negative for charge, Q is the nominal capacity measured in Ah, whose value for the EV used in this research is $80Ah$. The ϖ term refers to the internal losses caused by self-discharge, this value is lower than 3%, in this case it is discarded for the analysis obtaining a global accuracy of the model of at least, 97%. The factor β is defined as the product of parameters that depend on the performance between charge and discharge $f[v]$, temperature $f[T]$ and the number of cycles of the battery [41, 43, 44], this factor is shown in the following expression.

$$\beta = f[T]f[v]f[N_{cycles}] \tag{2.5}$$

The expression of temperature $f[T]$ is presented in [41], $f[T]$ can be calculated by taking the average of the ratios between each voltage value on the $25°C$ curve and the corresponding voltage values on other temperature curves. This relationship can be defined as:

$$f[T] = \frac{1}{k}\sum_{m=1}^{k}\frac{Voc_m|_{25°C}}{Voc_m|_{Other\_Temperature}} \tag{2.6}$$

where k is the total number of measured points. A comparison between the temperature of each cell on the $25°C$ curve with the experimental data (Fig. 2.3), shows that the temperature has an important effect on the behavior of the battery during discharge; therefore, it is proposed that $f[T]$ could be replaced by the expression considered as:

$$f[T] = aT^2 + bT + c \tag{2.7}$$

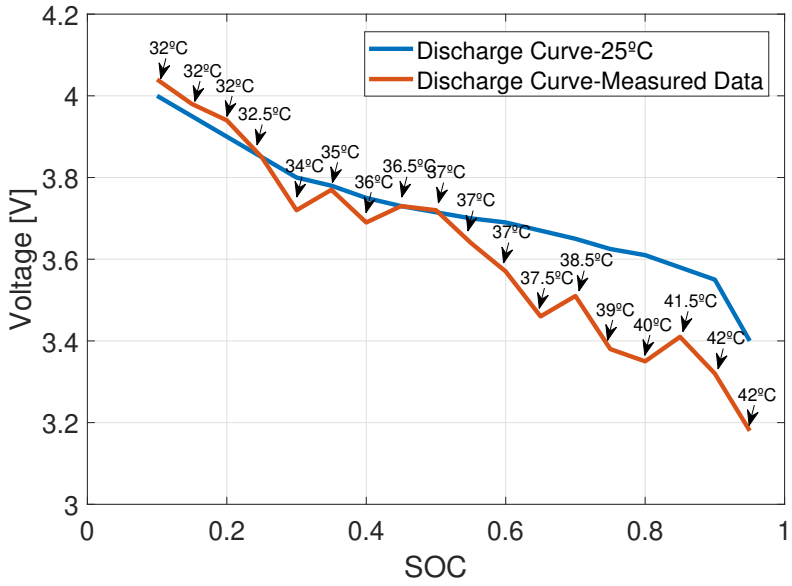

Fig. 2.3 Temperature influence during the discharge cycle of the batteries

where, a, b, and c are coefficients of the second-order polynomial found. Considering the equivalent circuit or the Thevenin model, which consists of an array of a Resistor-Capacitor (RC) network in series with a voltage source [42, 45–47], the proposal is replacing the RC circuit with a transfer function as shown in Fig. 2.4.

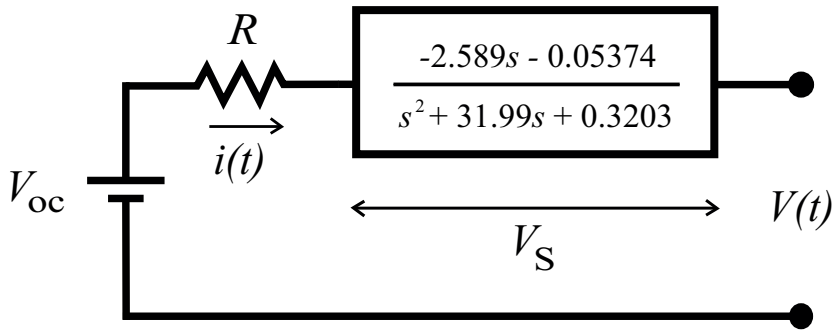

Fig. 2.4 Battery model using modified Thevenin circuit

where a, b and c are scalars coefficients for the second order polynomial in (2.7).

By using the least squares algorithm applied to Equation (2.6), the following parameters are obtained: $a = 0.000157$; $b = 0.00617$ and $c = 1.052$.

According to the data obtained during experiments on the EV battery during a previous research detailed in [42] , the fitted curve for the relationship between V_{OC} and SOC is shown in Figure 2.5 using $5th$ order regression, V_{OC} is represented as

$$V_{OC} = 1505SOC^5 - 4315SOC^4 + 4623SOC^3 - 2254SOC^2 + 556.9SOC + 288.1 \quad (2.8)$$

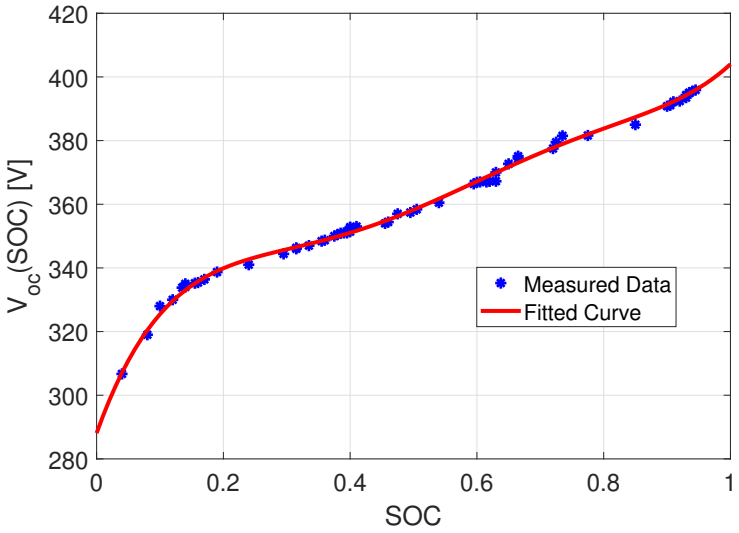

Fig. 2.5 Estimated and fitted V_{OC} vs. SOC

The method for determining $f[v]$ is to establish the relationship between the SOC from the characteristic curve of the battery and the measured data, as shown in Equation (2.9). This relationship is established when the battery cell is charged $(4.1V)$ and when the cell is discharged $(3.4V)$, the experimental data is presented in Table 2.2.

Table 2.2 Relationship for the Charging State and Discharging State

PARAMETER	CHARGED (4.1V)	DISCHARGED (3.3V)
SOC Curve	92%	9.5%
SOC Data	98%	8.9%

From the information presented, the formulation shown in (2.9) is applied to determine the factor $f[v]$, as follows:

$$f[v] = \frac{SOC_{oc}|Charging - Discharging\_Curve}{SOC_{oc}|Charging - Discharging\_Measured} \quad (2.9)$$

$$f[v] = 0.997 \quad (2.10)$$

Table 2.3 presents the factor for the number of cycles $f[N_{cycles}]$ for a Lithium Polymer battery GMB05230. It is considered that the distance covered by the EV is $20,000km$ and

each load reaches approximately 200km, implies at least 100 battery cycles, therefore it is taken as $f[N_{cycles}] = 1$ [10].

Table 2.3 Factor for the Number of Cycles

Cycle Number	100	200	300	400	500
$f[N_{cycles}]$	1	0.98	0.94	0.88	0.86

All the necessary values for the Equation (2.4) are replaced, obtaining the expression for the *SOC* given by:

$$SOC(t) = SOC(t_0) - 0.997(aT^2 + bT + c) \int_{t_0}^{t} \frac{i(\tau)}{80} \cdot d\tau \tag{2.11}$$

The *SOC* does not only depend on the current of the battery, this proposal also includes the effect of the temperature for the calculation. The expression (2.11) could be used to establish models that describe the complete dynamics of the battery of EVs.

The performance of the *SOC* model is evaluated in four realistic scenarios for EVs applications:

- Route 1 (Fig. 2.6a).- It includes the route of the *EV* between two cities, in such a way that the capacity of the battery is at its minimum. This route lasts around 7500 seconds.
- Route 2 (Fig. 2.6b).- Includes a journey around local areas of the city, with a duration of 7000 seconds.
- Route 3 (Fig. 2.6c).- Refers to a short route around the city with a duration of 3500 seconds.
- Route 4 (Fig. 2.6d).- For this experiment, a tour of steep slopes is carried out in such a way that in a certain sector the effect of the regeneration of the current towards the battery can be visualized.

Fig. 2.6 shows the response of the *SOC* model provided in Equation (2.11) and the data measured in each route. Fig. 2.6a, 2.6b and 2.6c show very close results for the modeled and measured *SOC* when the *EV* is discharging, however, Fig. 2.6d shows how the regenerative brake has more influence on the recharge of the battery in a section of the route, for this reason there is a small deviation of the modeled and measured values.This variation is due to non-linearities present in the braking mechanisms during aggressive driving conditions.

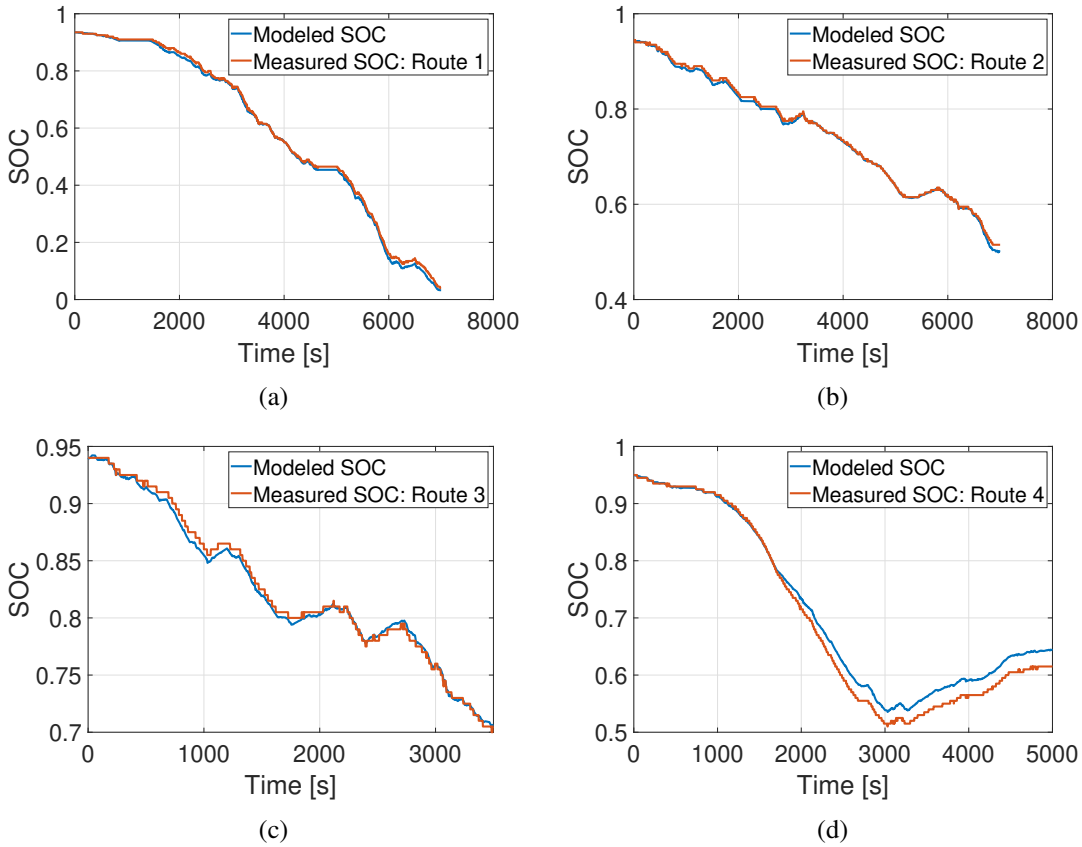

Fig. 2.6 Evaluating *SOC* model of the battery *EV* for different routes. (a) Route 1, (b) Route 2, (c) Route 3 and (d) Route 4

2.2.2 Battery Model Proposed

The two proposed models are based on the proposed structure to determine the *SOC*, where the current and temperature are the system inputs and the voltage of the battery is the output. These models will be evaluated with data from established routes for the *EV*.

For the internal resistance R_{int} described in Equation (2.12) the average variation of the current and voltage from the experimental data obtained from the pre-established routes is performed as follows:

$$R_{int} = \frac{1}{n}\sum_{i=1}^{n}\frac{\Delta V_i}{\Delta I_i} \tag{2.12}$$

The value for internal resistance is $R_{int} = 0.0498\Omega$

Equivalent electrical circuits are commonly used for modeling batteries, which consist in an array of a resistor capacitor network (*RC*) in series with a voltage source. The typically equivalent circuit model is the Thevenin model, see Fig. 2.7.

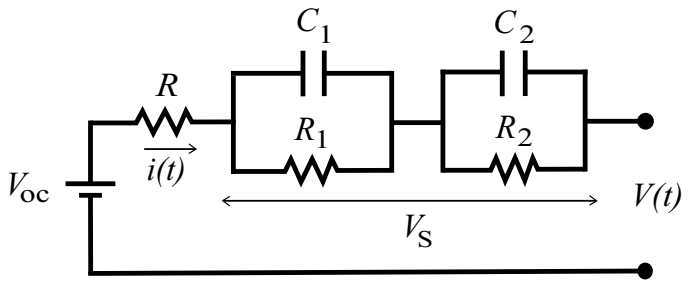

Fig. 2.7 Thevenin battery model (2RC model)

In this model, $V(t)$ is the voltage at the terminal of the battery, V_{oc} is the open circuit voltage of the battery cell, R is the internal resistance of the battery and the parameters R_1, C_1, R_2 and C_2 correspond to the RC network of the model. This parameters describe the polarization dynamics. According to the circuit theory, $V(t)$ in Fig. 2.7, can be defined as

$$V(t) = V_{oc} - Ri(t) - V_S \tag{2.13}$$

where V_S corresponds to the voltage that exists in the RC network when there is an $i(t)$ different from zero. To determine V_{oc} , several experiments of discharge events are performed to obtain a curve, which is used for fitting purposes (see Fig. 2.8).

2.2.3 Parameter Estimation

In this subsection a nonlinear least square (NLS) adaptive algorithm is used to estimate the parameters of the battery. Other methods could be in principle be used, but since in our problem NLS converges quickly and with low computational effort, it has been preferred to alternative methods. In order to minimize the squared error between the measured and calculated voltage, we define as the minimization target function, the error criterion known as chi square, and define it as follows:

$$\chi^2(\psi) = \sum_{i=1}^{M} \left[\frac{V(t_i) - \hat{V}(t_i, \psi)}{\sigma_{Vi}} \right]^2 \tag{2.14}$$

where $\hat{V}(\psi, t)$ is the estimated value of the $V(t)$ value defined in the output relation of Equation 3.9 and based on the parameter vector $\psi = [R \;\; R_1 \;\; C_1 \;\; R_2 \;\; C_2 \;\; V_{oc}]^T$, M is the number of data samples used and σ_{Vi} is the expected measurement error for the i-th sample $V(t_i)$.

By collecting all calculated and measured voltages $\hat{V}(t_i)$ and $V(t_i)$ in the $M \times 1$ vectors $\hat{V}$ and V respectively, and, further, collecting the reciprocal of all σ_{Vi} in the $M \times M$ diagonal matrix W, Equation (2.14) reduces to the quadratic form:

$$\chi^2(\psi) = (V - \hat{V})^T W (V - \hat{V}) \tag{2.15}$$

The minimum of the chi square error is searched by repeated use of the Levenberg-Marquardt algorithm, that we will briefly recall in the following paragraph, on small m sample sized partitions of the M sized available data.

In our setting, the Levenberg-Marquardt algorithm [48] is used to update the parameter vector and iteratively by solving the nonlinear optimization problem described in Equation (2.14). The algorithm adaptively updates the parameter estimates by combining the gradient descent update and the Gauss-Newton update [48] by tuning a damping parameter λ. The Marquardt's update equation is given by:

$$[J^T W J + \lambda \ \mathrm{diag}(J^T W J)]h = J^T W (V - \hat{V}) \tag{2.16}$$

where h is the parameter update vector, $\mathrm{diag}(\cdot)$ is an operator that extract the diagonal from a matrix, J is the Jacobian matrix of $V - \hat{V}$ with respect to ψ and λ is the damping parameter acting on the diagonal of $J^T W J$ and initially chosen to be large so that, initially, small steps in the steepest descent direction are taken. The Jacobian can be quickly updated (J_{new}) using the Broyden formula [49].

$$J_{new} = J + \frac{(\hat{V}(\psi + h) - \hat{V}(\psi) - Jh)h^T}{(h^T h)} \tag{2.17}$$

The damping factor λ is adjusted by checking the values obtained with the new parameter set against the previous values. One possible way to do this is by using a ρ factor [48, 50, 51] defined in Equation (2.18). The step is accepted if ρ is larger than a user-specified threshold, rejected otherwise and, in this case, λ is increased.

$$\rho(h) = \frac{\chi^2(\psi) - \chi^2(\psi + h)}{h^T(\lambda \ \mathrm{d}iag(J^T W J)h + J^T W (V - \hat{V}(\psi))}) \tag{2.18}$$

Different convergence criteria may be used, based on limit values for the gradient, for the chi square error, for the norm of the update vector or, simply, by the number of iterations. An adaptive algorithm is developed based on the above criterion. Given M time samples of current and voltage data $i(t)$ and $V(t)$, the sequence is initially split in sub-sequences of length m. The algorithm optimizes, for each sub-sequence, the chi

square cost function (2.15), obtained by estimating the electric parameter vector ψ of the battery and then calculating the voltage from the electrical parameters in ψ. The operation is repeated for each following sub-sequence using as initial condition for ψ the values obtained in the previous iteration. This process updates and adjusts the electrical parameters of the battery.

To determine V_{oc} from the measured data, a $5th$ order regression is used, as shown in Equation (2.19).

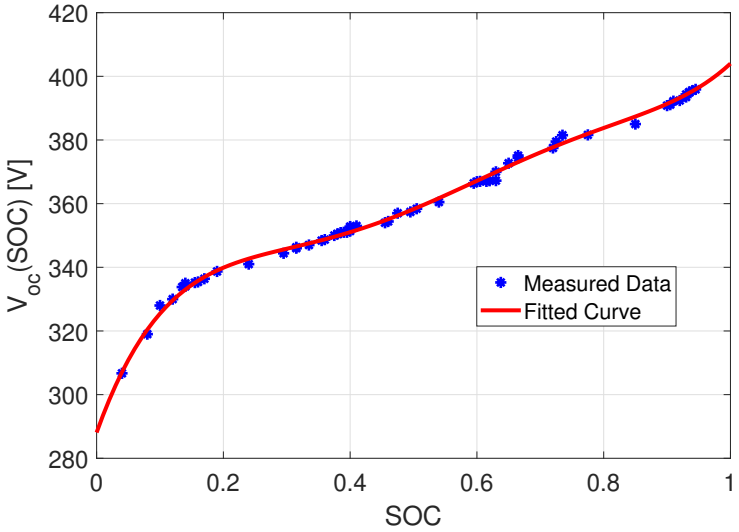

Fig. 2.8 Measured and fitted V_{oc} vs. SOC

$$\begin{aligned} V_{oc}(SOC) = 1505SOC^5 - 4315SOC^4 + 4623SOC^3 \\ - 2254SOC^2 + 556.9SOC + 288.1 \end{aligned} \tag{2.19}$$

The next term of the Equation (12) that is analyzed is the voltage V_S, this term refers to the combination of the *RC* network of the Thevenin model. A Thevenin model is established for each cell, this means the quantity of 96 *RC* networks in serial connection, increasing the difficulty to locate the value of the distribuited parameters *R* and *C* for each element that forms the complete model of the battery.

The proposal in this document is to modify the Thevenin model, replacing the *RC* network of the circuit by a transfer function, where the input is the current in the battery and its output is V_S.

For constructing a transfer function of RC network of battery pack from measured input-output data we use the System Identification Toolbox of MATLAB.

The transfer function found is:

$$\frac{V(s)}{I(s)} = \frac{-2.589s - 0.05374}{s^2 + 31.99s + 0.3203} \tag{2.20}$$

The resistor R refers to the internal resistance of the battery described in (2.12). Fig. 2.9 shows the modified circuit according to the proposal established in this paper.

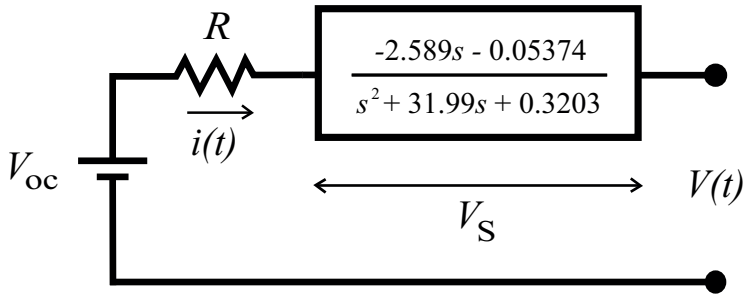

Fig. 2.9 Modified Equivalent Circuit Model

The modified equivalent circuit model successfully represents the behavior of lithium polymer battery in the EV along several established routes.

The error in models predictions is evaluated by the Root Mean Square Error $(RMSE)$. This indicator is given by:

$$RMSE = \sqrt{\frac{\sum_{i=1}^{n}(V_{measured,i} - V_{modeled,i})^2}{n}} \tag{2.21}$$

where, $V_{measured,i}$ is the ith measured data, $V_{modeled,i}$ is the ith simulated data and n is the number of measurements available for the analysis.

Table 2.4 RMSE Test Result for Models Battery

ROUTE	**Root Mean Squared Error (RMSE)**	
	Empirical Model	Modified Equivalent Circuit Model
Route 1	2.58	1.85
Route 2	4.95	3.47
Route 3	7.33	3.50
Route 4	3.44	3.20

Table 2.4 shows a comparison of the models according to *RMSE* index. The obtained indices make it clear that the constructed modified equivalent circuit model show higher prediction performance than the empirical model with lower *RMSE* index values for all routes. It has been demonstrated that the modified equivalent circuit model can be used

satisfactorily to predict *SOC* and output voltage of *EV* battery including the discharge and charge stages.

2.3 Inverter and Electric motor

The inverter is a key component of the *EV*, similar to the Engine Management System (*EMS*) of combustion vehicles, which determines driving behavior. The design of the inverters and the different topologies aim to transfer energy from the battery pack to the Permanent Magnet Synchronous Motor (*PMSM*), modifying the voltage and frequency according to their needs. The inverter is also responsible for transforming the energy obtained by the regenerative brake to power the batteries. As a result, the performance of the *EV* is directly related to the inverter efficiency [52–54].

In order to evaluate the performance of the inverter, measurements need to be taken of the battery power, motor performance, and the power delivered directly to the front wheels of the *EV*. These measurements were conducted using the MAHA LPS 3000 dynamometer bank during the experiment. The measurement experiment tests were made using the MAHA LPS 3000 dynamometer bank. Details can be found in Appendix A. In addition, the information obtained through the OBD II port directly from the ECU of *EV* is used by the authors in [55] in order to generate an analysis of losses and efficiency curves in the vehicle subsystems as shown in Fig. 2.10. Before starting with the experiments, MAHA LPS 3000 recommends establishing the following conditions: tires pressure must be 30 PSI, the tire tread temperature must reach $30°C$, secure the vehicle with tension straps, and follow the measurement protocol that governs the dynamometer bank [55, 56].

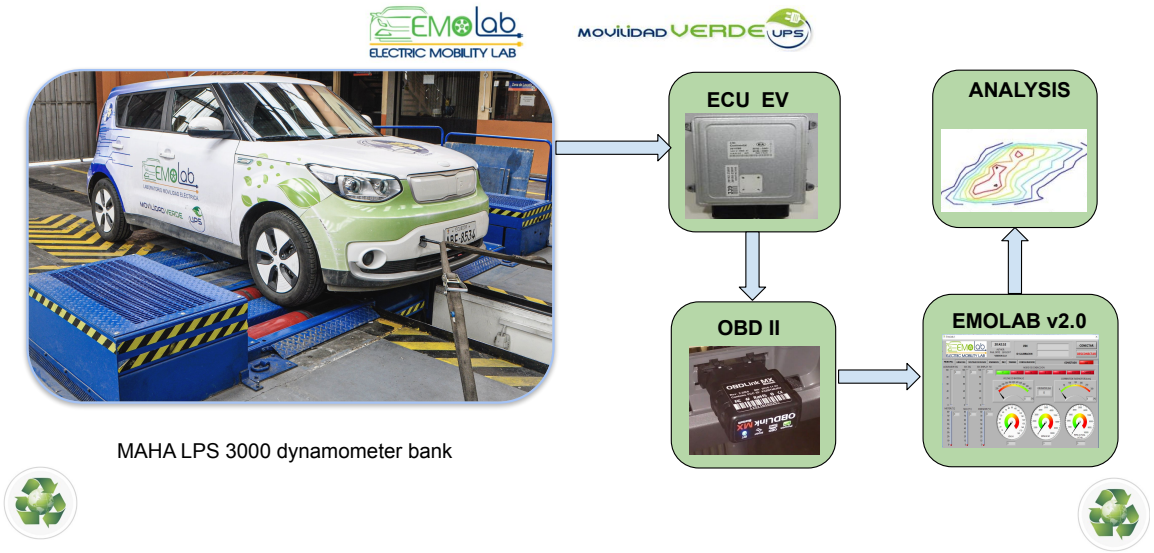

Fig. 2.10 Inverter and motor efficiency experiment setup on the dynamometer bank

After analyzing data from experiments, the inverter efficiency curve as a function of the motor's rotational speed is shown in Fig. 2.11 The inverter in this study shows minimum efficiency of 94 % at high speed and maximum efficiency of 99% at low speed.

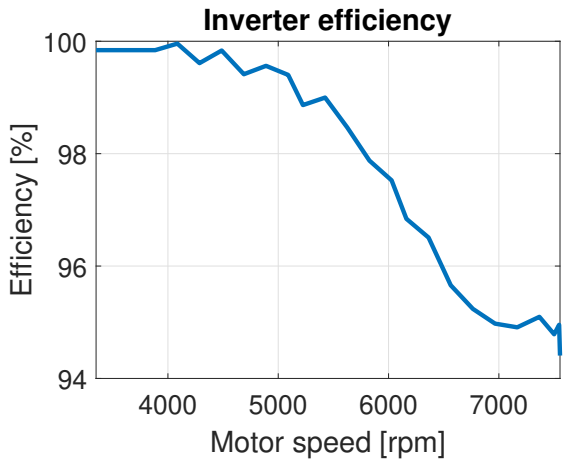

Fig. 2.11 Efficiency curves for inverter electrical device

The electric motor of the test *EV* is a (*PMSM*) and has advantages of high efficiency and torque current ratio, high power density, and wide speed range. These features are suitable for automotive applications, especially for *HEV* and *EV* [12, 55, 57–59]. Technical specifications declare the nominal parameters of the *PMSM* as 81.4 kW of maximum power, 400-V voltage, and 285 Nm maximum torque. The non-linear effects generated by the *PMSM* model, mechanical elements and the internal losses are

considered within the lookup tables that were generated through experimentation in the dynamometric bank.

According to data of experiments, the transmission and torque efficiency curves as a function of the motor's rotational speed are shown in Fig. 2.12, where the mechanical transmission torque efficiencies improve when increasing motor speed. It is essential to mention that Fig. 2.12 includes all losses between *PMSM* and gearbox, such as inertial losses, losses in couplings, and lubricant losses.

Fig. 2.12 displays the transmission and torque efficiency curves of the motor as a function of its rotational speed, as per the experimental data. The mechanical transmission torque efficiencies improve with an increase in the motor speed. It should be noted that Fig. 2.12 accounts for all losses, including inertial losses, losses in couplings, and lubricant losses, between the *PMSM* and gearbox.

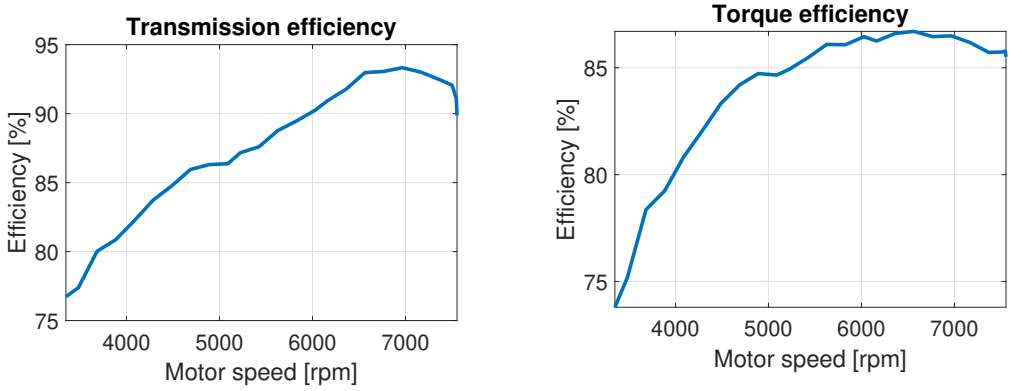

(a) (b)

Fig. 2.12 Result of efficiency curves based on speed

The PMSM mechanical power was calculated as follows

$$P_{mot}(k) = \eta_{MI}(\omega)P_{elec}(k) \tag{2.22}$$

The efficiency factor η_{MI} shown in Fig. 2.11 is obtained through mechanical power tests in the dynamometric bank and electrical power obtained from OBD data. Rewriting the Equation (2.22) in terms of torque, voltage, and current, it can be expressed as:

$$T_m(k)\omega(k) = V_{batt}(k)I_{batt}(k)\eta_{MI}(\omega) \tag{2.23}$$

The equation for motor torque can be expressed as follows

$$T_m(k) = \frac{V_{batt}(k)I_{batt}(k)\eta_{MI}(\omega)}{\omega(k)} \tag{2.24}$$

$$T_m(k) = \frac{30 V_{batt}(k) I_{batt}(k) \eta_{MI}}{\pi N_m} \tag{2.25}$$

where N_s is the motor rotational speed in (rpm). The mechanical power output of the transmission is calculated by:

$$P_{tra}(k) = \eta_{Tr}(k)(\omega) P_{mot}(k) \tag{2.26}$$

where η_{Tr} represents the efficiency factor shown in Fig. 2.11. Substituting from Equation (2.23) into Equation (2.26), the mechanical power output and torque of the transmission is obtained as

$$P_{tra}(k) = \eta_{Tr}(\omega) V_{batt}(k) I_{batt}(k) \eta_{MI}(\omega) \tag{2.27}$$

$$T_{Tra}(k) = \frac{\eta_{Tr}(\omega) \eta_{MI}(\omega) V_{batt}(k) I_{batt}(k)}{\omega(k)} \tag{2.28}$$

The *EV* model and its subsystems were implemented in MATLAB/Simulink. Experiments and power tests have previously validated the model feasibility and efficacy on a dynamometer bank. The measured experimental data also was used for the parameters adjustment of the mathematical model. The presented *EV* model leads to the calculation of torque, *PMSM* rotational speed, battery pack power, and the resulting energy consumption in each subsystem.

Chapter 3

A Virtual Sensor for Electric Vehicles' State of Charge Estimation

The increasing diffusion *EV* is not accompanied by a corresponding solid tradition in terms of data collection. The phenomenon is relatively new, and in particular, important for what concerns data related to battery observation. Often the models for determining the states of charge of vehicles are obtained in the laboratory and do not take into account the variability of driving styles; the use of auxiliaries, such as air conditioning; and the environmental conditions in which vehicles can be found. This leads to incorrect estimates of *SOC* of the batteries in the vehicle and failure of perception by the drivers [60–64].

Since the state of charge of a battery is not a directly observable quantity, the methods used for its estimation are strongly dependent on assumptions and model simplifications [65–67]. In addition, some methods require data measured in laboratory conditions that cannot be directly collected during the normal operation of a vehicle, making them unsuitable for real-world usage. Moreover, the models often depend on parameters that have to be calibrated manually with specific tests and are not appropriate for on-the-run analysis.

A critical factor in any *SOC* estimator is the quality of the information provided by the *EV* sensory system; e.g., battery current and voltage measurements. Then, a fault in any of these sensors can lead to a wrong *SOC* estimate and possible misuse of the battery [68]. The use of automatic learning techniques can bring about significant improvements, especially if combined with traditional techniques for estimating the battery model and state, which can then be improved by the data collected over time.

In this framework, the principal component analysis (PCA) is used to analyze the original data and reduce their dimensions, while the non-parametric machine learning

method named Support Vector Regression SVR, using kernel functions such as Gaussian kernel support vector regression $(GK-SVR)$ and polynomial kernel vector support regression $(PK-SVR)$ is used to estimate the battery current on a lithium iron phosphate $(LiFePo_4)$ battery.

3.1 Design of a virtual current sensor

The study employed a small (two-passenger) electric vehicle. It relies on a $LiFePo_4$ battery with a capacity of 150 Ah and a maximum voltage of 72 V. For more details, see [69]. The available measurements are the battery voltage (V), battery current (A), battery SOC $(\%)$, pedal position (% of angle) and vehicle speed (Km/h). All the variables are obtained from the $EV's$ controller area network (CAN) bus. The CAN bus messages are generated at different time intervals. Then, the CAN data is pre-processed to obtain samples at uniform time intervals for all the variables of interest and to remove eventual inconsistent data, which in some cases, are erroneously logged. The data used in this paper for training and testing are available at [70].

Four different itineraries have been considered; their characteristics are briefly summarized in Table 3.1.

Table 3.1 Itineraries used for training and testing

	Routes			
	Type	**Duration (s)**	**Init SOC**	**Max Speed**
1	urban(lt)	2000	89	60
2	urban(lh)	1100	81	55
3	mixed	1630	72	60
4	urban(lt)	1830	99	60

where "lt" stands for "light traffic conditions", "ht" for "heavy traffic" and "activity" represents the percentage of time the EV is moving at speed higher than 50 km/h.

The Routes have initial and final sections in urban conditions and a town's middle section. For the training step, 900 s of data were extracted from each route from random initial times, and testing was performed on the whole route data file.

The structure of the current virtual sensor is shown in Fig. 3.1. The battery voltage is obtained by adding the voltage of each of the 24 battery cells, the data of which is available on the CAN bus, rather than using the standard total battery voltage also available on the bus. The pedal position data is also available on the CAN bus, and the acceleration data are obtained by numerical differentiation of the speed measurements.

Two steps form the virtual sensor. First, a dimension reduction procedure based on *PCA* is applied to the inputs, and then, the resulting signal is applied to an *SVR* model that generates the current estimates.

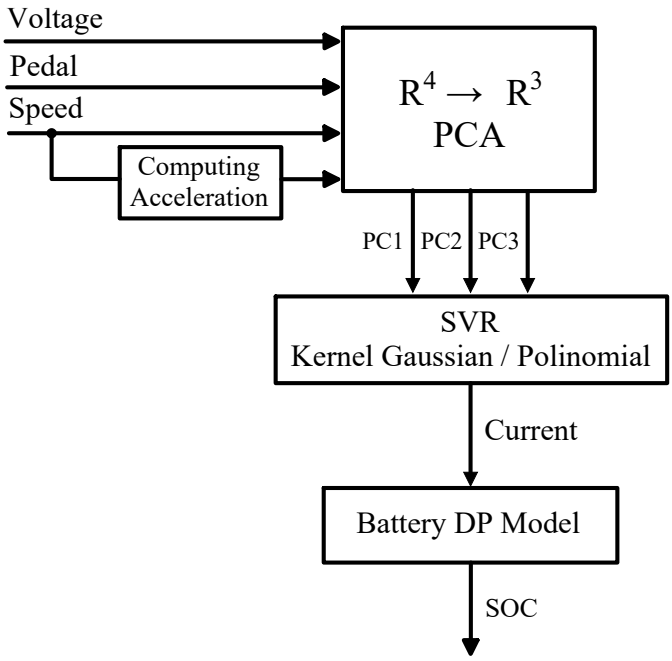

Fig. 3.1 General architecture for SOC estimation

PCA is used to reduce the dimension of input variable space [71]. This methodology allows one to find a new and reduced set of variables (*features*) as a linear combination of the original variables.

The expression of the principal components (PCs) can be written as:

$$PC_i = AZ_i \tag{3.1}$$

where, considering the i-th sample of input data, $PC_i \in \mathbb{R}^p$ is the vector of the p principal components, $Z_i \in \mathbb{R}^q$ the vector of q input variables and $A \in \mathbb{R}^{pxq}$ the *PCA* matrix. Each row a_k of matrix A is the eigenvector corresponding to the k-th principal component of the input sample being considered. If we are considering N samples of data, in our case time samples, we can write for all data $PC = AZ$ with $PC \in \mathbb{R}^{pxN}$ and $Z \in \mathbb{R}^{qxN}$. In principle p can be as large as q, but the main idea of PCA is to have $p < q$.

Before being fed to the *PCA* algorithm, the four input variables (i.e., voltage, pedal, speed and acceleration) are normalized in order to obtain the *PCA* input data vectors Z_p. Each variable is re-scaled as

$$Z_i = \frac{z_i - z_{min}}{z_{max} + z_{min}} \tag{3.2}$$

where z_{max} and z_{min} are respectively the maximum and minimum values of the original data samples. When applied to the data in Table 3.1, the *PCA* method finds that three principal components are sufficient to describe, respectively, the 99.75%, 99.78%, 99.58% and 99.66% of the total variance of the input variables for each one of the routes considered. While this means that the feasible order reduction is only one dimension, this reduction, as will be shown in the sequel, allows a substantially better performance of the SVR algorithm.

A geometric visualization of the four vectors representing the coefficient values that transform each input variable in the corresponding PC for Route 1 is shown in Fig. 3.2.

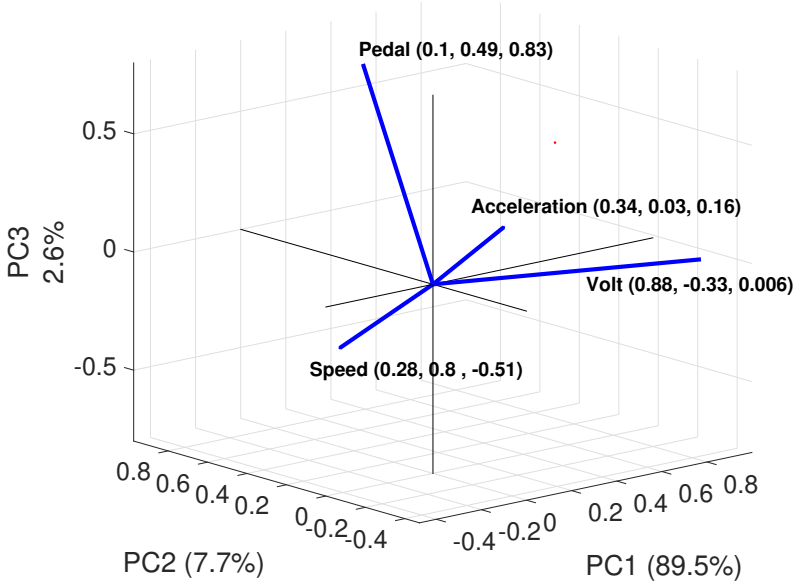

Fig. 3.2 Input variable vector representation in the principal components' space.

The support vector regression (SVR) method was first designed to solve nonlinear two-class classification problems [72, 73]. The *SVR* method is a non-parametric function approximation technique because it relies on kernel functions [74]. The relationship between the independent and dependent variables is represented by a deterministic function, defined as:

$$y = f(x) = w^T \phi(x) + b \tag{3.3}$$

where $x \in \mathbb{R}^n$ is the independent component of the data and the corresponding dependent value is $y \in \mathbb{R}$, so that each sample vector x_i corresponds to a scalar $yi\cdot$.

$w \in \mathbb{R}^m$, with m the dimension of the *"feature"* space, controls the flatness of the model; $\phi(\cdot)$ is a non-linear mapping function from the input space $\mathbb{R}^n$ to feature space $\mathbb{R}^m$; and $b \in \mathbb{R}$ is a bias term. Details of this algorithm can be found in Appendix B.

The approximation function $f(x)$ is represented by the following equation:

$$f(x) = \sum_{i=0}^{N} (\alpha_i - \alpha_i^*) G(x_i, x) + b \tag{3.4}$$

where α_i and α_i^* represent Lagrangian multipliers. The inner product $\langle \phi(x_i), \phi(x_j) \rangle$ is defined through a kernel function, that is, $G(x_i, x_j) = \langle \phi(x_i), \phi(x_j) \rangle$ [75–77]. Different kernel functions are determined as:
(a) Gaussian Kernel (GK) :

$$G(x_i, x_j) = -exp(\frac{\left\| x_i - x_j \right\|^2}{2\sigma^2}) \tag{3.5}$$

(b) Polynomial Kernel (PK) :

$$G(x_i, x_j) = (c + x_i^T x_j)^p \tag{3.6}$$

where σ^2 denote the variance for GK, p is the order of the kernel, and c is a constant that allows to trade off the influence of the higher and lower order term for PK. One of the aims of the paper is to show how the choice of the kernel is a key point in the proposed methodology. In the following, the SVR is based on the Gaussian kernel (GK) and the second and sixth order polynomial kernel ($PK2$ and $PK6$, respectively)

According to Equation B.6, the virtual sensor design problem can now be transformed into the following system of linear equations:

$$\hat{I}(x) = \sum_{i=0}^{N} (\alpha_i - \alpha_i^*) G(x_k, x_i) + b \tag{3.7}$$

where $\hat{I}(x)$ is the estimated battery current and $G(x_k, x_i)$ is the chosen kernel function; i.e., Gaussian or polynomial kernel.

The k-th input variable sample x_k used for training is set to x_k = [$PC1_k$, $PC2_k$, $PC3_k$] in the PCA case, or to x_k = [V_k, P_k, S_k, A_k], that is, the scaled voltage (V_k), pedal position (P_k), vehicle speed (S_k) and acceleration (A_k), when the SVR model is trained without resorting to PCA. The performance of the virtual sensor obtained from the SVR procedure, in terms of $RMSE$ (root mean square error) and MAE (mean absolute

error), for the *GK* and *PK*2 models, wherein *PCA* was not used, and the $PCA + GK$, $PCA + PK2$ and $PCA + PK6$ models, *PCA* based, are presented in Tables 3.2 and 3.3. In those experiments, different routes have been used for training models, and each model was then tested on the same set used for its training.

Table 3.2 RMSE (root mean square error) of SVR training for GK, PK2, PCA + GK, PCA + PK2 and PCA + PK6 models.

SVR Training RMSE					
Route	**GK**	**PK2**	**PCA + GK**	**PCA + GK2**	**PCA + PK6**
1	11.6	46.1	3.58	10.6	4.16
2	29.6	49.0	6.16	14.1	6.73
3	32.9	35.3	10.3	18.2	13.3
4	17.9	123	8.15	17.1	11.2

Table 3.3 Mean absolute error (MAE) of SVR training for GK, PK2, PCA + GK, PCA + PK2 and PCA + PK6 models.

SVR Training MAE					
Route	**GK**	**PK2**	**PCA + GK**	**PCA + GK2**	**PCA + PK6**
1	2.60	38.2	1.43	4.78	1.91
2	9.50	42.2	2.31	6.54	2.89
3	11.9	29.8	4.10	10.3	6.53
4	6.46	99.1	2.98	7.37	3.50

The $PCA + GK$ *SVR* method offers the best performance on the training sets, with the lowest *RMS* and *MAE* values. Additionally, the $PCA + PK6$ method yields good results, but is in general more expensive in terms of computational requirements. Note also that the route data used for training also has a relevant effect on the final quality of the model. In all cases, note how the use of *PCA* to pre-process the input variables yields much better results with both the polynomial and the Gaussian kernels. Fig. 3.3 shows the result for each method, except $PCA + PK6$, over a portion of the training data, in this case extracted from Route 1.

The MAE and RMSE indices in Tables 3.2 and 3.3 only show the average error in model operation and do not give any information about the error distribution. To overcome this problem we propose to use the developed discrepancy ratio (DDR) index, proposed in the literature for evaluating prediction models; see, e.g., [22–25].

The *MAE* and *RMSE* indices in Tables 3.2 and 3.3 only show the average error in model operation and do not give any information about the error distribution. To overcome this problem we propose to use the developed *DDR* index, proposed in the literature for evaluating prediction models; see, e.g., [78–81].

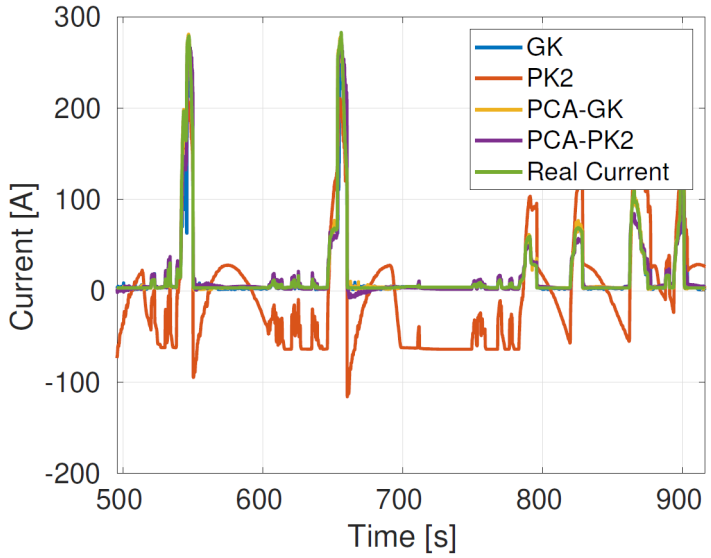

Fig. 3.3 A sample of predicted current on the same route used for training—in this case Route 1. The PCA + PK6 model is not shown.

$$DDR = \frac{PredictedValue}{MeasuredValue} - 1 \tag{3.8}$$

The error distribution can be visually described by drawing the histogram of the *DDR* for each one of the four different approaches considered. These results (see Fig. 3.4) show that during the training stage, the *DDR* values for the $PCA + GK$ method vary between -0.9 and 1; those for the $PCA + PK2$ method between -1 and 2; those for the *GK* method between -1 and 2; and those for the *PK*2 model between -5 and 5. Moreover, as it can be seen, the distribution for $PCA + GK$, and to a lesser degree, for $PCA + PK2$, has a smaller variance around the optimal zero value, and is thus more reliable than the other methods that do not rely on a preliminary *PCA* of input variables.

According to the results shown in Tables 3.2 and 3.3, and to the distribution of *DDR* values shown in Fig. 3.4, only the methods based on *PCA* "preprocessing" deserve being considered. As noted previously, training sets extracted from each one of the four routes considered result in different qualities of virtual sensor. Using, for example, data extracted from Route 1 (900s) to train the model, the battery current estimations obtained using the data from Routes 2, 3 and 4 are shown, respectively, in Figs 5–7. As expected, the Gaussian kernel based model $PCA + GK$ yields the best results, even if the $PCA + PK6$ model still gives accurate results. The RMSEs and MAEs of the three models considered, i.e., PCA+GK, PCA+PK2 and PCA+PK6, trained using a 15' section of each route in the data set, and then tested on the complete data of the four routes, are reported in Tables 3.4 and 3.5. In each table the column "score" represents the average by row of the *RMSE* and *MAE*. Note that the best results were obtained by

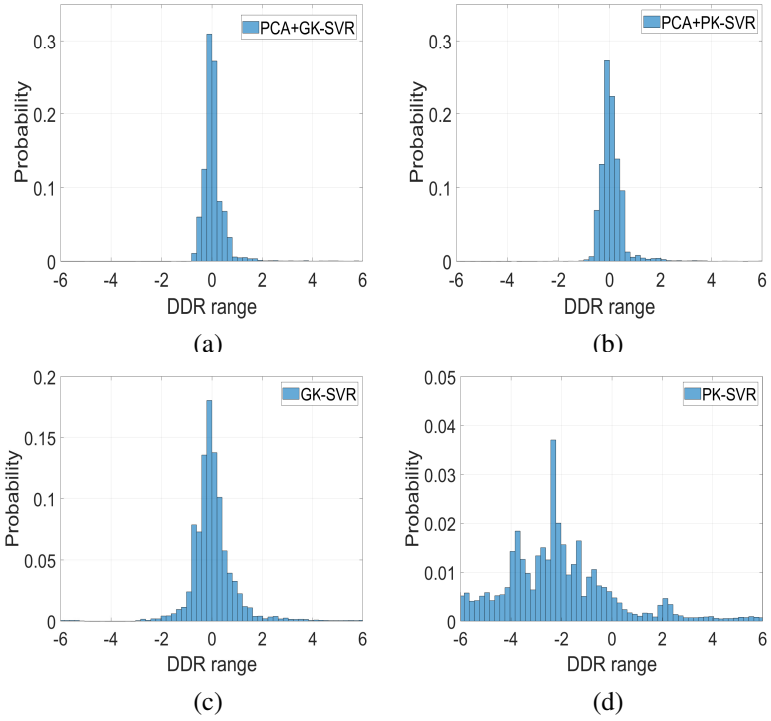

Fig. 3.4 Normalized histogram of the DDR values for the four methods in the training stage. (a) PCA+GK-SVM, (b) PCA+PK-SVM, (c) GK-SVM and (d) PK-SVM

using the $PCA-GK$ method trained using Route 1 followed by the $PCA-PK6$ method trained using Route 2. This shows that the characteristics of the routes chosen for the training of the virtual sensors should be carefully chosen to obtain a good representation of the behavior in different situations.

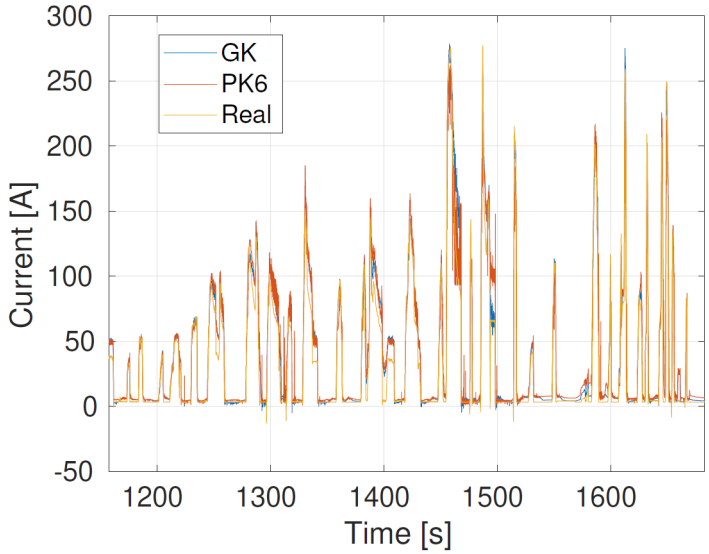

Fig. 3.5 Current prediction: Training using a 15' sample of Route 1 and Testing on a small portion of Route 2.

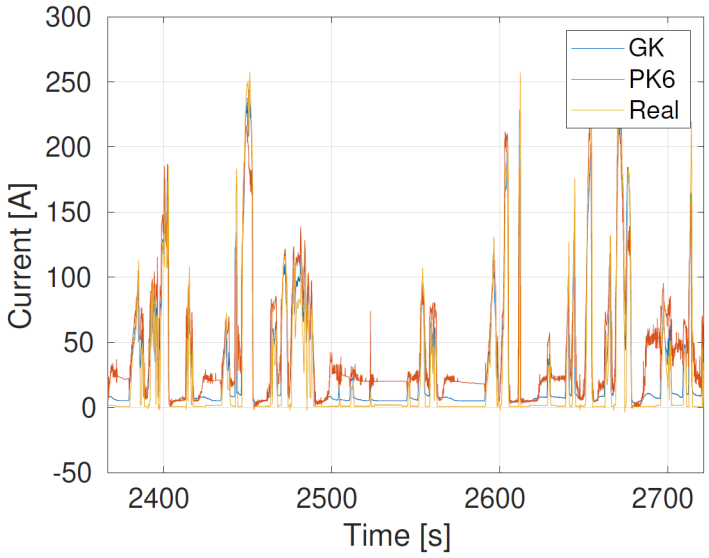

Fig. 3.6 Current prediction: Training using a 15' sample of Route 1 and Testing on a small portion of Route 3.

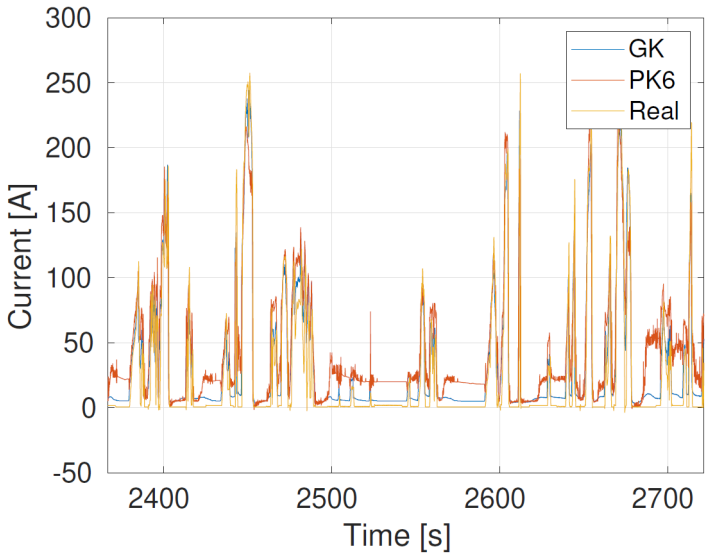

Fig. 3.7 Current prediction: Training using a 15' sample of Route 1 and Testing on a small portion of Route 4.

3.2 Battery Model and SOC Estimation

In order to estimate the *SOC*, the first step is to develop a reliable battery modeling. In this work, a model based on the dual polarization (DP) equivalent circuit model, composed of three parts, is employed to simulate the behavior of the battery [82, 37]. This model was described in the subsection 2.2.2.

Table 3.4 RMSEs of SVR PCA+GK, PCA+PK2 and PCA+PK6 models trained using four routes testedagainst the other routes.

	Training and Test Route				
Model-Route	**1**	**2**	**3**	**4**	**Score**
PCA+GK	1	3.98	14.44	14.77	16.91	12.53
	2	9.16	8.03	17.38	19.83	13.6
	3	16.93	19.71	12.21	16.18	16.26
	4	17.04	39.08	13.13	9.26	19.63
PCA+PK2	1	12.75	17.80	19.77	31.84	20.54
	2	19.49	15.30	19.85	18.88	18.38
	3	26.39	29.02	21.07	26.52	25.75
	4	22.26	24.32	21.32	19.43	21.83
PCA+PK6	1	4.99	15.80	14.26	27.33	15.60
	2	11.13	9.55	17.55	12.47	12.68
	3	20.97	20.13	15.01	16.58	18.17
	4	18.36	25.75	16.37	12.33	18.20

Table 3.5 MAEs of SVR PCA + GK, PCA + PK2 and PCA + PK6 models trained using four routes tested against the other routes.

	Training and Test Route				
Model-Route	**1**	**2**	**3**	**4**	**Score**
PCA+GK	1	1.74	6.89	7.17	7.12	5.73
	2	5.21	3.01	10.18	11.22	7.40
	3	8.38	10.01	7.13	7.83	8.34
	4	8.90	13.23	7.75	4.59	8.62
PCA+PK2	1	5.88	17.80	19.77	16.19	14.91
	2	9.22	8.13	11.00	9.99	99.59
	3	13.45	16.01	10.76	12.15	13.09
	4	10.07	13.11	10.13	9.93	10.81
PCA+PK6	1	2.01	7.98	7.15	14.98	8.03
	2	6.84	4.96	8.25	6.64	6.67
	3	11.09	10.33	7.56	8.28	9.32
	4	8.88	14.00	8.22	6.17	9.32

- An ideal voltage source representing the open circuit voltage of the battery V_{oc}; this voltage has a non linear relation with the state of charge of the battery. This relation depends on the type of battery, but also on its temperature and age.

- Internal resistors, specifically the "ohmic" resistance represented by R and the polarization resistances R_1 and R_2.
- Capacitors that, in combination with the polarization resistances, are used to characterize the transient response during the transfer of power, represented by C_1 and C_2.

Assuming the current through the battery as an independent variable, that is, the battery model is connected to an independent current source of value $i(t)$. Following modeling battery discharge or charge, the battery terminal voltage can be expressed in terms of the state equation and output relation given by:

$$\begin{bmatrix} \dot{V_1} \\ \\ \dot{V_2} \end{bmatrix} = \begin{bmatrix} -\frac{1}{R_1C_1} & 0 \\ \\ 0 & -\frac{1}{R_2C_2} \end{bmatrix} \begin{bmatrix} V_1 \\ \\ V_2 \end{bmatrix} + \begin{bmatrix} \frac{1}{C_1} \\ \\ \frac{1}{C_2} \end{bmatrix} i(t) \tag{3.9}$$

$$V(t) = V_{oc} + i(t)R + V_1 + V_2$$

where V_1 and V_2 are the voltages at C_1 and C_2 respectively; $V(t)$ is the voltage at the battery terminal; and $i(t)$ is the current in the battery. The states space of the battery model are represented by V_1 and V_2 and by the state of charge SOC, which defines the open circuit voltage V_{oc}. The methodology to obtain the value of these parameters was detailed in the previous chapter.

The identification results of electric parameters for the DP battery model are shown in Table 3.6.

Table 3.6 Battery Parameters Estimation

Identified item	**Value**
R	0.0056 Ω
R1	0.040858 Ω
R2	0.025259 Ω
C1	9484 F
C2	71.049 F
Optimal Value F	0.235

Finally, the relationship between the V_{oc} and the SOC can be described through polynomial data fitting. The fitted curve for the relationship between V_{oc} and SOC is presented in Fig. 2.5,

where the V_{oc} from the estimated data is fitted to the SOC value using the $4th$ order regression polynomial in Equation (3.10).

$$V_{oc}(SOC) = -157.9SOC^4 + 554.3SOC^3 - 696SOC^2 + 378.3SOC + 4.81 \quad (3.10)$$

3.3 Results and Discussion

In this section, the performance of the *SOC* estimation using the current virtual sensor based on the $PCA + GK$ and $PCA + PK2$ methods and the *DP* battery model is evaluated.

The voltage, the pedal position, the speed and the acceleration were measured and were used as input data to the model. *PCA* was applied, reducing the dimension of the inputs from R^4 to R^3. Then, the data were injected to the *SVR* model to estimate the current. Finally, the current provided by the virtual sensor was used as input for the DP battery model, to finally determine the *SOC*.

The estimation methods were validated with two routes, and the results can be seen in Fig.s 3.8 and 3.9, where the performance of the estimation methods vs. data reported by the existing *BMS* is shown.

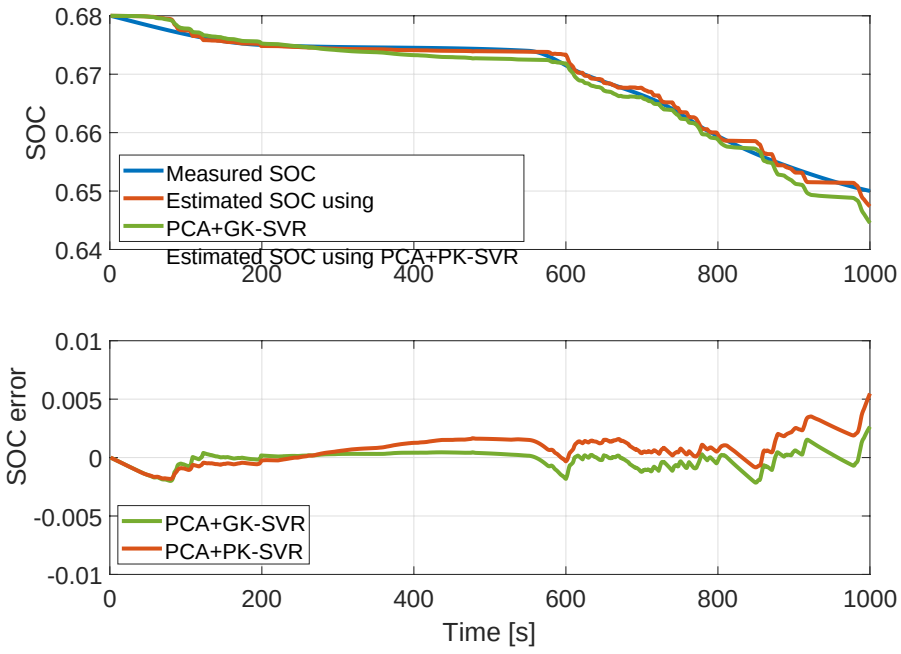

Fig. 3.8 Evaluating SOC model of the battery EV for Route 1

The *FIT* index was used to evaluate the quality of the proposed SOC estimation algorithm. This index is defined as

$$FIT = 100\left(1 - \frac{\|SOC_m - SOC_e\|}{\|SOC_e - \overline{SOC_m}\|}\right)\% \tag{3.11}$$

where $\|*\|$ is the norm of the argument, SOC_e is the SOC obtained with the estimation methods, SOC_m the measurements provided by the BMS and $\overline{SOC_m}$ is the average of $SOCm$ during the experiment.

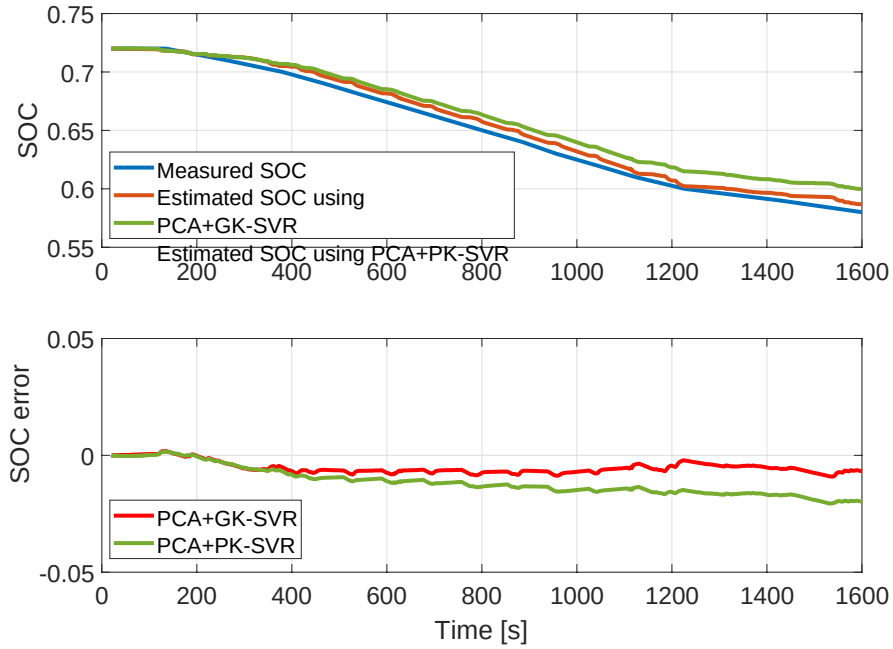

Fig. 3.9 Evaluating SOC model of the battery EV for Route 2

Table.3.7 shows a comparison of the methods according to FIT, $RMSE$ and MAE indexes for route 1. The obtained indices make it clear that the estimation $PCA + GK - SVR$ method shows higher prediction performance than the $PCA + PK - SVR$ method model, with $FIT = 91.8\%$.

Table 3.7 SOC Estimation Results for Route 1

	PCA+GK-SVR	**PCA+PK-SVR**
FIT	91.80%	85.423%
RMSE	0.007	0.014
MAE	0.005	0.011

For route 2, results are shown in Table.3.8. $PCA + GK - SVR$ method shows higher performance than the $PCA + PK - SVR$ method model, with $FIT = 87.49\%$.

Table 3.8 SOC Estimation Results for Route 2

	PCA+GK-SVR	**PCA+PK-SVR**
FIT	87.49%	71.76%
RMSE	0.058	0.127
MAE	0.053	0.114

Note that both models, $PCA + GK$ and $PCA + PK2$, provide adequate virtual current measurements that allow the estimation of the battery *SOC* from the battery voltage, accelerator pedal position and vehicle speed.

3.4 Conclusions

We have presented a solution for state of charge estimation in electric vehicle applications. The proposed strategy makes use of virtual sensors for the battery current estimation, replacing the physical sensor in case of failure.

The models are created by analyzing experimental data obtained from the *CAN* bus of a real electric vehicle. These models employ the battery voltage, vehicle speed, and acceleration pedal position to estimate the current signal when the actual measurement is unavailable. Support vector regressions and principal component analysis have been employed to build the virtual sensors. Gaussian and polynomial functions have been employed as kernel functions, and it was observed that the Gaussian kernel offers better performance on the available data sets. A principal component analysis allows one to reduce by one the dimension of the input to the virtual sensor, significantly increasing the final performance.

The estimated current signal is used as input to a dual polarization equivalent circuit model of the battery to estimate the state of charge and open circuit voltage during the vehicle's operation. The parameters of the equivalent circuit have been obtained through a non-linear least squares adaptive algorithm, using experimental data from the vehicle. The joint operation of the virtual sensor and the battery model allows one to estimate the state of charge with a fit higher than 87% when evaluated on fresh data not employed for the model adjustment. The methods herein proposed are scalable and can integrate knowledge from other sensors, such as temperature and torque, and can be combined with other machine learning methodologies. One of the limitations that we noticed in the the method is related to specific properties of the driving segments. Analyzing the entire route can lead to incorrect patterns due to different links between the magnitudes considered by the virtual sensor. For example, accelerations and currents have a very

different relation if the vehicle is traveling uphill or on flat terrain, or even downhill. The next extension of our work is to create a mixed method of classification and machine learning,to recognize specific peculiarities of the driving segment and select the correct model to apply.

Chapter 4

Energy-Efficiency Optimization Approach Based on Experimental Tests

The optimal energy management in electric vehicles becomes one of the challenges faced by new algorithms that include vehicle performance and driver behavior. The latter significantly influences the battery consumption and is difficult to forecast.

The main objective of research efforts in this field is to find a solution to improve energy efficiency and fuel savings in EV and HEV transportation systems, considering the maximum limits of the vehicle. This topic has been studied from different approaches in the literature.

4.1 Energy Efficiency Optimizer

In order to improve efficiency in EVs, in this section, an optimization algorithm for driving patterns will be proposed to achieve maximum energy efficiency; it is essential to understand the management of traction and the flow of energy consumption from the battery to the wheels of the EV. In addition, the power conditions and limitations of battery discharge EV during its operation were considered as studies showed in [83, 84]. The proposal includes the electric vehicle's dynamic model described in Equation (2.1), the battery model, the $PMSM$, and the inverter model as lookup tables. The proposed optimizer requires as input the torque, battery power from OBD data, and dynamometer lookup tables and the output of the optimizer is the reference signal Vr_{op}.

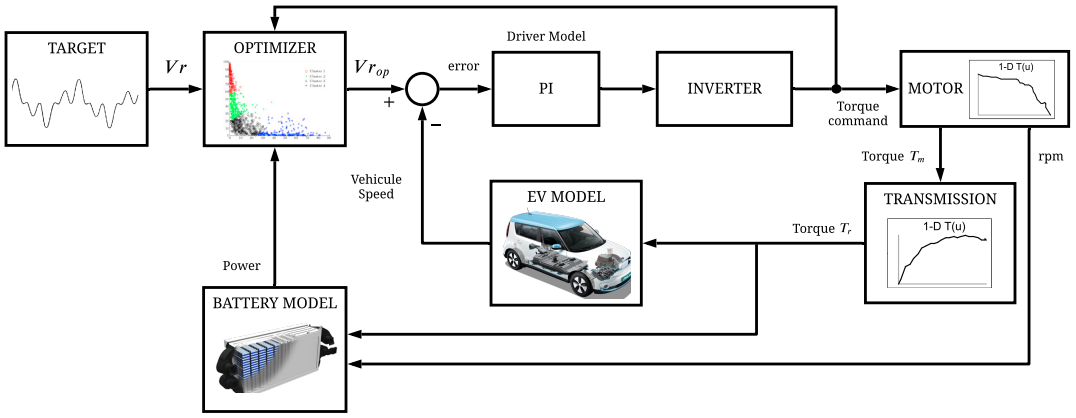

Fig. 4.1 Simulation schematic to optimization for drive cycles

For establishing a strategy for the optimizer, the objective function is obtained from the value analysis of the inverter and mechanical transmission efficiency lookup tables shown in Fig.s 2.11 and 2.12 obtained from the experiments presented in Chapter 2. The total energy-efficiency function between power supplied for battery and power wheel of the system is given as:

$$J\eta = \eta_{Tr}(\omega_k)\eta_{MI}(\omega_k) \tag{4.1}$$

It is fundamental to mention that the $J\eta$ represents the efficiency function between the battery and the transmission drive of EV. The decision variable of the optimization problem in (4.2) is the rotational velocity generated by $PMSM$ (Ns) expressed in rpm. The speed correction generated by the optimizer on the driving pattern can be assigned in real-time, improving the $EV's$ overall efficiency during its operation. The energy efficiency objective function was formulated according to the power and torque equations, and inequality constraints are given as follows.

$$\begin{aligned} \max_{N_s} \quad & J\eta_j = \frac{\pi T_e Ns}{30 V_{batt} I_{batt}} \\ \text{s.t.} \quad & 0 \leq T_m(j) \leq T_{max} \\ & 0 \leq V_{batt}(j) I_{batt}(j) \leq P_{max} \\ & 0 \leq \mid V_x - V_r \mid \leq \delta \end{aligned} \tag{4.2}$$

where j is the value obtained during the driving condition (DC) with a sampling period of 0.5 seconds and δ is the maximum variation between real and optimal velocity reference that depends on driving patterns. The optimal vehicle velocity depends on the

value of Ns found by the optimizer Ns_{op}, tire radius, and transmission ratio given as 8.2 for this vehicle, as shown in Equation (4.3).

$$Vr_{op} = \frac{\pi Ns_{op} radio}{30(8.2)} \tag{4.3}$$

To evaluate the optimizer's performance, real data collected on specific routes is used where the speed profile is determined by limits speed conditions and patterns driving. According to the established speed limits by Ecuador's traffic law, three test routes were established. Fig. 4.2 shows data for a route on highway roads where the speed limit is 90km/h, this route is considered as *DC* 1 in the analysis. *DC* 2 is considered the route generated by driving the EV in urban areas, where the maximum limit speed established is 50km/h. The data for this route is shown in Fig. 4.3 describe a typical driving pattern inside the city. Fig. 4.4 shows a combination of highways and urban areas, where variations in driving patterns can be seen. This route is considered as *DC* 3.

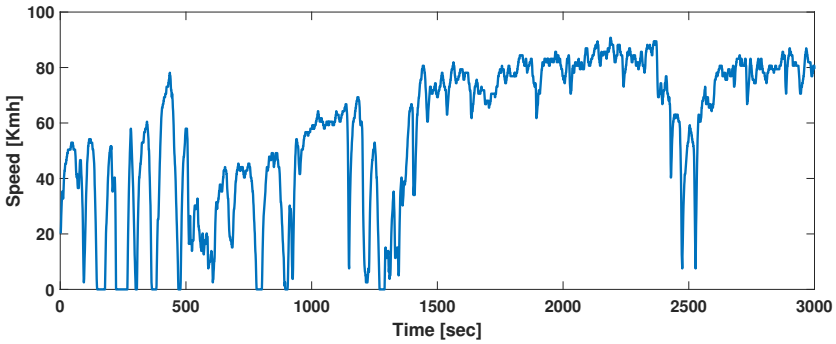

Fig. 4.2 Route 1: The route of the *EV* between two cities on the highway

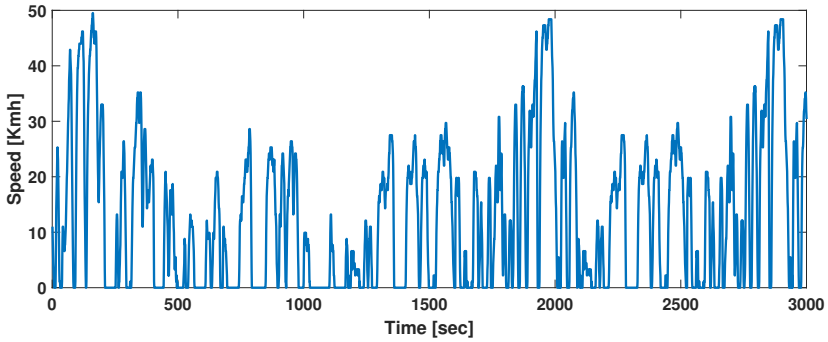

Fig. 4.3 Route 2: The route around local areas of the city, a short route around the city with medium-traffic roads

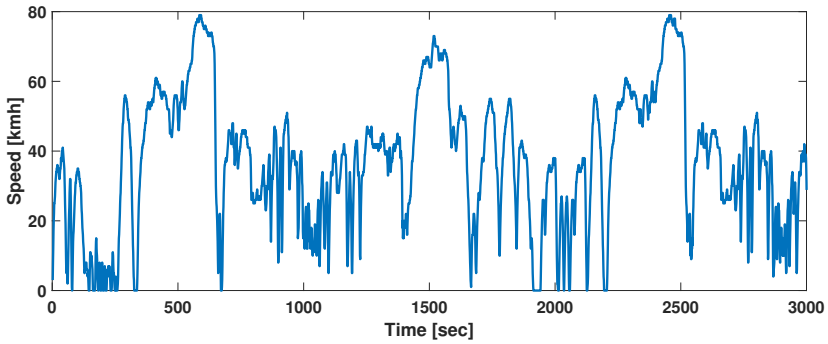

Fig. 4.4 Route3: high energy consumption in mountainous roads

The objective is to find a suitable optimization algorithm, among strategies used in the literature such as *GA*, *SA* and *PSO*. Table 4.1 presents the fitness values and computational time requirements for each algorithm. *PSO* obtains the best results on maximizing energy efficiency and minor computational time.

Table 4.1 Performance comparison of *GA*, *SA* and *PSO* algorithms

Algorithm	**The best efficiency value found** (%)	**Mean time execution (msec.)**
GA	79.15	0.79
SA	78.76	0.84
PSO	79.86	0.55

In this study, the *PSO*, introduced for Eberhart and Kennedy [85–88] for swarm behavior and social cooperation, is applied to solve the discontinuous and highly nonlinear objective function and inequality constraints.

Each iteration adjusts the particle position according to its own experience and neighboring, where it is established in the best position encountered by the swarm. The direction that the population takes is defined by particles neighboring the main particle and the swarm history experience. The velocity v_i and position x_i of particles are updated by the following Equations:

$$x_i(k+1) = x_i(k) + v_i(k) \tag{4.4}$$

$$v_i(k+1) = \omega v_i(k) + c_1 r_1(pbest_i(k) - x_i(k))) + c_2 r_2((gbest_i(k) - x_i(k))) \quad (4.5)$$

where, k is the iteration number, $gbest$ is the best value $global$ in iteration k , pbest is the best position of the best particle, r_1 and r_2 are random numbers in the range of $[0,1]$ and the particles number is defined since $i = 1,2,\ldots,N$. The PSO convergence depends on the learning factors c_1 and c_2, the inertial weight w, the maximum generation k of a PSO stage, and the number of particles N. Details of this algorithm can be found in Appendix C.

The objective function solution in Equation (4.2), is given in two-dimensional lookup tables with the desired motor rotational speed in a specific range of the desired speed. The proposed solving process for optimal driving employs the process described in the flowchart illustrated in Fig. 4.5.

The variation of the rotation speed of the $PMSM$ and the EV operating points are simulated under different driving pattern conditions, where the initial positions and the convergence of the particles during the execution of the algorithm are shown in Fig. 4.6. The performance of the algorithm shows that all particles converge towards the same point in an average of 6 iterations for each scenario while the EV is driven. As a result, the swarm's collective behavior converges to the same state, suggesting that a global minimum has been found.

- **Step 1** Parameter settings: the maximum number of iterations N, particle size X, the inertial weight factor ω, acceleration coefficients c_1 and c_2, random numbers for r_1 and r_2, and constraint conditions (P_{max}, T_{max} and $delta$);
- **Step 2** Fitness calculations and evaluation: compute the best value p_{best} and position g_{best} of the particle that maximizes the objective function in Equation (4.2) determined for j^th driven pattern sample;
- **Step 3** Compare value p_{best} and previous $J\eta$: If p_{best} is greater than $J\eta$ then update new velocity v_i and position x_i of particles using Equations (4.4) and (4.5), otherwise keep the previous values.
- **Step 4** If the maximum iteration is met, terminate the algorithm. Otherwise, go to step 2.
- **Step 5** Repeat the process for sample $j+1$.

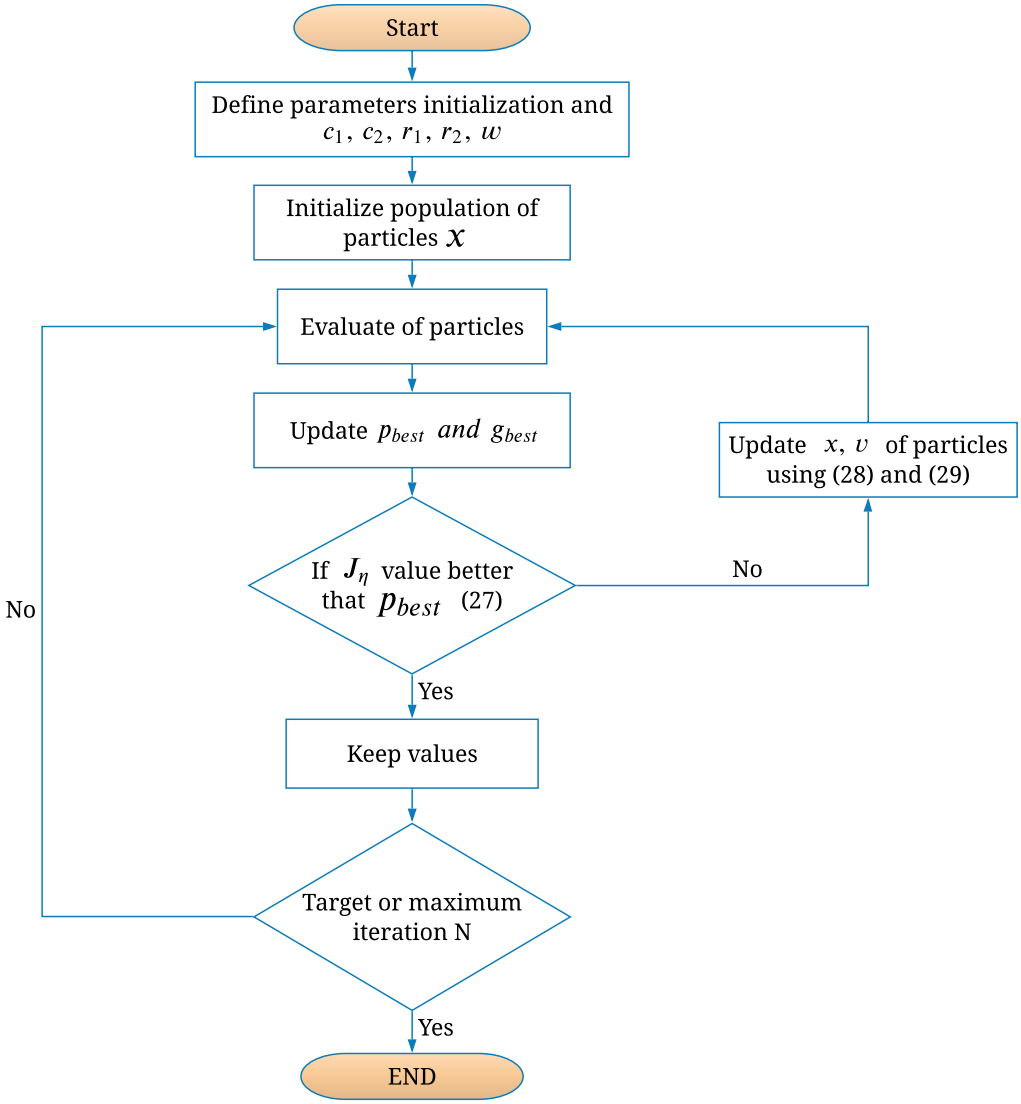

Fig. 4.5 PSO Algorithm flowchart.

4.2 Results and Analysis

In order to evaluate the energy efficiency algorithm presented in this paper, the dynamic modeling for a commercial *EV* and experimental tests, presented in the Chapter 2, and real *DCs* were used. The simulation model was built with Matlab/Simulink is shown in Fig. 4.1. All parameters used in the simulation are described in Table 2.1 and the solution for optimization problem (4.2) where using *PSO* flowchart shown in Fig. 4.5 for solving the optimization problem.

The algorithm proposal aims to make small changes (δ) in speed reference without affecting the driver's behavior. In other words, the algorithm intends to make small

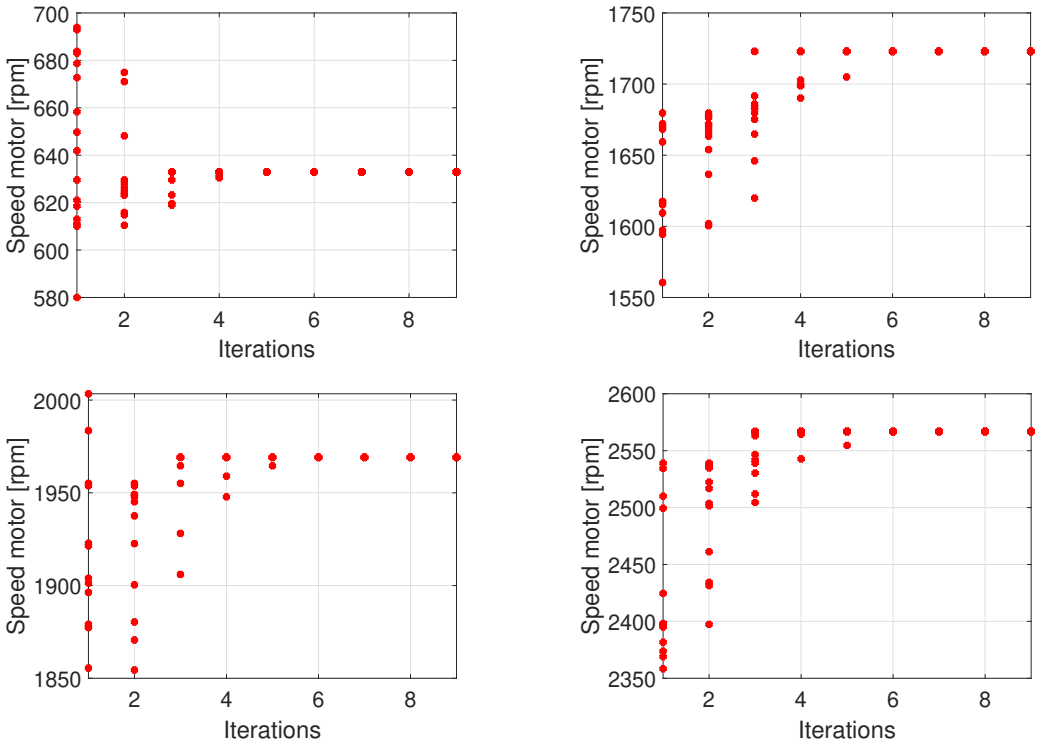

Fig. 4.6 Particles convergence of PSO algorithm in different motor speed scenarios

changes in the speed, improving the efficiency of the vehicle, without removing control of EV of the driver, Fig. 4.7.

Variations of the delta factor are considered, ranging δ factor between 0% and 10% with increases of 1% to determine the optimizer's performance. The results obtained from the simulations are presented in Table 4.2.

Table 4.2 shows that the *SOC* value of the battery, according to the model described in Figs 2.4 and 2.5, presents modifications below 1% without applying the optimizing algorithm. An optimizing algorithm is proposed to maximize the energy efficiency of the *EV*. The (EEOptimizer) is designed to make speed adjustments in the vehicle depending on the data of mechanical torque, battery power, and a maximum variation of δ. These adjustments are made by following the trajectory of a real-world driving cycle.

Given the variety and complexity of vehicle driving patterns, it is essential to consider several of them to evaluate optimizer performance. These driving patterns are created from various speed characteristics described as driving styles: conservative, moderate, and aggressive [89, 90].

The information is obtained by evaluating the *EV* on specific routes and real driving conditions described in Figs 4.2, 4.3 and 4.4 that include different driving styles. During the simulation, the following information from *ECU* is required: power in the wheel,

Table 4.2 Results of energy efficiency in *EV* applying the driver cycle optimizer in 3 tests with different variations in the reference speed.

	Variation	**Wheel power (kW)**	**Battery energy consumption (kWh)**	**Power efficiency** (%)	**SOC** (%)
	-	5.00	5.33	78.12	82.49
	1%	5.09	5.32	78.53	82.32
	2%	5.18	5.31	78.80	82.30
	3%	5.25	5.30	78.88	82.21
	4%	5.33	5.30	78.84	82.21
DC 1	**5%**	**5.42**	**5.29**	**79.22**	**81.99**
	6%	**5.47**	**5.26**	**79.41**	**81.81**
	7%	5.55	5.25	79.55	81.42
	8%	5.62	5.24	79.51	81.12
	9%	5.71	5.23	79.62	81.11
	10%	5.79	5.22	79.86	80.90
	-	3.20	3.62	73.76	86.51
	1%	3.24	3.61	73.96	86.44
	2%	3.26	3.56	74.19	86.42
	3%	3.28	3.51	74.14	86.43
	4%	3.17	3.49	74.48	86.35
DC 2	**5%**	**3.37**	**3.50**	**74.90**	**86.35**
	6%	**3.38**	**3.47**	**74.97**	**86.28**
	7%	3.39	3.43	75.27	86.31
	8%	3.41	3.41	75.34	86.21
	9%	3.45	3.41	75.34	86.01
	10%	3.50	3.40	75.42	86.00
	-	3.20	3.63	73.59	86.50
	1%	3.24	3.62	73.96	86.43
	2%	3.26	3.56	74.19	82.42
	3%	3.28	3.51	74.24	86.43
	4%	3.31	3.49	74.48	86.35
DC 3	**5%**	**3.37**	**3.50**	**74.90**	**86.36**
	6%	**3.27**	**3.47**	**75.35**	**86.28**
	7%	3.40	3.43	75.37	86.31
	8%	3.41	3.41	75.39	86.21
	9%	3.45	3.40	75.48	86.08
	10%	3.51	3.39	75.55	86.00

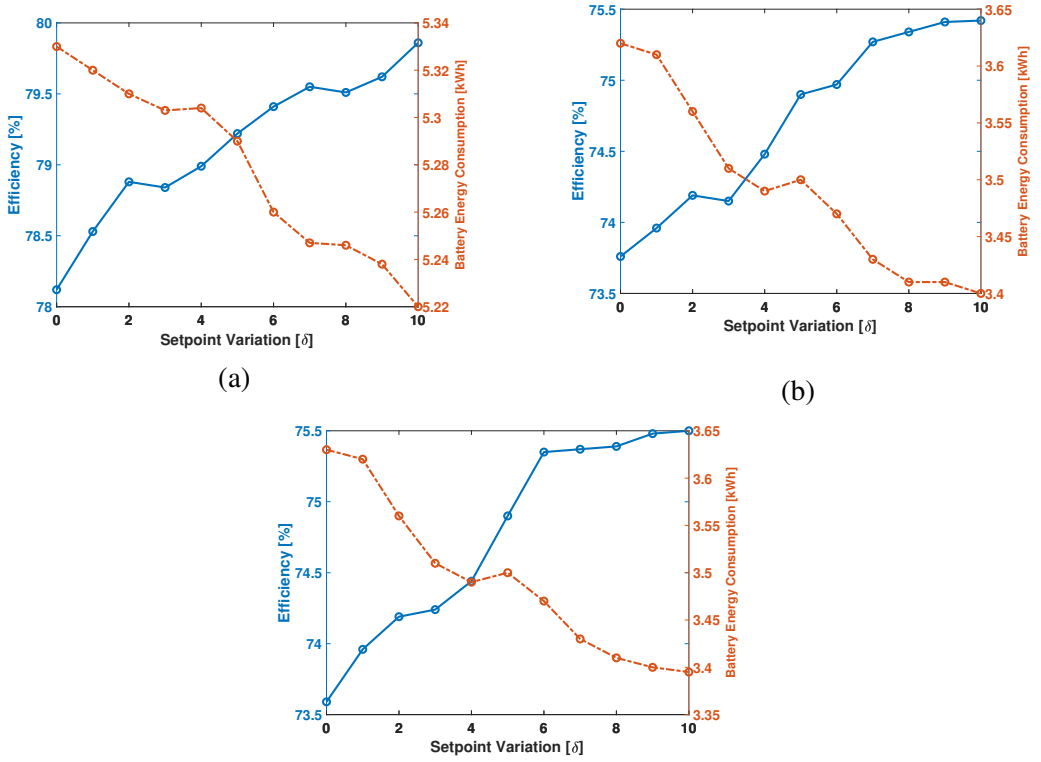

Fig. 4.7 Result of efficiency curves based on speed

battery power, energy efficiency, torque and *SOC* for each speed variation of δ defined in the optimization problem.

According to the performance of the *PSO* optimization algorithm presented in Fig. 4.6, the best locations of efficiency during the entire simulation time are located as a function of speed. In each *DC*, a specific driving pattern is presented, where results of the efficiency improvement for each *DC* are shown in Fig. 4.7.

The value of 0% for δ refers to the fact that the VE operates without the optimization algorithm through *DC*. Before starting with the simulations, it is necessary to take into account that the initial value of the *SOC* is 1 and a simulation time is 3000 seconds for each DC. According to the results shown in Table 4.2 and Fig. 4.7, it is possible to determine that the highest energy efficiency value is reached when δ is 10%. However, it is important to note that the evolution in the increase in efficiency is greater when the variation δ is between 5-6%. Fig. 4.7 (a) shows that for a 5% variation in speed the efficiency increases to 63% of the efficiency when δ is 10% and 74% when delta is 6%. For *DC* 2, Fig. 4.7 (b) shows the efficiency of 68% and 72% when δ is 5% and 6% respectively. Finally, Fig. 4.7 (c) presents 66% and 89% of the maximum efficiency value.

It is important to note that the power saving of the *DC* 3 is better than the others; This result corresponds to the test path that has moderate and aggressive style components in its driving pattern, therefore, the algorithm has several search spaces in the look-up tables.

On the other hand, when $\delta = 5$ %, it is considered the best solution given that the *SOC* value remains fixed while the energy efficiency increases for all *DC* simulations. In this scenario, it is verified that there is an improvement in the $EV's$ energy efficiency without causing additional consumption in the battery pack. Fig. 4.8(b) shows that the proposed algorithm does not generate significant changes in the speed adjustment in *EV* during its operation, ensuring the following of the trajectory at the reference speed.

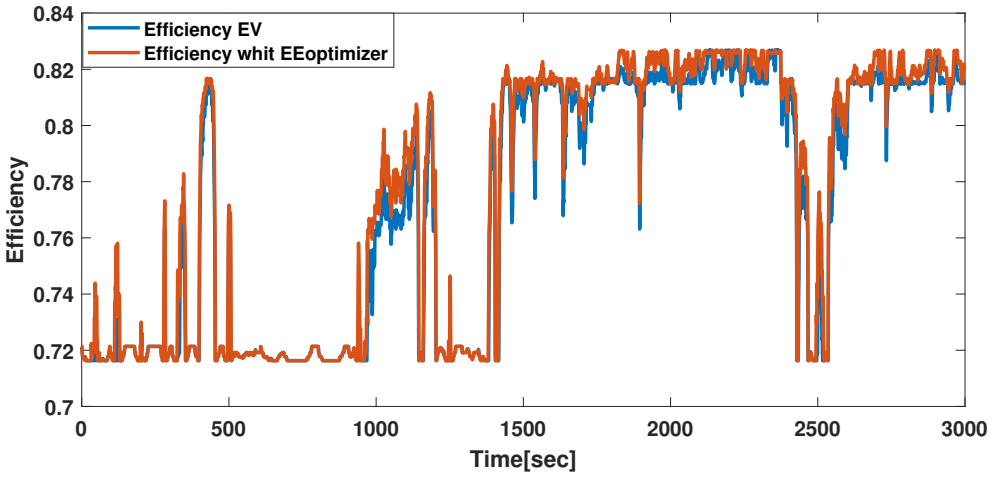

(a)

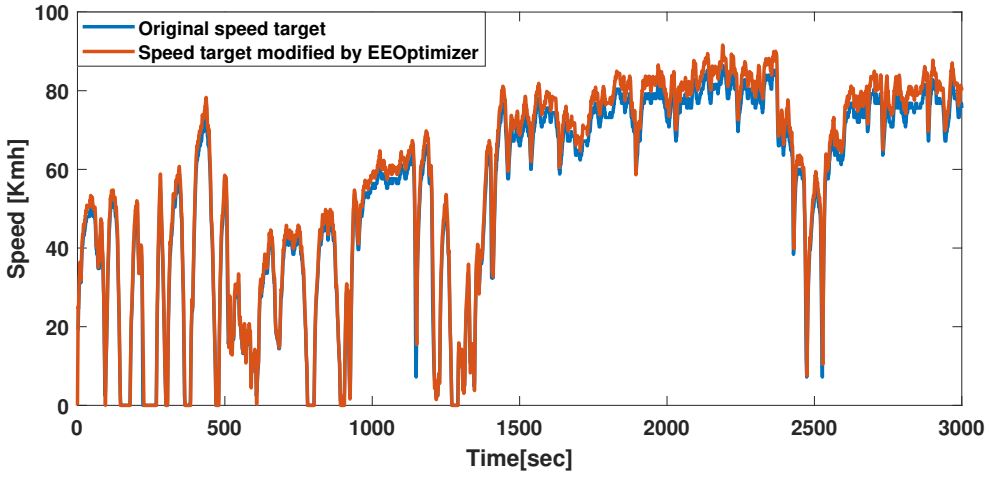

(b)

Fig. 4.8 Comparison of the original and optimal values for δ=5%: (a) Efficiency; (b) Speed

Fig. 4.8(a) presents the result of the variations carried out by the optimizer. The efficiency of the *EV* during operation shows an increase during the entire simulation process. This result verifies that the proposed optimizer adapts to any driving style, improving efficiency throughout the *EV* travel; besides, it can be applied for long driving times. Another advantage of this approach is the computational time required to execute the proposed algorithm. The formulation was carried out according to (4.2), the generated search tables and the metaheuristic algorithm used, present an average execution time of 0.55 milliseconds. Fig. 4.9 shows the calculation time required by the algorithm to generate a solution for each sample j of the *DC*. The sampling time of the vehicle measurements from OBD is 0.5 seconds, which implies the proposal can be implemented.

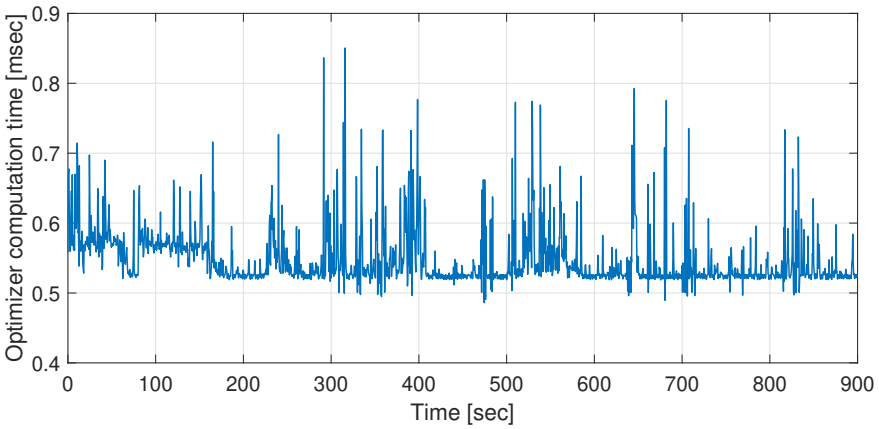

Fig. 4.9 The computation time during optimizer execute

To examine the effectiveness of the optimizer, the operation of the algorithm is compared with strategies reviewed in the literature that show the use of Dynamic Programming (DP) and iterative Dynamic Programming (iDP) as an alternative to find a solution to this problem. However, the computational cost increases depending on the amount of data it must process. The proposed optimizer keeps its computational cost in low levels, specifically 0.55 milliseconds average for any *DC*. Another aspect that can be emphasized is that during the formulation of the optimization problem, a δ factor is proposed such that guarantees that the algorithm works within a specific band according to the EV's speed. Finally, only the *PSO* algorithm is considered to generate the search for the best solution, because no prior training or identification of additional *DC* is necessary, avoiding hybrid algorithms. These features show the advantages of the proposed method over the strategies presented in the literature.

4.3 Conclusions

A strategy for improving energy-efficiency based on mathematical modeling, experimental data, optimization formulation problem, and driving patterns in electric vehicles was proposed in this study. The main conclusions are:

- The optimal rotational speed is calculated online corresponding to the driving requirements of *DC* using a metaheuristic algorithm and vehicle constraints (maximum torque and maximum power), ensuring minimal energy consumption between the battery pack and wheel over the road during driving.
- The mathematical model of the *EV* and the optimization algorithm proposed were designed for a commercial test vehicle. Its performance was verified using simulation on driving profiles described in Figs 4.2,4.3 and 4.4. This methodology could be applied to other electric propulsion vehicles with different architectures in the power train and even $HEVs$. For each variation in the speed reference, the proposal is improving efficiency. The results presented in Table 3 and Fig. 15 are evaluated with 3000 seconds (50 minutes). On a daily route, the average driving time for a common citizen is approximately 7200 seconds (120 minutes), which means that EV's energy efficiency can increase.
- According to the simulation results and considering improving the energy efficiency performance, the strategy showed that the best results are obtained when δ is 10%. However, according to the Fig. 4.7 is possible to determine that the major efficiency increment is when δ is between 5-6%. Therefore, this scenario can be considered to obtain the greatest increase in efficiency with low speed variation. The use of lookup tables and *PSO* for solving the optimization problem generates an alternative for implementation.
- The simulations have shown that the optimizer finds the best solution for each sample of *DC* in a 55 milliseconds average, considering that samples of *DC* have a rate of 0.5 seconds; thus, the optimizer has enough time to complete the whole process.

In future work, lateral forces and trajectories with curvature on the road can be considered for energy efficiency analysis. Furthermore, a combination of metaheuristics and machine learning algorithms can be applied to solve the optimization problem; However, it should be considered that the execution time increases, according to the reviewed literature.

Chapter 5

Assisted Regenerative Braking Control System

Advances in the electrification of transport are directed toward green mobility, focusing efforts on improving the performance of EV and HEV. The EV and HEV development main topic is increasing the driving autonomy range, which is the fundamental requirement. Consequently, regenerative braking control strategies are essential to increase vehicle autonomy.

The regenerative braking system (RBS) and the hydraulic braking system are essential to design a robust coordinate control strategy to recover braking energy. Existing research is mainly focused on developing control strategies to increase recovered energy while complying with braking regulations on emissions, energy consumption, safety and comfort ([91, 92]).

The control architecture of the *RBS* has various subsystems such as brake controller, regenerative brake controller, et al. In EV and HEV, the braking controller receives real-time inputs from various sensors such as wheel speed, battery *SOC*, motor, battery current and other vehicle inputs ([93]). With the inputs from the various sensors, the regenerative braking controller operates to maximize the regenerative braking efficiency and optimal usage of the stored battery power. After controller action, the respective output signals are sent to the motor control unit to optimize the vehicle's braking ([93]).

This chapter proposes an assisted control strategy applied to both mechanical and regenerative braking systems of electric vehicles, including model estimation algorithm and torque input limits.

5.1 Model of Energy Recovery System

As the braking torque is to be controlled, both mechanical friction brake and regenerative brake, it is fundamental to analyze the vehicle's braking system and generate a model that describes its dynamics.

The full braking force output demanded by the driver is achieved by combining hydraulic and regenerative brakes. In the event of a regenerative brake failure, the hydraulic brake system supplies the full braking force demanded by the driver. The general scheme of the braking system is presented in Figure 5.1.

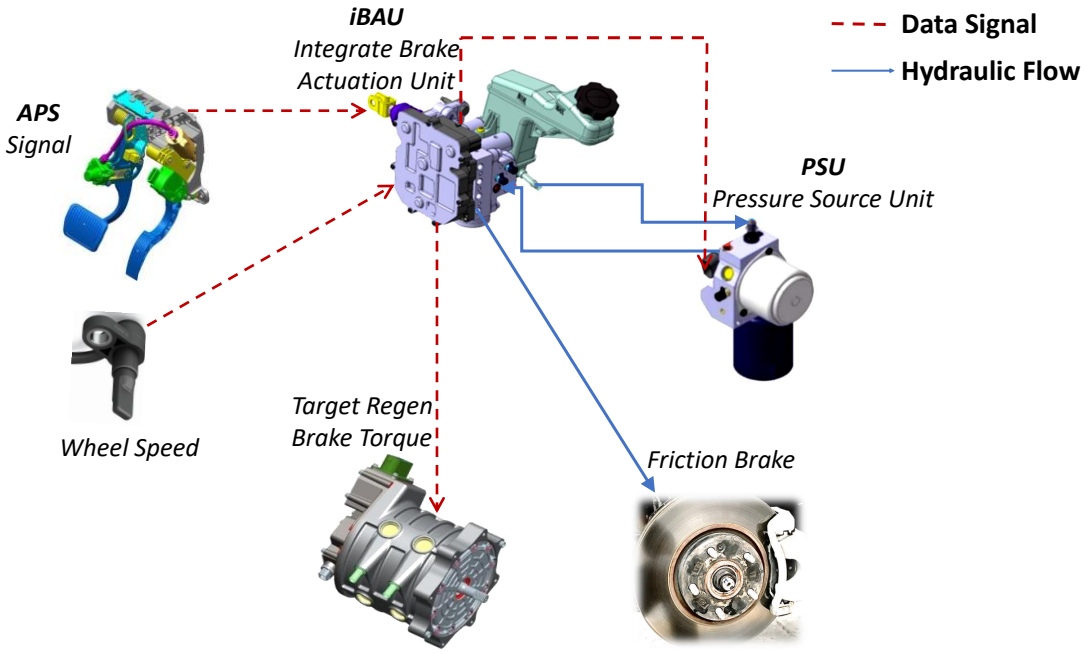

Fig. 5.1 The general architecture

The brake system is composed of the Pressure Source Unit (PSU) and the Integrated Brake Actuation Unit $(iBAU)$. The PSU generates the hydraulic pressure required for braking comparable to the boosting effect when the driver steps on the brake pedal in a system equipped with a vacuum booster. The hydraulic pressure stored in the cylinder is supplied to provide pressure on the entire brake line (front and rear wheels) ([94]).

The $iBAU$ delivers pressure generated by the PSU to a caliper on each wheel. Additionally, the $iBAU$ determines the necessary torque in the regenerative braking system. The level of brake force is determined by the brake pedal pressure and the wheel speed sensor.

In order to obtain the measurement of pressure in the wheels (front and rear) during braking, pressure sensors are placed at the end of the break hydraulic line, as shown in the Fig 5.2.

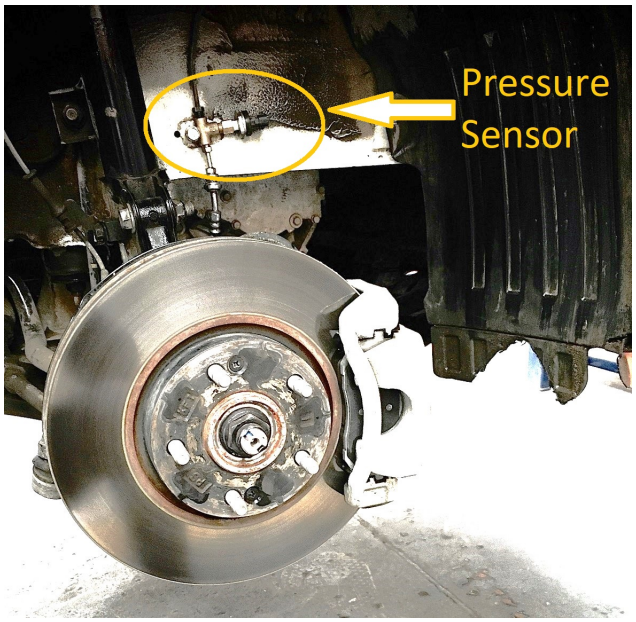

Fig. 5.2 Pressure sensor placed at the end of the hydraulic brake line

Fig.5.3 shows the results of the experimentation on the brake system. The figure shows that the pressure in the front and rear wheels cylinders are similar.

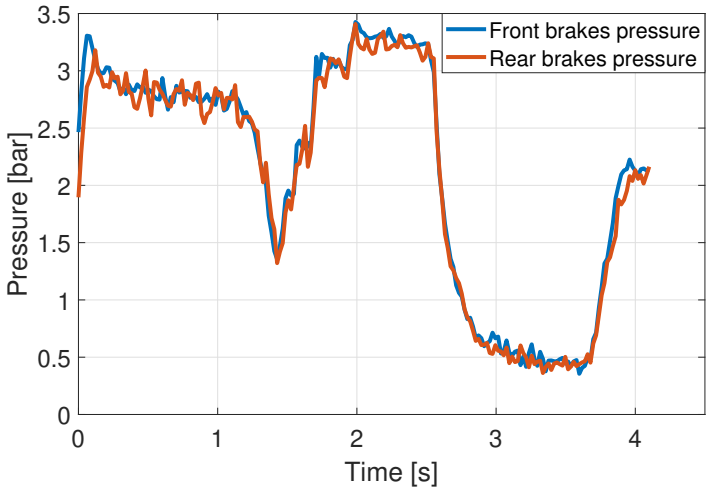

Fig. 5.3 Pressure sensor data

However, to calculate the torque is necessary to consider the characteristics of the friction brake, which refers to details of the calipers and brake discs on the front and rear wheels, as shown in the Fig.5.4.

Equation (5.1) shows the relationship between torque and pressure brake.

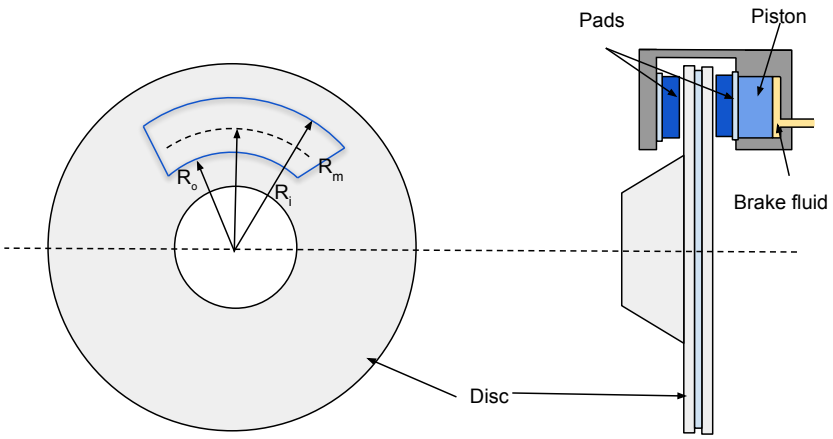

Fig. 5.4 Braking mechanism

$$T_{break} = P(t)\pi r_b^2 R_m N \mu_k \tag{5.1}$$

where $P(t)$ is the brake pressure shown in Fig. 5.3, r_b is the inner radius of the disc piston, R_m is the mean radius of brake pad force application on the brake rotor, N is the number of brake pads in the disk brake assembly and μ_k is the coefficient of kinetic friction of the mechanical brake ([95, 96]). It is essential to mention that the kinetic friction value is defined according to experiments detailed in ([97–99])

The value parameters are shown in Table 5.1.

Table 5.1 Parameters for Mechanical Friction Brake

Parameter	**Value**	**Unit**
Coefficient of kinetic friction	0.37	–
Front disc brake outer radius	0.150	mm
Rear disc brake outer radius	0.142	mm
Front disc piston inner radius	0.030	mm
Rear disc piston inner radius	0.019	mm
The mean radius of brake pad	0.12	m
Tire radius	0.325	m
Number of brake pad	2	–

Alternatively, also is possible to obtain the force information using the following equation

$$F_{break} = \frac{P(t)\pi r_b^2 R_m N \mu_k}{r_t} \tag{5.2}$$

were r_t is the radius of the vehicle tire. Using the information of pressure sensors and applying Equations (2.1), (5.1) and (5.2), it is possible to determine the friction brake torque contribution on front and rear wheels during the braking event, as is shown in Fig. 5.5.

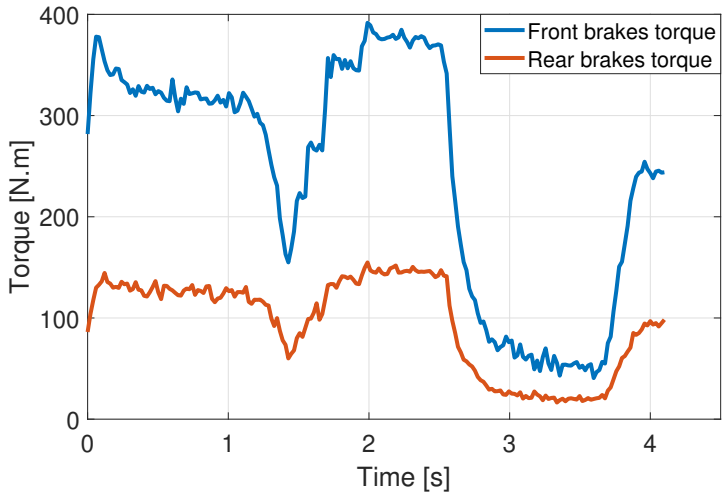

Fig. 5.5 Torque calculation in braking mechanism.

On the other hand, it is also possible to determine the contribution of the torque generated by *RBS* and the information of regenerative current during braking obtained through the *OBD* port directly from the *ECU* of *EV* used by the authors in [55]. Fig.5.6 shows the behavior of regenerative brake torque and the current generated while the vehicle speed decreases.

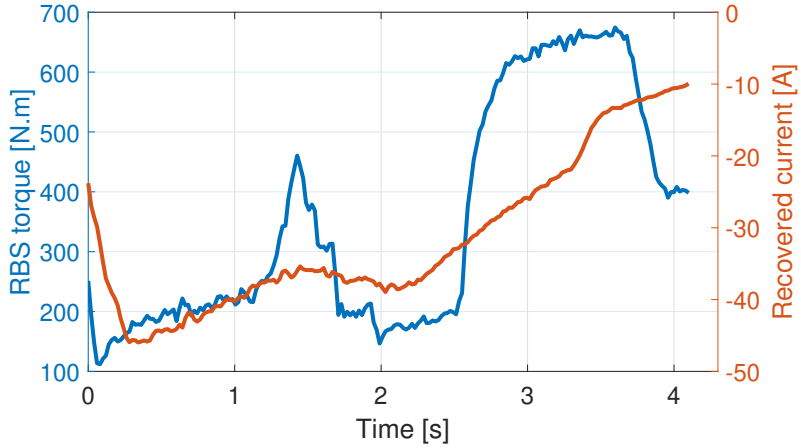

Fig. 5.6 Torque and recovered current of the RBS.

The experimental tests were realized considering regulation # 13 of the Economic Commission for Europe of the United Nations (UN/ECE) that provisions concerning the approval of vehicles with regard to braking ([100, 101]). In the process of braking on a horizontal road and the braking rate is defined as

$$z = \frac{F_f + F_r}{mg} \tag{5.3}$$

were F_f and F_r are the braking forces at the front and rear axles respectively, corresponding to the same front brake line pressure.

In order to guarantee the safety, stability and economy of braking and based on the recommendations in regulation # 13, the experimental data take into account the following considerations:

- The intensity of the braking rate to prevent wheel lockup or activation of the anti-lock braking system (ABS) must be less than 0.2.
- The emergency brake signal will not activate security safety systems while the vehicle deceleration is less than 4m/s^2.

The results of the braking process of the experiment are found in Table 5.2. In this table, five columns represent the braking characteristics, where it is possible to verify that the brake rate and acceleration values are according to the safety ranges analyzed previously.

Table 5.2 Performance Experimentation test

	Braking Rate (z)	**Average Deceleration (m/s^2)**	**Braking Time (s)**	**Initial Speed (km/h)**	**Final Speed (km/h)**
Test 1	0.12	1.43	4.58	40	14.9
Test 2	0.13	1.51	4.10	32.74	9.30
Test 3	0.19	2.20	4.46	50.22	14.48

In order to design the optimal controller, a simplified discrete time-invariant multivariable model from experimental data is necessary. The input signals are the mechanical brake torque and regenerative brake torque. The output signals are the speed vehicle and the recovered current.

The model is developed by employing the Numerical Subspace State Space System Identification ($N4SID$) method ([102]). $N4SID$ is considered due to the benefits of having improved performance in the presence of noise ([103, 104]).

The sampling time of the data acquisition measurements is 0.02 seconds. After acquiring the input-output data sets, the $N4SID$ method in the system identification toolbox of MATLAB is used to identify a conical linear state space model.

$$\begin{aligned} x_{k+1} &= A_m x_k + B_m u_k \\ y_k &= C_m x_k \end{aligned} \tag{5.4}$$

where $x_k \in \mathbb{R}^n$ are the estates, $u_k \in \mathbb{R}^p$ are the data inputs, $y_k \in \mathbb{R}^q$ is the estimated outputs, $A_m \in \mathbb{R}^{nxn}$, $B_m \in \mathbb{R}^{nxu}$, and $C_m \in \mathbb{R}^{rxn}$ are the state transition and output matrices respectively.

The best fit during the identification process is for a four-state multivariable model; therefore, $n = 4$, $p = 2$, $q = 2$ and $r = 2$. The fit for speed and current outputs of the model are 93.87% and 77.71%, respectively, as shown in Fig. 5.7.

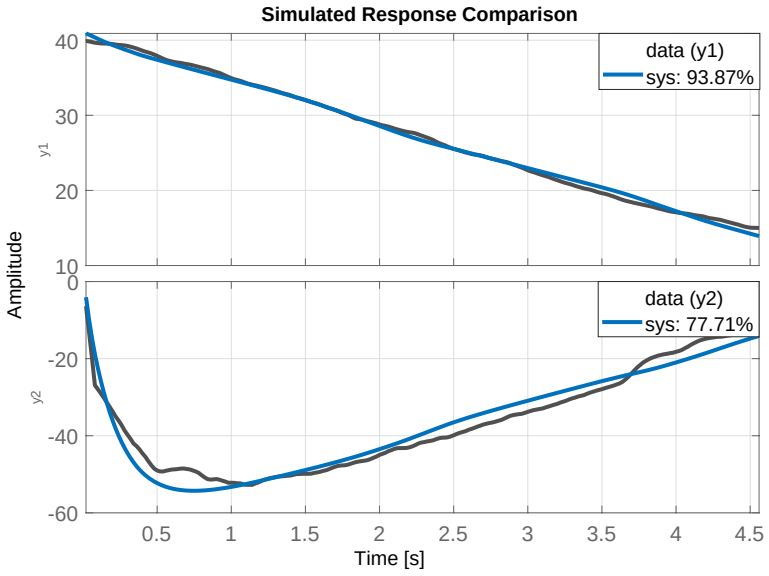

Fig. 5.7 Numerical Subspace State Space System Identification (N4SID) performance.

The detailed values of the matrices are presented in Equations (5.5), (5.6) and (5.7).

$$Am = \begin{bmatrix} 0 & 1 & 0 & 0 \\ 0.478 & 0.236 & 0.2067 & -0.235 \\ 0 & 0 & 0 & 1 \\ 0.2634 & -0.450 & -0.581 & 1.558 \end{bmatrix} \tag{5.5}$$

$$Bm = \begin{bmatrix} 0.0267 & 0.0195 \\ -0.0383 & -0.019 \\ -0.0312 & 0.002 \\ 0.001 & -0.011 \end{bmatrix} \tag{5.6}$$

$$Cm = \begin{bmatrix} 1 & 0 & 0 & 0 \\ 0 & 0 & 1 & 0 \end{bmatrix} \tag{5.7}$$

The eigenvalues of the A matrix are calculated in order to determine the system's stability, as shown following.

$$\begin{aligned} \lambda_1 &= 0.6503 \\ \lambda_2 &= 0.6094 \\ \lambda_3 &= 0.8487 \\ \lambda_4 &= 0.9874 \end{aligned} \tag{5.8}$$

According to 5.8, it is possible to verify the absolute value of the dominant eigenvalue less than 1 (λ_4); therefore, the identified discrete system is stable; even if a small perturbation is added to the system's states, it is asymptotically stable.

5.2 Proposal optimal torque control strategy of energy recovery system

The main objective of assisted control is to generate a braking torque control law that enhances the performance of the *RBS* of the vehicle, specifically increasing the amount of current recovered during the braking process. During this process, it is fundamental to consider that the desired braking torque is divided between the electrical and the mechanical system. This strategy must be adapted to the driver's driving profile by developing small changes in the target torque signals, both in the mechanical braking system and regenerative braking, as shown in Figure 5.8.

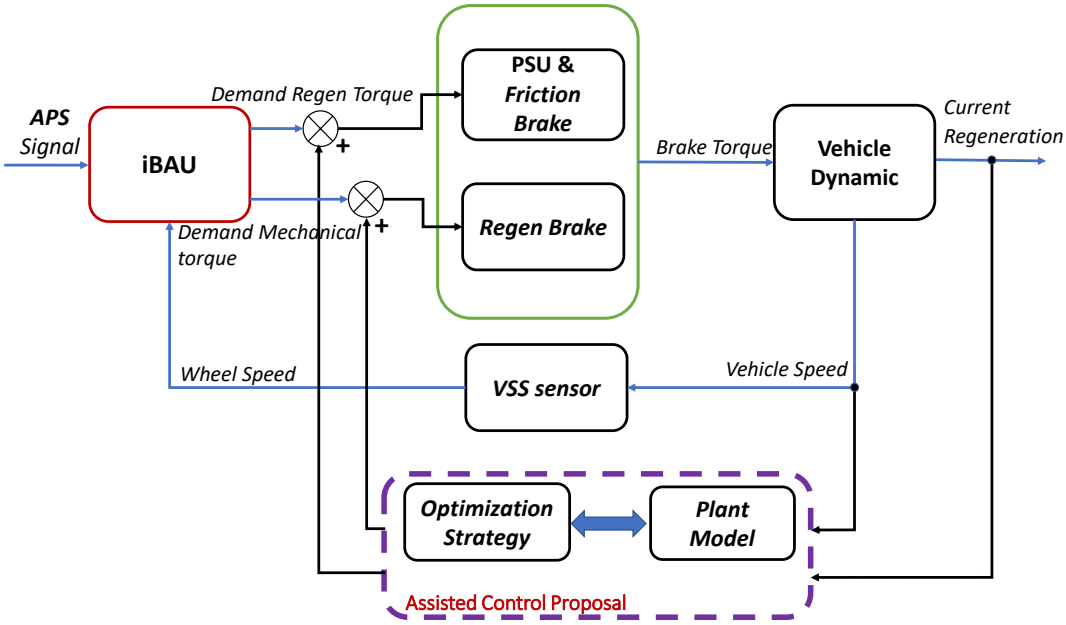

Fig. 5.8 General architecture of the control proposal.

5.2.1 Formulation of assisted optimal control strategy

In order to find the minimized solutions to the tracking speed signal established by the driver during the braking process, it is necessary to transform it into a model-based predictive control (MPC) problem, which is expressed by

$$J_{cost} = \sum_{i=1}^{H_p-1} [(y_{k+i} - yr_{k+i})^T Q(y_{k+i} - yr_{k+i})] + \sum_{i=1}^{H_c-1} [\Delta u_{k+i}^T R u_{k+i}] \tag{5.9}$$

where $Q \geq 0$ is the weighting matrix that reveals the system's ability to follow the reference road trajectory and $R \geq 0$ is the penalty matrix of the state vector. The solution of the MPC instance is to minimize the objective function of Equation (5.9) subject to the constraints in Equation (5.10) at each time step.

$$\begin{gathered} \min_u J_{cost} \\ \text{s.t.} \\ x_{k+1} = A_m x_k + B_m u_k \\ y_k = C_m x_k \\ y_k \leq w_k \\ u_{k-1}(1-\alpha) \leq u_k \leq u_{k-1}(1+\alpha) \\ \Delta u_{min} \leq \Delta u_k \leq \Delta u_{max} \\ k = 1, 2, \ldots, i \end{gathered} \tag{5.10}$$

where w_k is the value of the vehicle speed for each sample time obtained from the driver's driving profile, it is essential to mention that $w_k \leq y_k$ to ensure that the braking is done in equal time or less than the initial braking process. The α parameter defines the variation of the input signals. This parameter sets the input constraints that define the upper and lower limit.

5.3 Simulation results and analysis

Table 5.3 Results of energy efficiency in EV applying the driver cycle optimizer in 3 tests with different variations in the reference speed.

	Alpha Parameter	**Regenerative Current Improvement**	**Braking Time without control (s)**	**Braking Time with control (s)**
Test 1	0.10	6.11%	4.54	4.38
	0.15	6.41%	4.54	4.32
	0.20	6.51%	4.54	4.28
Test 2	0.10	5.52%	4.06	3.82
	0.15	7.02%	4.06	3.80
	0.20	8.02%	4.06	3.76
Test 3	0.10	7.36%	4.42	4.12
	0.15	10.6%	4.42	4.00
	0.20	13.4%	4.42	3.88

Simulations were performed to verify the feasibility and effectiveness of the assisted *MPC* controller for the *RBS*. According to the proposal control diagram shown in Figure 5.8, the *RBS* model obtained and the assisted control strategy described in section 5.2. The performance of the assisted multivariable control strategy in the braking system is evaluated by MATLAB simulations.

The proposed control strategy aims to make small changes set by the parameter (α) in the inputs of the *EV* braking system; this means that variations in friction braking torque and regenerative torque are defined, maximizing the current recovered by the *RBS* without affecting the braking process provided by the driver. To maintain a stable braking intensity according to the user's driving profile, the controller considers the speed and acceleration at the beginning of the braking process. The control action generates changes in this process, both in the friction brake torque signal that regulates the pressure in the brake cylinder and the commanded torque of the electric brake, as shown in Fig. 5.8

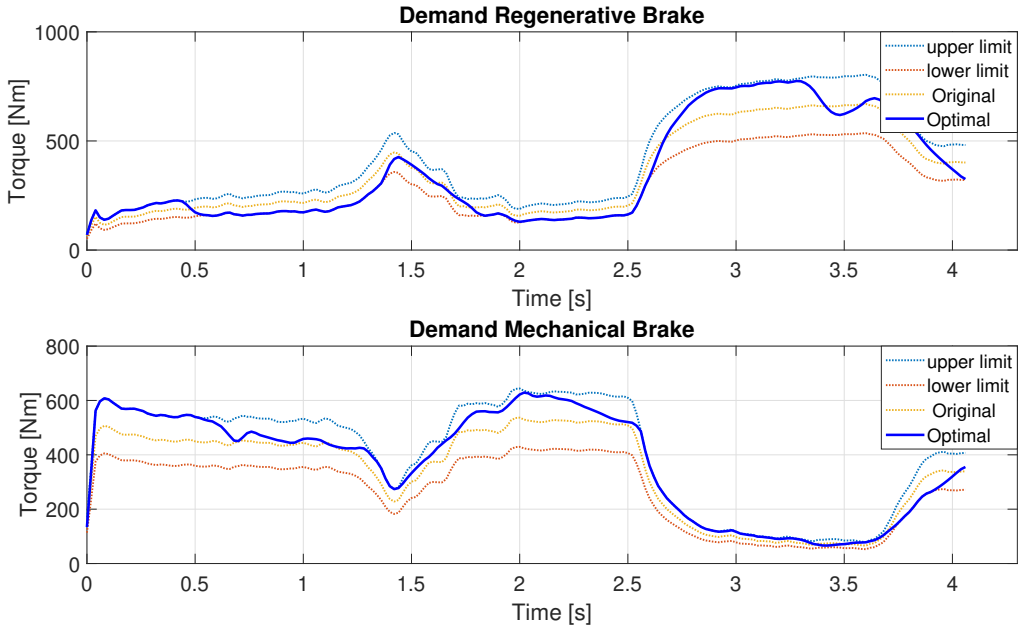

Fig. 5.9 Regenerative and friction braking torque generated by the MPC controller for test 2

Three braking process experiments have been considered to analyze the performance of the assited controller proposed. The results of the control performance simulations are shown in Figs. 5.9, 5.10 and 5.11. For each test is possible to verify that the controller generates variations in the input signals that represent the electrical and mechanical torque of the brake system. The variations of the input signal are limited according to the restrictions established in Equation 5.10.

During the simulation, the following information is required from the *ECU*: vehicle speed and recovery current, which represent two of the four system states described in Equations (5.5), (5.6). The other states are estimated using a KF. Figs 5.12, 5.13 and 5.14 show that in all cases, the assisted control guarantees the following speed generated by the user during the braking process. In fact, to ensure driving safety, the braking time provided by the controller is less than the braking time without the controller.

According to the results of the three scenarios, it is possible to determine that the significant increase in current recovery is reached when α is 0.2. However, it is essential to note that increasing α also reduces braking time, affecting the user's driving profile. One of the objectives of this research is to improve energy recovery, minimally affecting the user's driving behavior. In other words, the proposed assisted control must generate changes in the system in order to improve its performance without replacing the driver as the principal operator of the system.

In accordance with the table 5.3 and considering $\alpha = 0.2$ in test 1, it can be verified that there is a maximum braking time decrease of 0.26 seconds and a recovered current

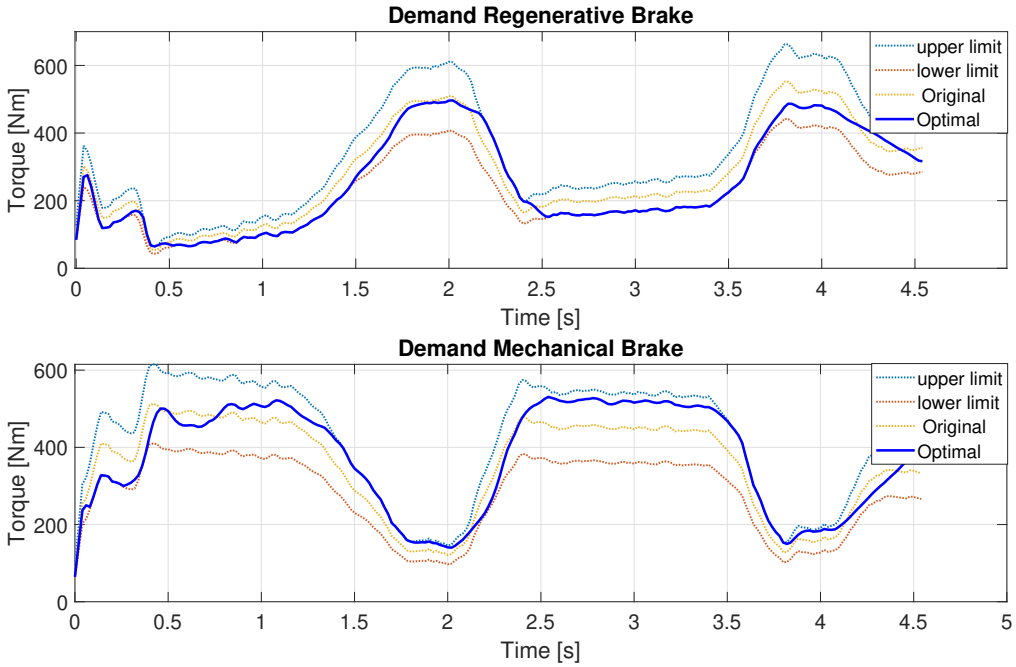

Fig. 5.10 Regenerative and friction braking torque generated by the MPC controller for test 2

improvement of 6.13%. In test 2, there is a maximum braking time decrease of 0.3 seconds and a recovered current improvement of 8.02%. Finally, in test 3, a reduction in the maximum braking time of 0.54 seconds and an improvement in the recovered current of 13.4%.

On the other hand, it is essential to indicate that the evolution in the recovered current is greater when the variation is between $\alpha = 0.1$ and $\alpha = 0.15$. Table 4 shows an increase in current improvement of 0.3%, 1.5% and 3.24% for tests 1, 2 and 3, respectively.

Additionally, it is possible to verify in Figure 5.15 the comparison of the percent of recovery current according to the α parameter.

In addition, it is possible to verify with these results that the most significant current recovery is generated when the vehicle speed before the braking process is greater, as shown in Table 3. However, it is essential to consider that for the assisted control algorithm to go into operation, it is fundamental to consider the braking and acceleration intensity conditions mentioned in the Chapter 2.

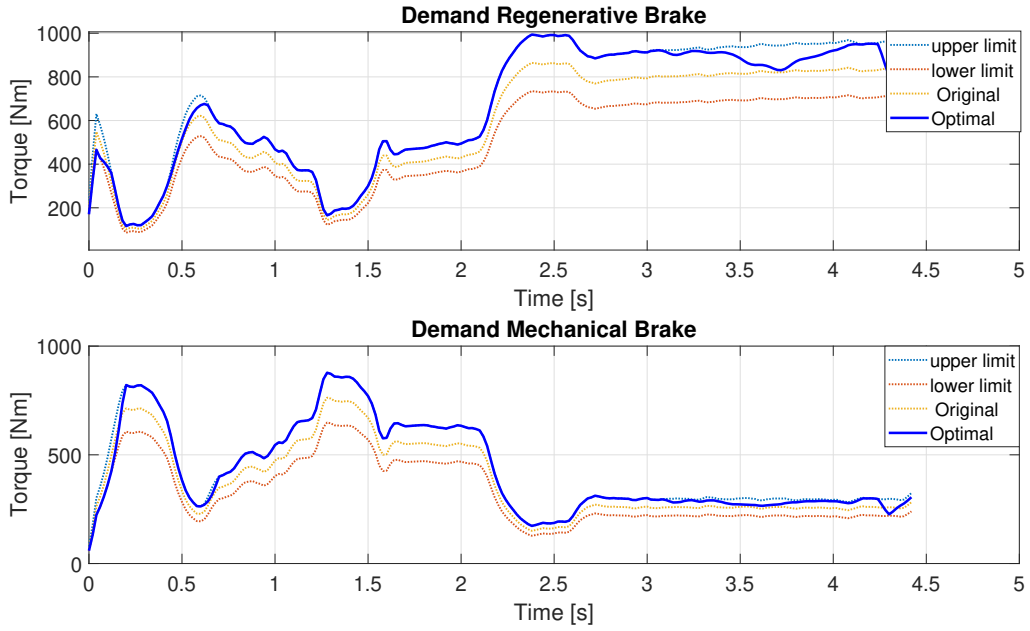

Fig. 5.11 Regenerative and friction braking torque generated by the *MPC* controller for test 3

5.4 Conclusions of the chapter

In this research, an assisted control strategy was proposed in the *RBS* in order to improve current recovery during the braking process. This proposal is based on mathematical models, experimental data and optimal controller design using *MPC* definitions. The main conclusions are:

The variations in the pressure line of the friction brake and the target torque requested in *RBS* follow the trajectory of the values delivered by the *iBAU* according to the controller constraints based on the braking profile of the driver.

Due to the fact that the proposed assisted controller will work at low vehicle speeds and according to the restrictions considered by the UN/ECE regulations, a linear model in *RBS* state space has been estimated. This methodology could be applied to other vehicles that have *RBS*, such as HEV and plug-in hybrid vehicles $(PHEV)$.

The results of the proposed assisted control performance were analyzed and it is verified that α is 0.15 is an appropriate value. This variation value shows that the assisted control intervention is almost imperceptible to the user or driver who operates the vehicle.

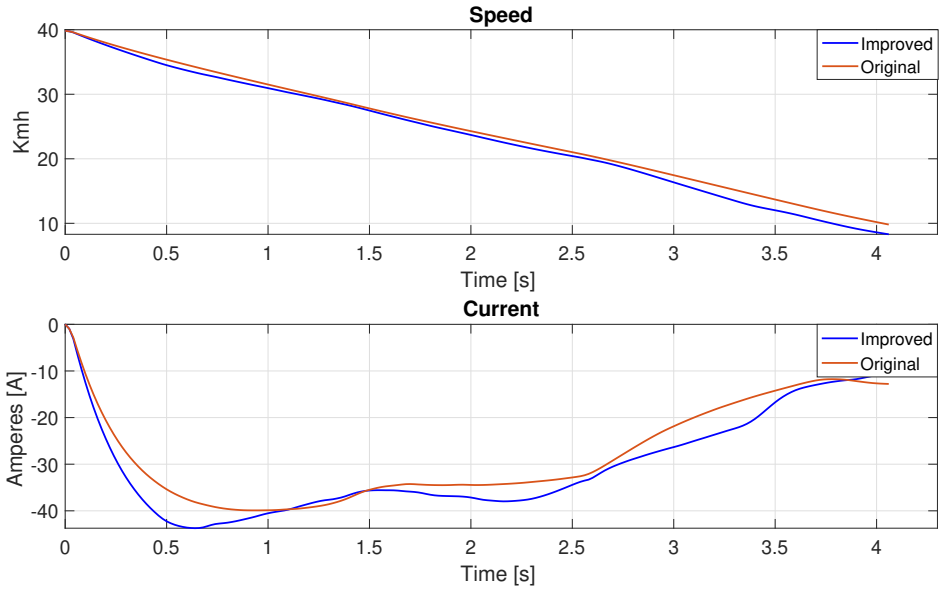

Fig. 5.12 Regenerative and friction braking torque generated by the MPC controller for test 1

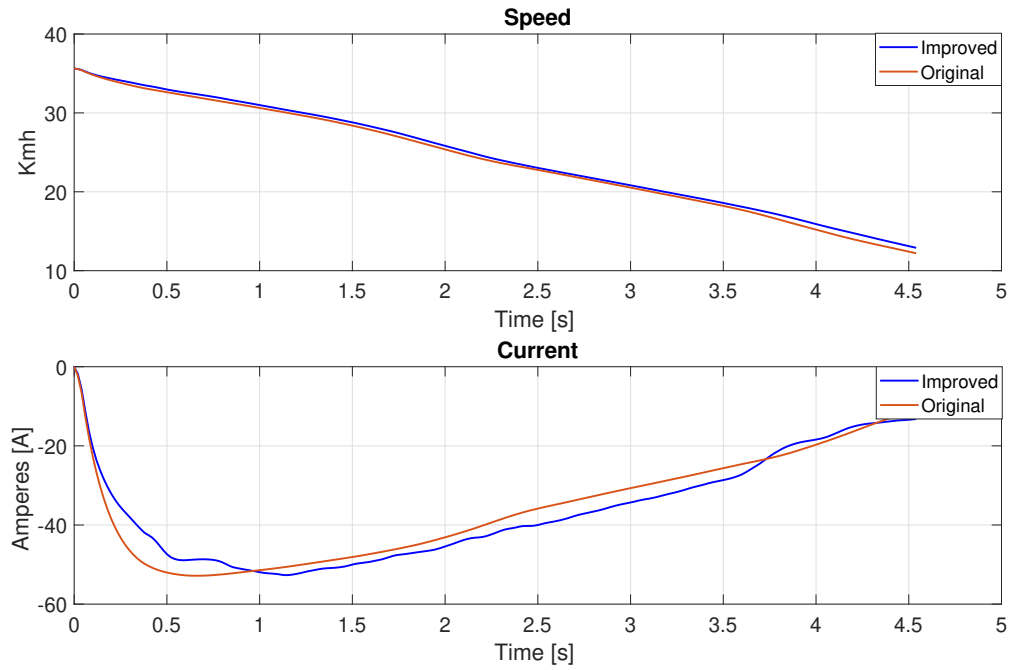

Fig. 5.13 Regenerative and friction braking torque generated by the MPC controller for test 2

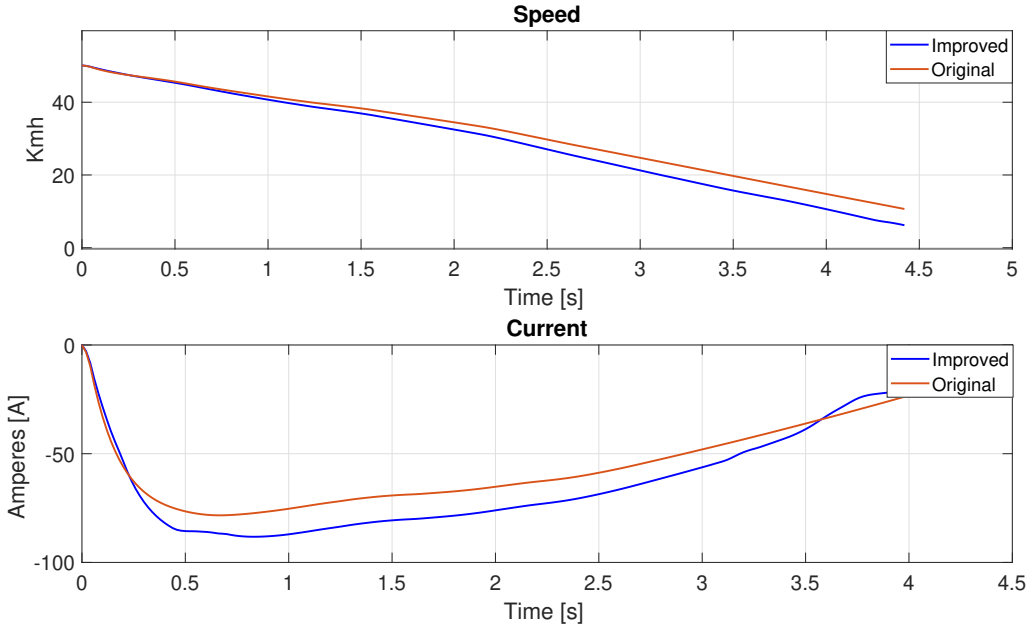

Fig. 5.14 Regenerative and friction braking torque generated by the MPC controller for test 3

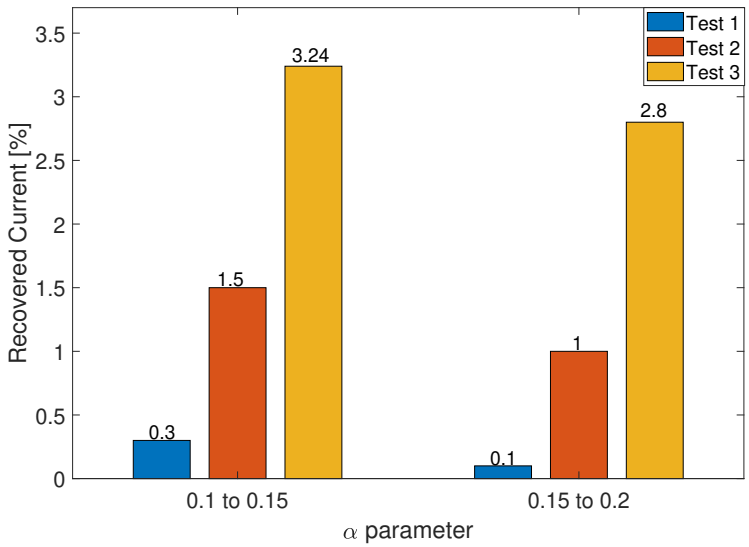

Fig. 5.15 Comparison of percent of recovery current according to α parameter

Chapter 6

Conclusions

The aim of the presented research is to develop assisted control strategies for *EV* systems, focused on enhancing the energy efficiency performance during driving operation and energy recovery through *RBS*. In the literature, *EV* system models and experimental test results have been reported. Selected models and lookup tables that are potentially useful for providing dynamic feature systems of *EV* have been considered. Therefore, the second chapter of this work presents a framework that defines the mechanical-electrical model of the system and the methodology to find them. In the framework, the steps are: to analyze the vehicles' battery, motor and dynamic models, taking into account their energy performance. These models are combined with experimental results to establish control and optimization strategies. In order to improve the efficiency of energy on *EVs*, this research proposes solutions to these challenges that are divided into three cores.

The first core proposes a design of a virtual current sensor replacing the conventional sensor in case of failure or complex measurement. This virtual sensor uses other variables available during *EV* operation, applying *PCA* and machine learning tools to establish a successful estimation, obtaining a fitting of 91% from $PCA + GK - SVR$. The current measurement or estimate and the battery model are essential for determining the *SOC*. The virtual current sensor is validated using experimental data from *EV*; these results were compared with the sensor and *SOC* data captured from the *CAN* bus.

The second core of this research deals with a methodology to improve de *EV* efficiency, considering the result in Chapter 2. The optimization strategy generates a correction in the rotational speed and torque for *PMSM*, ensuring minimal energy consumption between the battery pack and the wheel over the road during driving. This methodology uses a metaheuristic algorithm, specifically the *PSO* particle algorithm, to solve the optimization problem. During the simulation, the *PSO* algorithm shows

that solutions can be found in an average of 55 milliseconds, opening the possibility of implementation in future works.

Finally, the third core deals with generating an assisted control proposal for the *RBS*. This proposal has shown that assisted control improves the recovered current during a braking event. The simulations have shown the controller performance on the model obtained from the recovery system of the *EV* and the best results in the current recuperation considering an alpha factor of 0.15.

As future work, current results lead to consider that the key point is in the assisted controllers structure, which must be consistent with the plant structure; this would require specific considerations about the plant prior to estimating controller parameters. The experiments shown in this document must consider adequate instrumentation equipment and access from the vehicles *ECU*. Then, considering the proposals in this thesis, it is possible to generate future works that establish suggestions to implement control and optimization algorithms both during *EV* operation and in braking events. An alternative that can be examined is the intervention on a controller area network of the *RBS*, *VCU* and the intervention on the *IBAU* output signals.

References

[1] M. of Electricity and R. Energy, "Ecuador energy efficiency national plan 2016-2035 (planee)."

[2] J. Quirós-Tortós, L. Victor-Gallardo, and L. Ochoa, "Electric vehicles in latin america: Slowly but surely toward a clean transport," *IEEE Electrification Magazine*, vol. 7, no. 2, pp. 22–32, 2019.

[3] T. A. Skouras, P. K. Gkonis, C. N. Ilias, P. T. Trakadas, E. G. Tsampasis, and T. V. Zahariadis, "Electrical vehicles: Current state of the art, future challenges, and perspectives," *Clean Technologies*, vol. 2, no. 1, pp. 1–16, 2020.

[4] F. Un-Noor, S. Padmanaban, L. Mihet-Popa, M. N. Mollah, and E. Hossain, "A comprehensive study of key electric vehicle (ev) components, technologies, challenges, impacts, and future direction of development," *Energies*, vol. 10, no. 8, 2017.

[5] M. Sthel, J. G. R. Tostes, and J. R. Tavares, "Current energy crisis and its economic and environmental consequences: Intense human cooperation," *Natural Science*, vol. 5, pp. 244–252, 2013.

[6] R. Rajamani, "Longitudinal vehicle dynamics," in *Vehicle Dynamics and Control*, pp. 87–111, Springer, 2012.

[7] Shutterstock, "Electric vehicle sales in latin america double in 2021."

[8] A. de Empresas Automotrices del Ecuador, "Anuario aeade 2021."

[9] M. M. H. GmbH and C. KG, "Powerdyno lps 300," tech. rep., MAHA Maschinenbau Haldenwang GmbH and Co. KG, Germany, 2014.

[10] GMBPOWER, "GMB Li-ion Battery Individual Data Sheets," tech. rep., PowerStream Technology, Utah-USA, 2010.

[11] G. Gruosso, "Model based approach for evaluation of energy consumption of electrical vehicles," in *2017 IEEE Vehicle Power and Propulsion Conf. (VPPC)*, pp. 1–6, Dec 2017.

[12] J. D. Valladolid, H. D. Montesdeoca, M. B. Ortiz, and J. P. Ortiz, "Optimal adjustment of parameters for the powertrain model of an electric vehicle using experimental data," in *2020 IEEE International Conference on Industrial Technology (ICIT)*, pp. 939–944, 2020.

[13] S. Sarabi and L. Kefsi, "Electric vehicle charging strategy based on a dynamic programming algorithm," in *2014 IEEE International Conference on Intelligent Energy and Power Systems (IEPS)*, pp. 1–5, 2014.

[14] Y. Aguilar, I. Caldas, A. Rivera, and E. Tapia, "ESTUDIO DE LA INFLUENCIA DE LA APERTURA DE LAS VENTANAS Y LA VELOCIDAD DE CIRCULACILAÓN EN LA AERODINÁMICA DE UN VEHÍCULO DE TURISMO," *Ingenius. Revista de Ciencia y Tecnología* , pp. 7 – 13, 12 2017.

[15] E. A. Grunditz and T. Thiringer, "Performance analysis of current bevs based on a comprehensive review of specifications," *IEEE Transactions on Transportation Electrification*, vol. 2, no. 3, pp. 270–289, 2016.

[16] H. Iyama and T. Namerikawa, "Fuel consumption optimization for a power-split hev via gain-scheduled model predictive control," in *2014 Proceedings of the SICE Annual Conference (SICE)*, pp. 468–473, 2014.

[17] M. R. Ahssan, M. M. Ektesabi, and S. A. Gorji, "Electric vehicle with multi-speed transmission: A review on performances and complexities," *SAE International Journal of Alternative Powertrains*, vol. 7, pp. 169–182, dec 2018.

[18] A. R. Sparacino, G. F. Reed, R. J. Kerestes, B. M. Grainger, and Z. T. Smith, "Survey of battery energy storage systems and modeling techniques," in *Proc. IEEE Power and Energy Society General Meeting 2012*, pp. 1–8, July 2012.

[19] X. Liu, W. Li, and A. Zhou, "PNGV equivalent circuit model and soc estimation algorithm for lithium battery pack adopted in AGV vehicle," *IEEE Access*, vol. 6, pp. 23639–23647, 2018.

[20] A. Purwadi, A. Rizqiawan, A. Kevin, and N. Heryana, "State of charge estimation method for lithium battery using combination of coulomb counting and adaptive system with considering the effect of temperature," in *Proc. 2nd IEEE Conf. Power Eng. and Renewable Energy (ICPERE) 2014*, pp. 91–95, Dec 2014.

[21] L. Bascetta, G. Gruosso, and G. S. Gajani, "Analysis of electrical vehicle behavior from real world data: a v2i architecture," in *2018 Inter. Conf. of Electrical and Electronic Technol. for Automotive*, pp. 1–4, July 2018.

[22] A. Nugroho, E. Rijanto, F. D. Wijaya, and P. Nugroho, "Battery state of charge estimation by using a combination of coulomb counting and dynamic model with adjusted gain," in *Proc. Int. Conf. Sustainable Energy Eng. and Appl. (ICSEEA) 2015*, pp. 54–58, Oct 2015.

[23] G. L. Plett, "Extended kalman filtering for battery management systems of lipb-based hev battery packs: Part 3. state and parameter estimation," *J. Power Sources*, vol. 134, no. 2, pp. 277–292, 2004.

[24] Y. Wang, C. Zhang, and Z. Chen, "State-of-charge estimation of lithium-ion batteries based on multiple filters method," *Energy Procedia*, vol. 75, pp. 2635–2640, 2015.

[25] H. Fang, X. Zhao, Y. Wang, Z. Sahinoglu, T. Wada, S. Hara, and R. A. de Callafon, "State-of-charge estimation for batteries: A multi-model approach," in *Proc. American Control Conf.*, pp. 2779–2785, June 2014.

[26] G. Gruosso, "Model based approach for evaluation of energy consumption of electrical vehicles," in *2017 IEEE Vehicle Power and Propulsion Conf. (VPPC)*, pp. 1–6, Dec 2017.

[27] F. Jin, H. Yongling, and W. Guofu, "Comparison Study of Equivalent Circuit Model of Li-Ion Battery for Electrical Vehicles," *Res. J. Appl. Sci. Eng. Technol*, vol. 6, no. 20, pp. 3756–3759, 2013.

[28] J. Fang, L. Qiu, and X. Li, "Comparative study of Thevenin model and GNL simplified model based on kalman filter in SOC estimation," *Inter. J. Advanced Research in Computer Engineering & Technology*, vol. 6, no. 11, pp. 1660–1663, 2017.

[29] A. Hentunen, T. Lehmuspelto, and J. Suomela, "Time-domain parameter extraction method for thévenin-equivalent circuit battery models," *IEEE Trans. Energy Convers.*, vol. 29, pp. 558–566, Sept 2014.

[30] N. Koirala, F. He, and W. Shen, "Comparison of two battery equivalent circuit models for state of charge estimation in electric vehicles," in *Proc IEEE 10th Conf. Ind. Elec. Appl. (ICIEA) 2015*, pp. 17–22, June 2015.

[31] M. Bahramipanah, D. Torregrossa, R. Cherkaoui, and M. Paolone, "Enhanced equivalent electrical circuit model of lithium-based batteries accounting for charge redistribution, state-of-health, and temperature effects," *IEEE Trans. Transp. Electrific.*, vol. 3, pp. 589–599, Sept 2017.

[32] J. Chen, Q. Ouyang, C. Xu, and H. Su, "Neural network-based state of charge observer design for lithium-ion batteries," *IEEE Trans. Control Syst. Technol.*, vol. 26, pp. 313–320, Jan 2018.

[33] H. Chaoui and C. C. Ibe-Ekeocha, "State of charge and state of health estimation for lithium batteries using recurrent neural networks," *IEEE Trans. Veh. Technol.*, vol. 66, pp. 8773–8783, Oct 2017.

[34] I. Li, W. Wang, S. Su, and Y. Lee, "A merged fuzzy neural network and its applications in battery state-of-charge estimation," *IEEE Trans. Energy Convers.*, vol. 22, pp. 697–708, Sept 2007.

[35] M. S. E. Din, A. A. Hussein, and M. F. Abdel-Hafez, "Improved battery soc estimation accuracy using a modified ukf with an adaptive cell model under real ev operating conditions," *IEEE Trans. Transp. Electrific.*, vol. 4, pp. 408–417, June 2018.

[36] H. Tian and B. Ouyang, "Estimation of EV battery SOC based on KF dynamic neural network with GA," in *Proc. Chinese Control Decision Conf. (CCDC)*, pp. 2720–2724, IEEE, 2018.

[37] H. He, R. Xiong, X. Zhang, F. Sun, and J. Fan, "State-of-charge estimation of the lithium-ion battery using an adaptive extended kalman filter based on an improved thevenin model," *IEEE Trans. Veh. Technol.*, vol. 60, pp. 1461–1469, May 2011.

[38] X. Gong, R. Xiong, and C. C. Mi, "Study of the characteristics of battery packs in electric vehicles with parallel-connected lithium-ion battery cells," *IEEE Trans. Ind. Appl.*, vol. 51, pp. 1872–1879, March 2015.

[39] A. Lievre, A. Sari, P. Venet, A. Hijazi, M. Ouattara-Brigaudet, and S. Pelissier, "Practical online estimation of lithium-ion battery apparent series resistance for mild hybrid vehicles," *IEEE Trans. Veh. Technol.*, vol. 65, pp. 4505–4511, June 2016.

[40] B. G. Kim, D. D. Patel, and Z. M. Salameh, "Circuit Model of 100 Ah Lithium Polymer Battery Cell," *J. Power Energy Eng.*, vol. 1, no. 06, pp. 1–8, 2013.

[41] Y. Cao, R. C. Kroeze, and P. T. Krein, "Multi-timescale parametric electrical battery model for use in dynamic electric vehicle simulations," *IEEE Trans. Transp. Electrific.*, vol. 2, no. 4, pp. 432–442, 2016.

[42] J. D. Valladolid, D. Patiño, J. P. Ortiz, I. Minchala, and G. Gruosso, "Proposal for modeling electric vehicle battery using experimental data and considering temperature effects," in *2019 IEEE Milan PowerTech*, pp. 1–6, 2019.

[43] R. Rao, S. Vrudhula, and D. N. Rakhmatov, "Battery modeling for energy aware system design," *Computer*, vol. 36, pp. 77–87, Dec 2003.

[44] Lijun Gao, Shengyi Liu, and R. A. Dougal, "Dynamic lithium-ion battery model for system simulation," *IEEE Transactions on Components and Packaging Technologies*, vol. 25, no. 3, pp. 495–505, 2002.

[45] G. Gruosso, G. S. Gajani, J. D. Valladolid, D. Patino, and F. Ruiz, "State of charge estimation of lifepo4 battery used in electric vehicles using support vector regression, pca and dp battery model," in *2019 IEEE Vehicle Power and Propulsion Conference (VPPC)*, pp. 1–5, 2019.

[46] G. Gruosso, G. Storti Gajani, F. Ruiz, J. D. Valladolid, and D. Patino, "A virtual sensor for electric vehicles' state of charge estimation," *Electronics*, vol. 9, no. 2, 2020.

[47] X. Ma, D. Qiu, Q. Tao, and D. Zhu, "State of charge estimation of a lithium ion battery based on adaptive kalman filter method for an equivalent circuit model," *Applied Sciences*, vol. 9, no. 13, 2019.

[48] S. Bellavia, S. Gratton, and E. Riccietti, "A levenberg–marquardt method for large nonlinear least-squares problems with dynamic accuracy in functions and gradients," *Numerische Mathematik*, 06 2018.

[49] H. Mohammad and M. Y. Waziri, "On broyden-like update via some quadratures for solving nonlinear systems of equations," *Turkish Journal of Mathematics*, vol. 39, no. 3, pp. 335–345, 2015.

[50] M. Transtrum and J. Sethna, "Improvements to the levenberg-marquardt algorithm for nonlinear least-squares minimization," *arXivLabs*, pp. 1–33, 01 2012.

[51] J. Qiao, L. Wang, C. Yang, and K. Gu, "Adaptive levenberg-marquardt algorithm based echo state network for chaotic time series prediction," *IEEE Access*, vol. 6, pp. 10720–10732, 2018.

[52] S. Chakraborty, H.-N. Vu, M. M. Hasan, D.-D. Tran, M. E. Baghdadi, and O. Hegazy, "Dc-dc converter topologies for electric vehicles, plug-in hybrid electric vehicles and fast charging stations: State of the art and future trends," *Energies*, vol. 12, no. 8, 2019.

[53] J. Urkizu, M. Mazuela, A. Alacano, I. Aizpuru, S. Chakraborty, O. Hegazy, M. Vetten, and R. Klink, "Electric vehicle inverter electro-thermal models oriented to simulation speed and accuracy multi-objective targets," *Energies*, vol. 12, no. 19, 2019.

[54] A. Kolli, A. Gaillard, A. De Bernardinis, O. Bethoux, and D. Hissel, "A review on dc/dc converter architectures for power fuel cell applications," *Energy Conversion and Management*, vol. 105, pp. 716 – 730, 2015.

[55] J. D. Valladolid, R. Albarado, D. Mallahuari, and D. Patiño, "Experimental performance evaluation of electric vehicles (ev) based on analysis of power and torque losses," in *2020 IEEE International Conference on Industrial Technology (ICIT)*, pp. 933–938, 2020.

[56] A. Irimescu, L. Mihon, and G. Pãdure, "Automotive transmission efficiency measurement using a chassis dynamometer," *International Journal of Automotive Technology*, vol. 12, pp. 555–559, Aug 2011.

[57] J. Wu, J. Wang, C. Gan, Q. Sun, and W. Kong, "Efficiency optimization of pmsm drives using field-circuit coupled fem for ev/hev applications," *IEEE Access*, vol. 6, pp. 15192–15201, 2018.

[58] C. Lai, G. Feng, J. Tian, Z. Li, Y. Zuo, A. Balamurali, and N. C. Kar, "Pmsm drive system efficiency optimization using a modified gradient descent algorithm with discretized search space," *IEEE Transactions on Transportation Electrification*, pp. 1–1, 2020.

[59] J. O. Estima and A. J. Marques Cardoso, "Efficiency analysis of drive train topologies applied to electric/hybrid vehicles," *IEEE Transactions on Vehicular Technology*, vol. 61, no. 3, pp. 1021–1031, 2012.

[60] V. R. Tannahill, D. Sutanto, K. M. Muttaqi, and M. A. Masrur, "Future vision for reduction of range anxiety by using an improved state of charge estimation algorithm for electric vehicle batteries implemented with low-cost microcontrollers," *IET Electrical Systems in Transportation*, vol. 5, no. 1, pp. 24–32, 2015.

[61] S. Sautermeister, M. Falk, B. Bäker, F. Gauterin, and M. Vaillant, "Influence of measurement and prediction uncertainties on range estimation for electric vehicles," *IEEE Transactions on Intelligent Transportation Systems*, vol. 19, no. 8, pp. 2615–2626, 2018.

[62] S. Scheubner, A. T. Thorgeirsson, M. Vaillant, and F. Gauterin, "A stochastic range estimation algorithm for electric vehicles using traffic phase classification," *IEEE Transactions on Vehicular Technology*, vol. 68, no. 7, pp. 6414–6428, 2019.

[63] E. Kontou, Y. Yin, and Z. Lin, "Socially optimal electric driving range of plug-in hybrid electric vehicles," *Transportation Research Part D: Transport and Environment*, vol. 39, pp. 114–125, 2015.

[64] S. Srinivasa Raghavan and G. Tal, "Influence of user preferences on the revealed utility factor of plug-in hybrid electric vehicles," *World Electric Vehicle Journal*, vol. 11, no. 1, 2020.

[65] M. A. Hannan, M. M. Hoque, A. Hussain, Y. Yusof, and P. J. Ker, "State-of-the-art and energy management system of lithium-ion batteries in electric vehicle applications: Issues and recommendations," *IEEE Access*, vol. 6, pp. 19362–19378, 2018.

[66] R. Xiong, J. Cao, Q. Yu, H. He, and F. Sun, "Critical review on the battery state of charge estimation methods for electric vehicles," *IEEE Access*, vol. 6, pp. 1832–1843, 2018.

[67] A. Fotouhi, D. J. Auger, K. Propp, S. Longo, and M. Wild, "A review on electric vehicle battery modelling: From lithium-ion toward lithium–sulphur," *Renewable and Sustainable Energy Reviews*, vol. 56, pp. 1008–1021, 2016.

[68] Z. Liu and H. He, "Model-based sensor fault diagnosis of a lithium-ion battery in electric vehicles," *Energies*, vol. 8, no. 7, pp. 6509–6527, 2015.

[69] L. Bascetta, G. Gruosso, and G. S. Gajani, "Analysis of electrical vehicle behavior from real world data: a v2i architecture," in *2018 International Conference of Electrical and Electronic Technologies for Automotive*, pp. 1–4, 2018.

[70] G. Storti Gajani, G. Gruosso, and J.-D. Valladolid, "Electric vehicle speed, pedal, accel, voltage and current data over four different roads," 2019.

[71] T. ArchanaH and S. Deshmukh, "Dimensionality reduction and classification through pca and lda," *International Journal of Computer Applications*, vol. 122, pp. 4–8, 07 2015.

[72] V. N. Vapnik, *Statistical Learning Theory*. Wiley-Interscience, 1998.

[73] S. Salcedo-Sanz, J. L. Rojo-Álvarez, M. Martínez-Ramón, and G. Camps-Valls, "Support vector machines in engineering: an overview," *WIREs Data Mining and Knowledge Discovery*, vol. 4, no. 3, pp. 234–267, 2014.

[74] H. Drucker, C. J. C. Burges, L. Kaufman, A. Smola, and V. Vapnik, "Support vector regression machines," in *Advances in Neural Information Processing Systems* (M. Mozer, M. Jordan, and T. Petsche, eds.), vol. 9, MIT Press, 1996.

[75] B. Schölkopf and A. Smola, *Learning with Kernels: Support Vector Machines, Regularization, Optimization, and Beyond*. Adaptive Computation and Machine Learning, Cambridge, MA, USA: MIT Press, Dec. 2002. Parts of this book, including an introduction to kernel methods, can be downloaded here.

[76] Y. Ding, L. Cheng, W. Pedrycz, and K. Hao, "Global nonlinear kernel prediction for large data set with a particle swarm-optimized interval support vector regression," *IEEE Transactions on Neural Networks and Learning Systems*, vol. 26, pp. 2521–2534, Oct 2015.

[77] J. L. Rojo-Álvarez, M. Martínez-Ramón, J. Muñoz-Marí, and G. Camps-Valls, *Advances in Kernel Regression and Function Approximation*, p. 333. IEEE, 2018.

[78] R. Noori, A. Khakpour, B. Omidvar, and A. Farokhnia, "Comparison of ann and principal component analysis-multivariate linear regression models for predicting the river flow based on developed discrepancy ratio statistic," *Expert Systems with Applications*, vol. 37, no. 8, pp. 5856 – 5862, 2010.

[79] A. H. Haghiabi, A. Parsaie, and S. Ememgholizadeh, "Prediction of discharge coefficient of triangular labyrinth weirs using adaptive neuro fuzzy inference system," *Alexandria Engineering Journal*, vol. 57, no. 3, pp. 1773 – 1782, 2018.

[80] F. Hooshyaripor, A. Tahershamsi, and K. Behzadian, "Estimation of peak outflow in dam failure using neural network approach under uncertainty analysis," *Water Resources*, vol. 42, pp. 721–734, Sep 2015.

[81] Y. Huang and B. Clerckx, "Relaying strategies for wireless-powered mimo relay networks," *IEEE Transactions on Wireless Communications*, 05 2016.

[82] S. Barcellona, F. Ciccarelli, D. Iannuzzi, and L. Piegari, "Modeling and parameter identification of lithium-ion capacitor modules," *IEEE Transactions on Sustainable Energy*, vol. 5, no. 3, pp. 785–794, 2014.

[83] I.-G. Jang, C.-S. Lee, and S.-H. Hwang, "Energy optimization of electric vehicles by distributing driving power considering system state changes," *Energies*, vol. 14, no. 3, 2021.

[84] F. Mohammadi, G.-A. Nazri, and M. Saif, "A bidirectional power charging control strategy for plug-in hybrid electric vehicles," *Sustainability*, vol. 11, no. 16, 2019.

[85] S. Sengupta, S. Basak, and R. A. Peters, "Particle swarm optimization: A survey of historical and recent developments with hybridization perspectives," *Machine Learning and Knowledge Extraction*, vol. 1, no. 1, pp. 157–191, 2019.

[86] Y. Wang, Y. Li, L. Jiang, Y. Huang, and Y. Cao, "Pso-based optimization for constant-current charging pattern for li-ion battery," *Chinese Journal of Electrical Engineering*, vol. 5, no. 2, pp. 72–78, 2019.

[87] S. Cheng, H. Lu, L. Xiujuan, and Y. Shi, "A quarter century of particle swarm optimization," *Complex & Intelligent Systems*, vol. 4, 04 2018.

[88] I. Rahman, P. M. Vasant, B. Mahinder, and M. Abdullah, "On the performance of accelerated particle swarm optimization for charging plug in hybrid electric vehicles," *Alexandria Engineering Journal*, vol. 55, no. 1, pp. 419 – 426, 2016.

[89] C. Lv, X. Hu, A. Sangiovanni-Vincentelli, Y. Li, C. M. Martinez, and D. Cao, "Driving-style-based codesign optimization of an automated electric vehicle: A cyber-physical system approach," *IEEE Transactions on Industrial Electronics*, vol. 66, no. 4, pp. 2965–2975, 2019.

[90] X. Zeng, C. Cui, Y. Wang, G. Li, and D. Song, "Segemented driving cycle based optimization of control parameters for power-split hybrid electric vehicle with ultracapacitors," *IEEE Access*, vol. 7, pp. 90666–90677, 2019.

[91] X. Lin and D. Görges, "Robust model predictive control of linear systems with predictable disturbance with application to multiobjective adaptive cruise control," *IEEE Transactions on Control Systems Technology*, vol. 28, no. 4, pp. 1460–1475, 2019.

[92] S. Eben Li, K. Li, and J. Wang, "Economy-oriented vehicle adaptive cruise control with coordinating multiple objectives function," *Vehicle System Dynamics*, vol. 51, no. 1, pp. 1–17, 2013.

[93] B. Xiao, H. Lu, H. Wang, J. Ruan, and N. Zhang, "Enhanced regenerative braking strategies for electric vehicles: Dynamic performance and potential analysis," *Energies*, vol. 10, no. 11, p. 1875, 2017.

[94] KIA, "kia soul ev specification." https://www.kia.com/content/dam/kwcms/kme/uk/en/assets/vehicles/soul-ev/specification/kia-soul-ev-specification.pdf, May 2019.

[95] M. Blundell and D. Harty, "Chapter 6 - modelling and assembly of the full vehicle," in *The Multibody Systems Approach to Vehicle Dynamics (Second Edition)* (M. Blundell and D. Harty, eds.), pp. 451–533, Oxford: Butterworth-Heinemann, second edition ed., 2015.

[96] K. Han, S. B. Choi, J. Lee, D. Hyun, and J. Lee, "Accurate brake torque estimation with adaptive uncertainty compensation using a brake force distribution characteristic," *IEEE Transactions on Vehicular Technology*, vol. 66, no. 12, pp. 10830–10840, 2017.

[97] M. Mróz, A. Orłowicz, G. Wnuk, O. Markowska, W. Homik, and B. Kolbusz, "Coefficient of friction of a brake disc-brake pad friction couple," *Archives of Foundry Engineering*, no. No 4, 2016.

[98] N.-J. Lee and C.-G. Kang, "The effect of a variable disc pad friction coefficient for the mechanical brake system of a railway vehicle," *PLOS ONE*, vol. 10, pp. 1–18, 08 2015.

[99] A. A. Yevtushenko and P. Grzes, "Initial selection of disc brake pads material based on the temperature mode," *Materials*, vol. 13, no. 4, 2020.

[100] Q. He, Y. Yang, C. Luo, J. Zhai, R. Luo, and C. Fu, "Energy recovery strategy optimization of dual-motor drive electric vehicle based on braking safety and efficient recovery," *Energy*, vol. 248, p. 123543, 2022.

[101] "Regulation no 13 of the economic commission for europe of the united nations (un/ece) — uniform provisions concerning the approval of vehicles of categories m, n and o with regard to braking [2016/194]," Feb 2016.

[102] P. Van Overschee and B. De Moor, "N4sid: Subspace algorithms for the identification of combined deterministic-stochastic systems," *Automatica*, vol. 30, no. 1, pp. 75–93, 1994. Special issue on statistical signal processing and control.

[103] L. Dosiek, N. Zhou, J. W. Pierre, Z. Huang, and D. J. Trudnowski, "Mode shape estimation algorithms under ambient conditions: A comparative review," *IEEE Transactions on Power Systems*, vol. 28, no. 2, pp. 779–787, 2013.

[104] S. B. Javed, A. A. Uppal, R. Samar, and A. I. Bhatti, "Design and implementation of multi-variable h robust control for the underground coal gasification project thar," *Energy*, vol. 216, p. 119000, 2021.

Appendix A

Dynamometric Bench MAHA

In this Appendix, the dynamometric bench LPS 3000 MAHA is presented based on [9]. The hardware features used to generate the experimentation in this research are presented in Table A.1.

Table A.1 Parameters for the dynamometric bench whit Roller Set R200/2

Parameter	**Value**	**Unit**
Roller Length	900	*mm*
Roller Width	1100	*mm*
Roller Height	800	*mm*
Roller Diameter	318	*mm*
Roller axle separation	656	*mm*
Axle load	15	tons (t)
Smallest test-able wheel	12	*inch*
Weight incl. packing	2500	*kg*
Lifting Bar	up to max. 40	*bar*
Eddy current brake	2x200	*kW*
Power supply	400v/60Hz	$--$
Test speed	max 200	km/h
Wheel power	max 400	*kW*
Traction	15	*kN*
Measurement accuracy	$\pm$ 2%	$--$

Adittionally, It is possible to drive according to a speed profile with a fixed time and a speed run on the dynamometer using the Drive cycle button.

Appendix B

Support Vector Regression

Support Vector Regression (SVR) is a supervised machine learning algorithm which can be used regression challenges.In this algorithm, we plot each data item as a point in n-dimensional space (where n is number of features you have) with the value of each feature being the value of a particular coordinate.

SVR is considered a non parametric technique because it relies on kernel functions. The relationship between the independent and dependent variables is given by a deterministic function, defined as:

$$f(x) = W^T \phi(x) + b \tag{B.1}$$

where x is the input data in $\mathbb{R}^n$,$f(x)$ is the output value in $\mathbb{R}$, W is controls the smoothness of the model, $\phi(.)$ is a non-linear mapping function from input space $\mathbb{R}^n$, and b is the input data.

To maximize flatness, a vector w with a small norm is desired; for this reason the coefficients of ware estimated by minimizing:

$$\min_{w,\xi,\xi^*} \frac{1}{2} w^T w + C \sum_i (\xi_i + \xi_i^*)^2 \tag{B.2}$$

subject to constraints

$$\begin{aligned} w^T \phi(x_i) + b - y_i &\leq \varepsilon + \xi_i^* \\ y_i - w^T \phi(x_i) + b &\leq \varepsilon + \xi_i \end{aligned} \tag{B.3}$$

where ε is the acceptable output error. C represents a positive constant that determines the degree of penalized loss when a training error larger than ε occurs. ξ_i and ξ_i^*

are non negative slack variables specifying the upper and lower "additional" training errors with respect to the allowed error tolerance ε.

The optimization dual problem is solved using Lagrangian multipliers, where the optimum is a saddle point of the Lagrangian Eq. (B.4) subjected to Eq. (B.5).

$$\begin{aligned} \min \quad & \frac{1}{2}\sum_{i,j=0}^{N}(\alpha_i-\alpha_i^*)(\alpha_j-\alpha_j^*)\langle\phi(x_i),\phi(x_j)\rangle \\ & +\varepsilon\sum_{i,j=0}^{N}(\alpha_j+\alpha_j^*)-\sum_{i,j=0}^{N}y_i(\alpha_j-\alpha_j^* \end{aligned} \tag{B.4}$$

subject to

$$\begin{aligned} \textstyle\sum_{i=0}^{N}(\alpha_i-\alpha_i^*)=0 \\ 0\leq\alpha_i,\alpha_i^*\leq C \\ i=1,2,...,N \end{aligned} \tag{B.5}$$

where N is the number of training samples.

The approximation function $f(x)$ is represented as the following equation:

$$f(x)=\sum_{i=0}^{N}(\alpha_i-\alpha_i^*)G(x_i,x)+b \tag{B.6}$$

where G is the kernel function

Appendix C

Particle Swarm Optimization

Particle Swarm Optimization (PSO) is a non-linear mataheuristic algorithm using collective behavior to converge to a solution into the parameter search-space. We implemented a constriction PSO, which stabilizes the algorithm by dampening the velocity of the particles in the search space. We used the optimal settings described by [85]. The topology of the swarm of particles establishes a measure of the degree of connectivity of its members to the others. It essentially describes a subset of particles with whom a particle can initiate information exchange.

The velocity v_i and position ψ_i are updated as follow:

$$v_i = v_i + c_1 r_1 [pb_i - \psi_i] + c_2 r_2 [gb - \psi_i] \tag{C.1}$$

$$\psi_i = \psi_i + v_i \tag{C.2}$$

where c_1 and c_2 are positive constants, and r_1 and r_2 are two random functions in the range [0, 1] and are different for each dimension and each particle.

The parameters c_1 and c_2, are weights that capture how much a particle should weigh moving towards its cognitive attractor (pb)or its social attractor (gb). The exchange of information between particles mean they are inherently cooperative, thus implying that an unbiased choice of the acceleration coefficients would make them equal.

The following equations describe the velocity and position update mechanisms in a standard PSO algorithm:

$$v_{i+1} \leftarrow v_i + c_1 r_1 [pb_i - \psi_i] + c_2 r_2 [gb - \psi_i] \tag{C.3}$$

$$\psi_{i+1} \leftarrow \psi_i + v_{i+1} \tag{C.4}$$

The procedure of particle swarm optimization algorithm is given in Algorithm 1.

Algorithm 1: PSO algorithm to determine the best rotational speed of the PMSM

```
Initialize population 𝒫
Initialize velocity v
Input: w, c1, c2, iter_max, 𝒫
while iter < iter_max do
    iter=iter+1;
    for i = 1 𝒫 do
        if F(ψ_i) < F(bp) then
            F(bp) = F(ψ_i);
            bp = ψ_i;
        end
        if F(bp) < F(gb) then
            F(gp) = F(pb_i);
            gp = pb_i;
        end
        r1 = rand();
        r2 = rand();
        v_i=v_i+c1 r1 [pb_i − ψ_i]+c2 r2 [gb − ψ_i];
        ψ_i = ψ_i + v_i
    end
end
Result: ψ best global
```

According to the PSO algorithm, the code in Matlab is presented.

function [EfiOp1, rpmop1 ,PotOP1 ,Top1]= Optimizer(T, rpm, Pbat,PP)
v1= [99.7500 99.4500 99.4500 99.2500 99.2500 99.0497 99.0477 99.0457... 99.0417 99.0317 99.0099 99.0012 98.8352 98.4135 98.3627 98.2013... 98.0646 98.0280 98.0051 97.8760 97.5246 96.8411 96.5071 95.6584... 95.2380 94.9754 94.9097 95.0961 94.7861 94.9544 94.4073 93.010];

x1= [0 500 1000 1500 2000 2500 3348.775 3482.726 3683.652 3884.579... 4085.505 4286.432 4487.359 4688.285 4889.212 5090.138 5224.089... 5425.016 5625.942 5826.869 6027.795 6161.746 6362.673 6563.599... 6764.526 6965.452 7166.379 7367.305 7501.256 7546.269 7554.234 8000] ;

v2= [73.7932 73.7932 73.7932 73.7932 75.1829 78.3659 79.2471 80.8057... 82.0410

```
83.3204 84.1930 84.7308 84.6597 84.9331 85.4738 86.0920... 86.0809 86.4555 86.2524
86.6050 86.7047 86.4594 86.4950 86.1859... 85.7237 85.7339 85.7750 85.5122];

x2= [ 0 100 1000 3348.775 3482.726 3683.652 3884.579 4085.505 4286.432... 4487.359
4688.285 4889.212 5090.138 5224.089 5425.016 5625.942... 5826.869 6027.795
6161.746 6362.673 6563.599 6764.526 6965.452... 7166.379 7367.305 7501.256
7546.269 7554.234];


    Max_iter=40; % max iterations
Part_N=30; % Number of particles
x=zeros(Part_N,2);
obj_func=zeros(Part_N,1);
Nva_obj_func=zeros(Part_N,1);
EfiOp1=EfiOp
rpmop1=rpmop;
PotOP1=PotOP;
Top1=Top;
if isempty(Pbat);Pbat=0;end
if isempty(rpm);rpm=0;end
if isempty(T);T=0;end
Wm=rpm*2*pi/60;
if Wm<1
if isempty(Wm); Wm=1;end
Wm=1;end
% Lower and Upper boundaries are calculate
if rpm<=100
l= [0 , 0];
u=[284 , rpm]; else
l= [0 , rpm-rpm*PP];
u=[284 , rpm+rpm*PP];end
% % % % Initial Positions % % % %
x(:,1)=l(1)+rand(Part_N,1).*(u(1)-l(1));
x(:,2)=l(2)+rand(Part_N,1).*(u(2)-l(2));
% % % % % % % % % % % % % %
% % % The objective function is evaluated % % %
for i=1:Part_N
obj_func(i,:)=(T*interp1(x1,v1,x(i,2))*interp1(x2,v2,x(i,2))*(x(i,2)*2*pi/60))/(Pbat);
end
```

```
% % % % % % % % % % % % % % % % % %
% % % The best global vector % % [global_opt ind]=max(obj_func);
G_opt=ones(Part_N,1);
G_opt(:,1)=x(ind,2);
Mejor_pos=[x(ind,2)];
Loc_opt=x(:,2);
v=zeros(Part_N,1);
t=1;
while t<Max_iter
% % % The new speed values are calculated % %
v = v+rand(Part_N,1).*(Loc_opt-x(:,2))+rand(Part_N,1).*(G_opt-x(:,2));
% % % The new position values are calculated % %
x(:,2)=x(:,2)+v;
for i=1:Part_N
% % % constrain particle positions % %
if x(i,2)>u(2); x(i,2)=u(2);
elseif x(i,2)<l(2); x(i,2)=l(2);
end
Nva_obj_func(i,:)=(T*interp1(x1,v1,x(i,2))*interp1(x2,v2,x(i,2))*(x(i,2)*2*pi/60))/(Pbat);
if Nva_obj_func(i,:) > obj_func(i,:)
Loc_opt(i)=x(i,2);
obj_func(i,:)=Nva_obj_func(i,:);
end
end
% % %The best value of the particles is obtained% % [Nvo_global_opt ind]=max(obj_func);
if Nvo_global_opt>global_opt
global_opt=Nvo_global_opt;
G_opt(:,1)=x(ind,2);
Mejor_pos=[x(ind,2)];end
t=t+1; end
EfiOp=global_opt;
rpmop=x(ind,2);
PotOP=T*interp1(x1,v1,x(i,2))*interp1(x2,v2,x(ind,2))*(x(i,2)*2*pi/60);
Top=Pbat/(interp1(x1,v1,x(i,2))*interp1(x2,v2,x(ind,2))*(x(i,2)*2*pi/60));
% % % Algorithm output values % % Top1=Top;
EfiOp1=EfiOp;
rpmop1=rpmop;
PotOP1=PotOP;
```